From the field of human and molecular biology
Theoretical Medicine and Biosciences
of the Faculty of Medicine
of University of Saarland,
Homburg/Saar

DYNAMIC INTERACTION BETWEEN FIBROBLASTS AND TUMOR CELLS AND THEIR EXOSOMES IN ADVANCED PROSTATE CANCER

DISSERTATION

for the award of the degree of Doctor of Natural Sciences
of the Faculty of Medicine
of the
UNIVERSITY OF SAARLAND

2025

Submitted by:
Aishwarya Tagat
Born on 01.12.1994 in
Mysuru, Karnataka, India

1 DATA SHEET

Dynamic interaction between fibroblasts and tumor cells and their exosomes in advanced prostate cancer

Department for Clinical-Experimental Research

Clinic for Urology and Pediatric Urology

Saarland University Hospital

Name, Given Name:	Tagat, Aishwarya
Matriculation Number:	7013541
Address:	Rheinstrasse 37
	79189, Hausen an der Möhlin, Bad Krozingen, Germany
Phone:	+49 (0) 176 35813432
E-mail:	tagat22@gmail.com

Date of Delivery:	26.09.2025
Dean:	Univ.-Prof. Dr. med. dent. Matthias Hannig

2 STATUTORY DECLARATION

I hereby assure that I have composed the present thesis entitled Dynamic interaction between fibroblasts and tumor cells and their exosomes in advanced prostate cancer independently and have used no other appliances and reagents than indicated. Parts gathered from other works according to wording or meaning have been indicated in every single case by the declaration of the source.

Furthermore, I have produced my work according to the principles of good scientific practice in compliance with the valid "Richtlinien der Universität des Saarlandes zur Sicherung guter wissenschaftlicher Praxis".

Date: 26.09.2025

Name: Aishwarya Tagat

3 TABLE OF CONTENTS

1 DATA SHEET 2
2 STATUTORY DECLARATION 3
3 TABLE OF CONTENTS 4
4 LIST OF FIGURES 7
5 LIST OF TABLES 8
6 LIST OF ABBREVIATIONS 9
7 ABSTRACT 12
8 ZUSAMMENFASSUNG 14
9 ACKNOWLEDGMENT 16
10 INTRODUCTION 17
10.1 Epidemiology of Prostate Cancer 17
10.2 Prostate Cancer 18
10.3 Molecular Biology and Pathophysiology of Prostate Cancer 20
10.4 Prostate Tumor Microenvironment 23
10.5 Extracellular Vesicles 24
10.5.1 Biogenesis of Extracellular Vesicles 25
10.5.2 Exosomes in Prostate Tumor Microenvironment 27
10.5.3 Exosomes in Prostate Cancer Metastasis 28
10.5.4 Role of Exosomal miRNAs in Prostate Cancer 29
11 HYPOTHESIS AND AIM OF THE STUDY 31
12 MATERIALS 33
12.1 Patient Samples 33
12.2 Cell lines 33
12.3 Medium, reagents, and chemicals 34
12.4 Antibodies and Primers 35
12.5 Kits 35
12.6 Buffers and Solutions 36
12.7 Consumables 37
12.8 Devices 38
12.9 Softwares 39
13 METHODS 40
13.1 Cell Culture 40
13.1.1 Preservation and Storage of Cells 40
13.1.2 Thawing and Culturing of Cells 40
13.1.3 Subcultivation 41
13.1.4 Cell Counting and Seeding 41

13.1.5 Cell Lysis 41
13.2 Isolation of Exosomes 42
13.2.1 Production of Exosome-free Medium 42
13.2.2 Isolation of Exosomes from Cell Culture 42
13.3 Characterization of Cells and their Exosomes 44
13.3.1 Nanoparticle Tracking Analysis 44
13.3.2 Transmission Electron Microscopy 45
13.3.3 Protein separation using SDS –PAGE 46
13.3.4 Western Blotting 47
13.4 Co-culture Assays 50
13.4.1 Viability Assay 50
13.4.2 Proliferation Assay 52
13.4.3 Migration Assay after cellular co-culture 53
13.4.4 Migration Assay after exosomal treatment 55
13.5 miRNA Expression Analysis 56
13.5.1 Total RNA isolation from cells and exosomes 56
13.5.2 miRNA Microarray Analysis 57
13.5.3 Validation of miRNA-expression by qPCR 59
14 RESULTS 61
14.1 Characterization of cells and their exosomes 61
14.1.1 Particle Size and Concentration Profiling of Exosomes from Primary Prostate Fibroblasts 61
14.1.2 Morphological Analysis of Exosomes from Primary Prostate Fibroblasts 63
14.1.3 Profiling of Exosome-Specific Markers in Prostate Fibroblasts-derived Exosomes 64
14.1.4 Expression Profiling of α-SMA in Prostate Fibroblasts 65
14.2 Functional assessment of fibroblasts and their exosomes-mediated effects on prostate cancer cells 66
14.2.1 Influence of patient-derived fibroblasts in regulating prostate cancer viability 66
14.2.2 Influence of patient-derived fibroblasts in regulating prostate cancer proliferation 68
14.2.3 Influence of patient-derived fibroblasts in regulating prostate cancer motility 70
14.2.4 Influence of exosomes derived from patient-derived fibroblasts in regulating prostate cancer viability 72
14.2.5 Influence of exosomes derived from patient-derived fibroblasts in regulating prostate cancer migration 74
14.3 Functional assessment of prostate cancer exosomes-mediated effects on patient-derived fibroblast viability 76
14.4 Effect of prostate cancer cells and their exosomes on immortalized hTERT foreskin fibroblasts 77
14.5 Assessment of α-SMA in hTERT fibroblasts after co-culture with prostate cancer cells 79
14.6 Identification and Validation of miRNA Pattern in Patient-derived Prostate Fibroblasts and their exosomes 79
14.6.1 Microarray-Based Identification of Differentially Expressed miRNAs 80
14.6.2 Validation of selected upregulated miRNAs 82
15 DISCUSSION 84
15.1 Exosome Characterization and Compliance with MISEV 84
15.2 Functional Influence of NCAFs and CAFs on Prostate Cancer Progression 86
15.3 Functional Influence of NCAF- and CAF-Exosomes on Prostate Cancer Progression ... 89

15.4 Reciprocal Effects of Prostate Cancer Cells and their Exosomes on Patient-derived Fibroblasts 91
15.5 miRNA Profiling and Its Potential Role in Prostate Cancer through Cargo Packaging .93
16 FUTURE PROSPECTS AND CLINICAL RELEVANCE 97
17 LIMITATIONS 99
18 BIBLIOGRAPHY 100
19 SCIENTIFIC CONTRIBUTION AND AWARDS 124
19.1 Presentations at National and International Conferences (First Author only) 124
19.2 Poster Presentations at National and International Conferences (First Author only) 124
19.3 Awards and Prizes 124
20 CURRICULUM VITAE 125

4 LIST OF FIGURES

Figure 1: Incidence of Prostate Cancer in men among Western Countries. (Cancer WHO n.d.). 17
Figure 2: Schematic representation of the prostate gland anatomy. (Hoofring 2007) 19
Figure 3: Schematic Representation of Prostate Tumor Microenvironment (Image created using (BioRender n.d.)) 24
Figure 4: Biogenesis and classification of extracellular vesicles (EVs) (Linxweiler and Junker 2020) 26
Figure 5: Steps in the isolation of exosomes by ultracentrifugation (UC) [Image created using (BioRender n.d.)] 43
Figure 6: Principle of Nanoparticle Tracking Analysis (NTA)(Nanopartikel-Tracking-Analyse (NTA) n.d.) 45
Figure 7: Stepwise illustration of viability assay [Image created using (BioRender n.d.)] 51
Figure 8: Schematic overview of prostate cancer (PCa) cell migration following co-culture with CAFs and NCAFs (Image created using (BioRender n.d.)) 53
Figure 9: Nanoparticle Tracking Analysis (NTA) of exosomes isolated from prostate fibroblasts 62
Figure 10: Transmission electron microscopy (TEM) images of exosomes isolated from prostate fibroblasts 63
Figure 11: Western blot analysis of exosomal protein markers in prostate fibroblasts 64
Figure 11: Western blot analysis of α-SMA expression in primary prostate fibroblasts 65
Figure 13: Effect of patient-derived fibroblasts on prostate cancer viability 67
Figure 14: Effect of patient-derived fibroblasts on prostate cancer proliferation. 69
Figure 15: Effect of patient-derived fibroblasts on prostate cancer migration 71
Figure 16: Effect of fibroblast-derived exosomes on prostate cancer viability. 73
Figure 17:Effect of fibroblast-derived exosomes on prostate cancer migration. 75
Figure 18: Effect of prostate cancer cells-derived exosomes on patient-derived fibroblast viability. 77
Figure 19: Effect of prostate cancer cells and their exosomes on hTERT fibroblast viability. 78
Figure 20: α-SMA expression in hTERT fibroblasts after co-culture with prostate cancer cells. 79
Figure 21: Global microarray profiling of cellular and exosomal miRNAs derived from patient prostate fibroblasts. 80
Figure 22: qPCR validation of cellular and exosomal miRNAs from NCAFs and CAFs. 83

5 LIST OF TABLES

Table 1. Cell lines used.....33
Table 2. List of medium, reagents, chemicals and enzymes used.....34
Table 3. List of Antibodies and Primers used.....35
Table 4. List of kits used.....35
Table 5. List of Buffers and Solutions.....36
Table 6. List of consumables used.....37
Table 7. List of devices used.....38
Table 8. List of software used.....39
Table 9. Primary antibodies used for WB.....48
Table 10. Secondary antibodies used for WB.....49
Table 11. Scanning instructions for microarray.....58
Table 12. Pipetting scheme and PCR program for reverse transcription.....59
Table 13. Program for qPCR.....60
Table 14. Exosome concentration and size distribution.....61
Table 15. List of expressed cellular and exosomal miRNAs.....81

6 LIST OF ABBREVIATIONS

ABBREVIATION	EXPLANATION
Ab	Antibody
ALIX	ALG-2-interacting protein X (ALIX)
AR	Androgen Receptor
BCA	Bicinchoninic Acid
BPHFs	Benign Prostatic Hyperplasia-associated Fibroblasts
BrdU	Bromodeoxyuridine
CAF	Cancer-associated fibroblast
CCD	Charge-coupled device
CHAPS	3-[(3-cholamidopropyl)dimethylammonio]-1-propanesulfonate
CI	Cell Index
CIM plate	Cellular Invasion/ Migration plate
CM	Conditioned Medium
cm^2	square centimeter
CRPC	Castration-resistant Prostate Cancer
Ct	Crossing point
CTCs	Circulating Tumor Cells
DMEM	Dulbecco´s Modified Eagle Medium
DMSO	Dimethyl sulfoxide
DPBS	Dulbecco´s Phosphate Buffer Saline
DTT	Dithiotriol
DUBs	Deubiquitylating Enzymes
ECM	Extracellular matrix
ED-FCS	Exosome-Deficient Fetal Calf Serum
EMT	Epithelial-mesenchymal transition
ESCRT	Endosomal Sorting Complex Required for Transport
EVs	Extracellular Vesicles
EZH2	Zeste homolog 2
GDP	Global Domestic Product

h	hour
H_2SO_4	Sulfuric acid
HDI	Human Development Index
HIF	Hypoxia-inducible Factor
HnRNPA1	heterogenous nuclear ribonucleoprotein A1
HRP	Horseradish peroxidase
hTERT	hTERT-immortalized foreskin fibroblasts
ILVs	intraluminal vesicles
ISEV	International Society of Extracellular Vesicles
kDa	kilodaltons
LN_2	Liquid Nitrogen
LNA	Locked Nucleic Acid
MeOH	Methanol
MMPs	Metalloproteinases
min	minute
miRNAs	microRNAs
ml	milliliter
MVBs	multivesicular bodies
NaCl	Sodium Chloride
NED	Neuroendocrine Differentiation
NTA	Nanoparticle Tracking Analysis
NCAF	Non-cancer-associated fibroblast
ncRNAs	Non-coding RNAs
NF-kB	Nuclear Factor-kappa B
NK	Natural Killer
PCa	Prostate Cancer
PFA	Paraformaldehyde
pI	Isoelectric point
PI	Protease Inhibitor
PRC2	polycomb Repressive Complex 2
PSA	Prostate-specific Antigen
PVDF	Polyvinylidene Difluoride
qPCR	quantitative real-time polymerase chain reaction

RBP	RNA-binding protein
RNA	Ribonucleic Acid
RPMI-1640	Roswell Park Memorial Institute-1640
RT	Room Temperature
SDS	Sodium Dodecyl Sulfate
SDS-PAGE	Sodium Dodecyl Sulfate Polyacrylamide Gel Electrophoresis
sEVs	small extracellular vesicles
TBS-T	Tris-buffered saline with Tween 20
TEM	Transmission Electron Microscopy
TME	Tumor Microenvironment
Tris	Tris(hydroxymethyl)aminomethane
UC	Ultracentrifugation
WB	Western Blot
Wnt	wingless related integration site

7 ABSTRACT

Prostate Cancer (PCa) is the most commonly diagnosed malignancy among men worldwide and remains a significant cause of cancer-related deaths in men. Despite advances in diagnostics and therapeutics, the disease often progresses to aggressive, therapy-resistant stages. Increasing evidence highlights the tumor microenvironment (TME) as a critical regulator of disease progression. Among its components, fibroblasts, particularly cancer-associated fibroblasts (CAFs) and their secreted exosomes, play an important role in modulating tumor growth, invasion and treatment response. However, the mechanisms by which patient-derived fibroblasts and their exosomes influence prostate cancer remain incompletely understood.

This work investigated the dynamic interaction between primary patient-derived prostate fibroblasts, their exosomes, and PCa tumor cells, focusing on functional regulation and exosome-mediated signaling. Four pairs of CAFs and non-cancer-associated fibroblasts (NCAFs) were isolated from patients after radical prostatectomy and were comprehensively characterized. Exosomes were successfully isolated and confirmed using nanoparticle tracking analysis, transmission electron microscopy, and western blotting for canonical markers, establishing their identity as exosomes. Functional co-culture studies revealed patient-specific but distinct effects of fibroblasts on PCa cells. CAFs generally enhanced tumor cell viability and motility, whereas NCAFs showed a stronger influence on promoting proliferation. Exosome treatments partially mirrored these effects, demonstrating that fibroblast-derived exosomes can recapitulate key functional alterations in tumor cells. Importantly, context-specific responses were observed between the two PCa cell lines studied. The androgen-dependent LNCaP cells and the androgen-independent, more aggressive LNCaP C4-2 cells. While LNCaP cells remained largely non-migratory, CAFs and their exosomes significantly promoted migration in LNCaP C4-2 cells, suggesting that fibroblast-derived exosomes may contribute to metastatic progression.

To further investigate reciprocal signaling, PCa cells-derived exosomes were applied to fibroblasts and hTERT-immortalized foreskin fibroblasts. While LNCaP C4-2-derived exosomes increased fibroblast viability, they failed to induce significant activation in patient fibroblasts. They unexpectedly reduced α-SMA expression in hTERT cells, indicating

variable fibroblast responses to tumor-derived signals. Additionally, global microRNA profiling of fibroblasts and their exosomes revealed a distinct expression pattern differentiating CAFs from NCAFs. Several miRNAs associated with cancer-related pathways were enriched in CAFs and their exosomes, and validation experiments confirmed their selective packaging. These findings highlight a potential role of fibroblast-derived exosomal miRNAs in modulating PCa cell behavior and provide insight into their contribution to tumor progression.

Overall, this work demonstrates that patient-derived fibroblasts and their exosomes are not passive bystanders but active modulators of PCa biology. The study provides new insights into the molecular and functional interplay between stromal and tumor cells, identifies potential biomarkers for disease stratification, and emphasizes the therapeutic relevance of targeting tumor-stroma communication. By advancing our understanding of the role of fibroblast-derived exosomes in PCa, these findings open avenues for developing novel diagnostic strategies and more personalized treatment approaches for advanced disease.

8 ZUSAMMENFASSUNG

Das Prostatakarzinom (PCa) ist weltweit die am häufigsten diagnostizierte Krebserkrankung bei Männern und nach wie vor eine bedeutende Ursache für krebsbedingte Todesfälle bei Männern. Trotz Fortschritten in der Diagnostik und Therapie entwickelt sich die Erkrankung häufig zu aggressiven, therapieresistenten Stadien fort. Immer mehr Hinweise deuten darauf hin, dass die Tumormikroumgebung (TME) eine entscheidende Rolle bei der Regulierung des Krankheitsverlaufs spielt. Unter ihren Komponenten spielen Fibroblasten, insbesondere krebsassoziierte Fibroblasten (CAFs) und die von ihnen sekretierten Exosomen, eine wichtige Rolle bei der Modulation des Tumorwachstums, der Invasion und dem Ansprechen auf die Behandlung. Die Mechanismen, durch die Fibroblasten und ihre Exosomen den Prostatakrebs beeinflussen, sind jedoch noch nicht vollständig geklärt.

In dieser Arbeit wurde die dynamische Interaktion zwischen primären, von Patienten stammenden Prostata-Fibroblasten, ihren Exosomen und PCa-Tumorzellen untersucht, wobei der Schwerpunkt auf der funktionellen Regulation und der exosomvermittelten Signalübertragung lag. Vier Paare von CAFs und nicht-krebsassoziierten Fibroblasten (NCAFs) wurden nach radikaler Prostatektomie isoliert und umfassend charakterisiert. Die Exosomen wurden erfolgreich isoliert und mittels Nanopartikel-Tracking-Analyse, Transmissionselektronenmikroskopie und Western Blotting für kanonische Marker bestätigt, wodurch ihre Identität als Exosomen bestätigt wurde. Funktionelle Co-Kultur-Studien zeigten patientenspezifische, unterschiedliche Auswirkungen von Fibroblasten auf PCa-Zellen. CAFs erhöhten im Allgemeinen die Lebensfähigkeit und Motilität der Tumorzellen, während NCAFs einen stärkeren Einfluss auf die Förderung der Proliferation zeigten. Exosomenbehandlungen spiegelten diese Effekte teilweise wider und bestätigten, dass von Fibroblasten stammende Exosomen wichtige funktionelle Veränderungen in Tumorzellen induzieren können. Die Unterschiede zwischen den beiden untersuchten PCa-Zelllinien waren besonders deutlich. Die androgenabhängigen LNCaP-Zellen reagierten nur schwach auf die Signale der Fibroblasten und ihrer Exosomen und zeigten kaum Migrationsverhalten. Im Gegensatz dazu reagierten die androgenunabhängigen und aggressiven LNCaP C4-2 Zellen mit einer deutlichen Zunahme der Migration, wenn sie CAFs oder deren Exosomen ausgesetzt waren. Diese unterschiedliche Reaktion zeigt

deutlich, dass die Wirkung von aus Fibroblasten stammenden Exosomen auch vom biologischen Kontext der Tumorzellen abhängt und in fortgeschrittenen Stadien der Erkrankung zur Metastasierung beitragen kann.

Um die wechselseitige Signalübertragung weiter zu untersuchen, wurden aus PCa-Zellen stammende Exosomen mit Fibroblasten und hTERT-immortalisierte Vorhautfibroblasten ko-kultiviert. Während aus LNCaP C4-2 stammende Exosomen die Lebensfähigkeit der Fibroblasten erhöhten, konnten sie keine signifikante Aktivierung in den Fibroblasten der Patienten induzieren. Sie reduzierten unerwarteterweise die α-SMA-Expression in hTERT-Zellen, was auf variable Reaktionen der Fibroblasten auf tumorabgeleitete Signale hindeutet. Darüber hinaus ergab die globale microRNA-Profilierung von Fibroblasten und ihren Exosomen ein deutliches Expressionsmuster, das CAFs von NCAFs unterscheidet. Mehrere miRNAs, die mit krebsbezogenen Signalwegen assoziiert sind, waren in CAFs und ihren Exosomen angereichert, und Validierungsexperimente bestätigten ihre selektive Verpackung. Diese Ergebnisse unterstreichen die potenzielle Rolle von Fibroblasten-abgeleiteten exosomalen miRNAs bei der Modulation des PCa-Zellverhaltens und geben Aufschluss über ihren Beitrag zur Tumorprogression.

Insgesamt zeigt diese Arbeit, dass von Patienten stammende Fibroblasten und ihre Exosomen aktive Modulatoren der PCa-Biologie sind. Die Studie liefert neue Erkenntnisse über die molekulare und funktionelle Wechselwirkung zwischen Stroma- und Tumorzellen, identifiziert potenzielle Biomarker für die Krankheitsstratifizierung und unterstreicht die therapeutische Relevanz der gezielten Beeinflussung der Kommunikation zwischen Tumor und Stroma. Durch die Vertiefung unseres Verständnisses der Rolle von Fibroblasten-abgeleiteten Exosomen bei PCa eröffnen diese Ergebnisse neue Wege für die Entwicklung neuartiger Diagnosestrategien und personalisierterer Behandlungsansätze für fortgeschrittene Erkrankungen.

9 ACKNOWLEDGMENT

First and foremost, I would like to sincerely thank Prof. Dr. Med Kerstin Junker of the Department for Clinical-Experimental Research, Clinic for Urology and Pediatric Urology, Saarland University Hospital, for her invaluable counsel, recommendations, unwavering support, and involvement throughout the entire doctoral thesis process. I appreciate the effort and support from Dr. Hiresh Ayoubian in constantly guiding me through the miRNA experimentation and providing me with inputs concerning the microarray data of the prostate fibroblast cells and their exosomes, which helped me further progress my research.

I want to thank M.Sc Greta Jaschkowitz and M.Sc Sabrina Rau for constantly engaging me in scientific discussions, which helped me optimise various biological experiments. I would also like to thank all the technicians from the research group for supporting me in conducting experiments and procuring hands-on experience in the department.

Finally, I must express my profound gratitude to my parents for encouraging me to embark on this career track and to my spouse, Chetan Mallikarjunaiah Megalamane, for his unfailing support and constant encouragement throughout my years of doctoral research. This would not have been achievable without them.

10 INTRODUCTION

10.1 Epidemiology of Prostate Cancer

Based on the statistics from the World Health Organization, as of 2025, cancer is still the second most significant cause of death worldwide, accounting for nearly 10 million deaths in 2020 behind ischemic heart disease (Cancer WHO n.d.). As of 2022, prostate cancer (PCa) was the most frequently diagnosed cancer in men worldwide, representing 7.3% of all cancers (Bray et al. 2024).

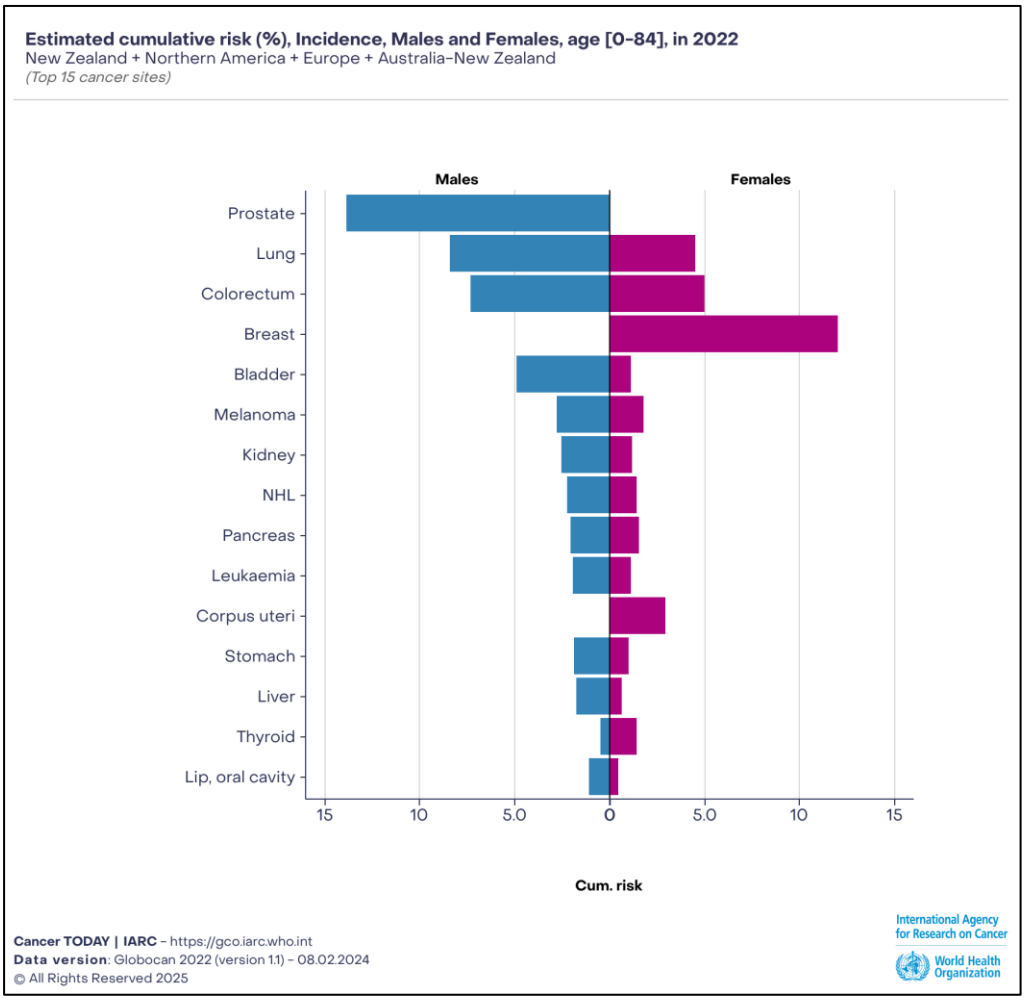

Figure 1: Incidence of Prostate Cancer in men among Western Countries. (Cancer WHO n.d.).

Total estimated risk (%) of cancer incidence in 2022 for both men and women (ages 0–84) in high-income areas (Europe, North America, Australia/New Zealand). Prostate cancer is the most frequent cancer in men, surpassing lung and colorectal cancers, whereas breast and colorectal cancers are more common in women. This emphasizes the gender-specific cancer burden, highlighting the importance of focused screening and prevention methods

Globally, the incidence of PCa has a positive correlation with both global domestic product (GDP) and human development index (HDI), indicating higher incidences in developed countries in comparison to developing nations (Wong et al. 2016). Remarkably, while prevalence is rapidly rising in Asian countries, some countries like Japan and Korea have lower prevalence than Western countries with similar HDIs (Kakehi et al. 2017)(Ito 2014). Australia and New Zealand in Oceania, North America and Europe, and South American countries like Brazil have the highest prevalence (Wong et al. 2016) (**Figure 1**). Southern and Central Asia, and sub-Saharan Africa, which encompass many of the world's low-income nations, have the lowest incidence of PCa but highest rates of annual increase in incidences currently (Chen et al. 2014). Increased screenings are linked to higher incidence through overdiagnosis as a result of greater awareness of PCa due to availability of diagnostic screening in many of these regions (Finne et al. 2010). Therefore, despite having a lower incidence rate globally, PCa is the most diagnosed cancer among men in Western countries, including Germany, which can be attributed to the widespread practice of Prostate-specific antigen (PSA) testing and biopsies (Ciatto et al. 2000). Although access to early diagnosis is expected to lower mortality rates, these regions have the highest age-standardized rates of prostate cancer mortality (Wong, et al. 2016) (Chen, et al. 2014). This can be potentially linked to PCa risk factors contributed by higher economic development, surpassing the advantages of the advanced public healthcare and treatment.

In 2019, 72,600 men developed PCa in Germany, which accounts for the most common type of cancer (26%) and the third leading cause of cancer related deaths (10%) in men excluding malignant neoplasms of the skin (Ciatto et al. 2000) (RKI 2020 n.d.). The risk factor for PCa increases with age and it is rarely diagnosed in men below 50. Therefore, the chances of someone below 35 years of age developing PCa in Germany in the next 10 years are less than 0.1% but that of a 75-year-old male is around 7% giving rise to the need for improvement in current therapies and diagnostics (RKI 2020 n.d.).

10.2 Prostate Cancer

The prostate is an acorn-shaped male exocrine gland located below the bladder and in front of the rectum, surrounding the urethra that produces essential components of seminal fluid for fertility and keeps the sperm viable (McNeal 1981) (**Figure 2**). The prostate undergoes several stages during organogenesis, such as canalization, cytodifferentiation,

branching morphogenesis, organ specification and epithelial budding (Francis and Swain 2018). These mechanisms are strictly regulated during development by male hormones androgens, epigenetics and other signaling pathways to regulate transcriptional programs to form a fully functional prostate gland (Francis and Swain 2018). According to Abate-Shen & Shen, the reactivation and dysregulation of many complex biological mechanisms, such as proliferation and migration, and genes crucial for organogenesis, could lead to cancer development (Abate-Shen and Shen 2000).

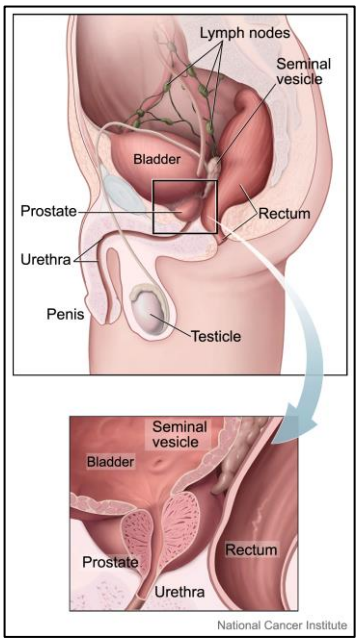

Figure 2: Schematic representation of the prostate gland anatomy. (Hoofring 2007)

Anatomical illustration of the male pelvic region highlighting the prostate gland. The prostate is located below the bladder, surrounding the urethra, and positioned in front of the rectum. The inset provides a magnified view showing the spatial relationship between the prostate, bladder, seminal vesicles and rectum: structures critical in PCa progression and diagnosis.

PCa is often referred to as a "silent" cancer since it usually progresses without any noticeable symptoms in early stages, making early diagnosis difficult and leading to diagnoses at a later and less curable stage. This is partially due to the slow growth of many prostate tumors as well as the limits of existing screening technologies such as the PSA test, digital rectal examination and biopsies, which can lead to overdiagnosis of indolent cases (Schröder et al. 2014)(Kohaar, Petrovics, and Srivastava 2019; US Preventive Services Task Force et al. 2018). Biopsy remains. the gold standard but is invasive. Although risk stratification has improved due to imaging and novel biomarkers, it is still challenging to differentiate between aggressive and non-aggressive disease (Bjurlin et al. 2013; Rebello et

al. 2021). Ablative radiotherapy, radical prostatectomy and active surveillance are available treatments for localized cancer; however, these might have serious side effects, such as sexual and urinary dysfunction, which can lower the quality of life (Bergman and Litwin 2012). Treatment options for advanced or metastatic PCa, including chemotherapy, androgen deprivation and new drugs (e.g., abiraterone, enzalutamide, PARP inhibitors), can prolong survival but are not curative and frequently lead to the development of resistance (Rebello, et al. 2021).

PCa is also complicated and heterogeneous, and because genetic and molecular knowledge is constantly changing, no one treatment is suitable for every patient (Rebello et al. 2021; Sekhoacha et al. 2022). There has been widespread innovative research in areas like liquid biopsy, nanotechnology and artificial intelligence which seem promising but further validation and integration into clinical practice is needed (Crocetto, et al. 2022). To improve prognostic and treatment outcomes, further research is needed to identify appropriate biomarkers, develop effective and less toxic medications, and generate more precise and less intrusive diagnostic tools (Sekhoacha, et al. 2022). Thus, continued research into prostate epigenetics, systemic mechanisms, cell-cell interactions within the tumor microenvironment (TME) and signaling pathways will help advance understanding of PCa; thereby opening newer diagnostics and therapies, ultimately increasing patients' survival and quality of life.

10.3 Molecular Biology and Pathophysiology of Prostate Cancer

PCa development involves a complex network of biological processes, including hormonal regulation, genetic predispositions and changes within the TME. Another process central to disease progression is the enhanced activity of the androgen receptor (AR) for both androgen-dependent and hormone-independent PCa. Androgens such as testosterone and dihydrotestosterone bind to the AR, a transcription factor in PCa that regulates several genes involved in cell proliferation, survival and differentiation. Upon binding, it promotes nuclear translocation, dimerization and subsequent binding to androgen response elements within AR target genes, such as PSA (Li et al. 2002). This process is essential for both normal prostate development and tumorigenesis. Various signaling pathways interact with AR to influence its activity. For instance, the mTOR pathway has been shown to modulate AR transcription, impacting cell proliferation and survival (Wang et al. 2008).

Additionally, the activation of nuclear factor-kappa B (NF-kB) promotes AR-driven survival pathways under androgen-deprivation conditions, a characteristic of castration-resistant PCa (CRPC) (Nadiminty et al. 2013). Another significant component of AR signaling is the interaction with the transcription factor c-myc, which enhances the expression of heterogeneous nuclear ribonucleoprotein A1 (HnRNPA1). HnRNPA1 plays an important role in the alternative splicing of AR mRNA, thereby producing splice variants that contribute to therapy resistance (Nadiminty et al. 2015; Tummala et al. 2017). C-myc can also antagonize AR activity, affecting the gene networks crucial for PCa progression (Barfeld et al. 2017; Qiu et al. 2022). This dual role of c-myc further highlights the complexity of AR signaling of PCa progression. Several other pathways, such as the mitogen-activated protein kinase (MAPK) activation, promote feedback loops that sustain AR-mediated gene expression and further promote survival of PCa cells in the absence of androgen (Lopez et al. 2016). The polycomb Repressive Complex 2 (PRC2) pathway enhances zeste homolog 2 (EZH2), which is associated with persistence of androgen-responsive programs in CRPC cells, contributing to the expression of active AR splice variants such as AR-V7 critical for tumor survival (Fong et al. 2017; Qu et al. 2015)

Elevated activity of AR plays a critical role in both early and more aggressive forms of PCa, with coactivators such as SRC-1 further enhancing the function of AR (Agoulnik et al. 2005). Even when tumors evolve to a hormone-refractory state and do not rely on androgens, they often retain AR expression. This enables the reactivation of tumor-survival-promoting pathways despite patients undergoing androgen deprivation therapy (Chen et al. 2005). These shifts in AR signaling are central to the development of treatment resistance. Dong et al. demonstrated that increased AR expression makes cancer cells sensitive to minimal androgen levels, further complicating the therapeutic landscapes (Dong et al. 2005). The growth, survival and dysregulation often observed in (CRPC) is also linked to AR signaling (Guo, Li, and Xin 2015). Moreover, Luo et al. also examined the link between AR and wingless-related integration site (Wnt) signaling, revealing that the activation of the Wnt/β-catenin pathway promotes growth in CRPC. This persistent activity of AR in CRPC signifies the need for strategies that inhibit AR directly or indirectly by disrupting the downstream pathways (Lopez et al. 2016)(Mohler et al. 2004).

AR splice variants are critical to developing resistance to androgen deprivation therapy, especially in CRPC. These splice variants, such as AR-V7, often lack ligand-binding domain and signals in a ligand-independent manner, sustaining AR activity (Yang et al. 2011). Studies have also indicated that elevated levels of full-length AR and its variants have been observed in various hormone-resistant tumors thereby contributing to persistence of AR signaling and cancer cell survival (Decker et al. 2012; Mostaghel et al. 2011). Guo et. al further demonstrated that AR splice variants can regulate distinct transcriptional programs that differ from those controlled by full-length AR, thereby complicating therapeutic strategies (Guo et al. 2009). Furthermore, the distinct splicing mechanisms that drive the production of these variants are important because alterations in splicing factors and genomic context can significantly influence the function of AR variants in TME (Seo et al. 2013).

In addition to the hormonal regulation, genetics significantly shape disease progression. Notably, BRCA mutations are associated with aggressive phenotypes and serve as a biomarker for treatment responses. Gallagher et al. found that BRCA-associated tumors retained sensitivity to taxane chemotherapy (Gallagher et al. 2012), while BRCA1 has been shown to enhance AR transactivation, revealing a complex interplay between genetic mutations and hormonal influence (Yeh et al. 2000). Beyond these factors, the TME also influences disease progression. A reactive stroma indicates disease severity and poor prognosis, suggesting a crosstalk between tumor and stroma. A particularly challenging adaptation is the neuroendocrine differentiation (NED), which often arises in response to AR-targeted therapy. Further, Weng et al. implicated that LYN, a SRC family tyrosine kinase, promoted cell migration and invasion in PCa, implicating another layer of molecular complexity (Weng et al. 2023). Recent studies have also highlighted the regulatory function of miRNAs in PCa. For example, Rao et al. showed that miR-512-3p upregulation enhances cell proliferation and cell cycle progression through G1 phase checkpoints (Rao et al. 2017). Natani et al. reported that miR-147b can induce NED by modulating the activity of ribosomal protein, leading to more aggressive and therapy-resistant phenotypes (Natani et al. 2023).

In summary, the molecular pathophysiology of PCa encompasses many factors, including androgenic dependency and signaling, genetic mutations, the relationship between AR and its splice variants, the influence of miRNAs and the dynamic response of the tumor

and its microenvironment. Therefore, a comprehensive understanding and integration of these molecular insights is pivotal in improving the clinical management of PCa.

10.4 Prostate Tumor Microenvironment

One of the well-known characteristic of PCa is its significant heterogeneity due to genomic, epigenetic and phenotypic aspects. This impacts the prognostic landscape and therapy possibilities, leading to varying clinical outcomes, highlighting the necessity for a better understanding of the PCa as a complex tumor disease including TME (Han et al. 2022; Shoag and Barbieri 2016). Firstly, their genetic variability makes the management of PCa more difficult. According to earlier research, PCa has significant intra-tumoral heterogeneity, with several tumor areas displaying unique genetic profiles. Multi-region sequencing studies have demonstrated that localized prostate tumors exhibit mutational variants and genomic instability, which are associated with patient outcomes like biochemical recurrence following surgery or radiation therapy (Boutros et al. 2015; Haffner et al. 2013; Rao et al. 2024). Furthermore, the multifocal tumor nodules, presents diagnostic problems since separate foci may have different histological and genetic fingerprints.(Yan et al. 2024; Zhao et al. 2022).

The TME is crucial to the development of PCa and regulates tumor progression by interacting between immune cells, endotheliala cells and stromal cells, including distinct subsets of cancer-associated fibroblasts (CAFs), non-cancer-associated fibroblasts (NCAFs) and the tumor cells themselves (Ding et al. 2025; Wu et al. 2022). CAFs are activated fibroblasts which are known to have an active role in reprogramming tumor behavior by promoting epithelial-mesenchymal transition (EMT), cytokines and extracellular matrix components (ECM) secretion, and stemness of cancer through paracrine signaling (Giannoni et al. 2010a). By changing the molecular properties of the ECM, CAF-derived products have been demonstrated to promote the migration and invasion of many types of cancer cells, generating a favorable condition for tumor development (Wang et al. 2024). Moreover, signaling pathways such as TGF-β pathway activation may further promote this pro-invasive phenotype by inducing a fibroproliferative response (Barcellos-de-Souza et al. 2016). In contrast to CAFs, NCAFs are relatively inactive but can be transformed into CAFs by factors secreted by cancer cells, illustrating the mutual interaction of the signaling of cancer and stromal cells in the TME (Barcellos-de-Souza et al. 2016).

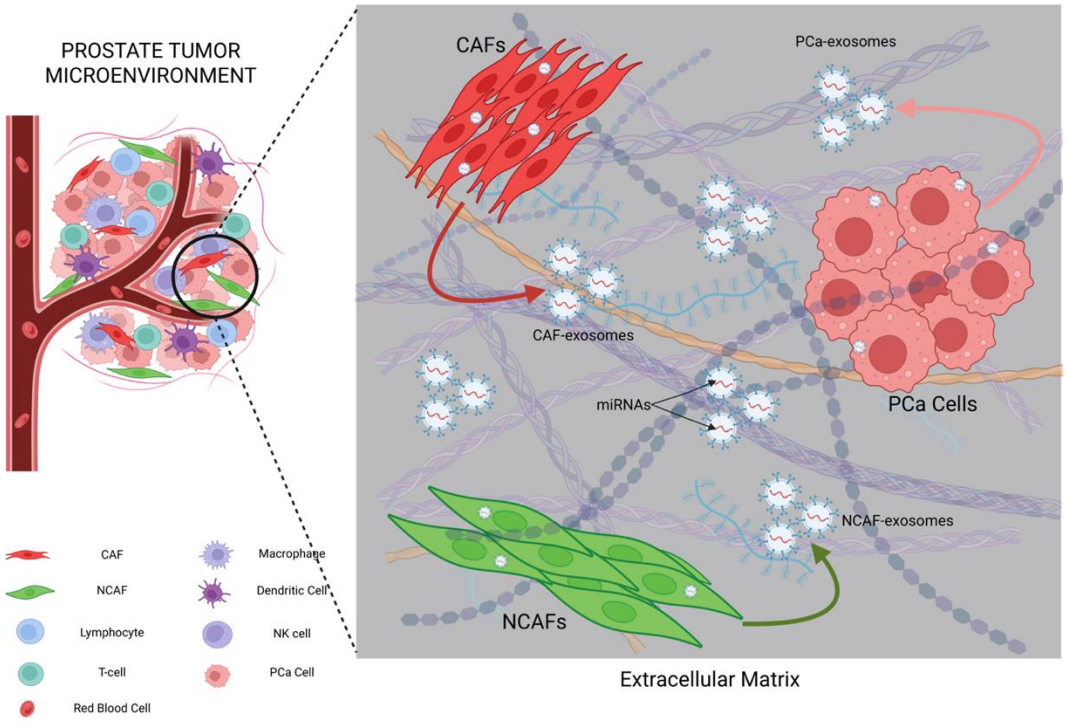

Figure 3: Schematic Representation of Prostate Tumor Microenvironment (Image created using (BioRender n.d.))

Illustrates the complex interactions between prostate cancer (PCa) cells, cancer-associated fibroblasts (CAFs) and non-cancer-associated fibroblasts (NCAFs). Both PCa cells and stromal cells (CAFs and NCAFs) release exosomes carrying molecular cargo, including microRNAs (miRNAs), which can be taken up by neighboring cells. This bidirectional exchange of exosomal contents facilitates tumor progression, remodeling of the extracellular matrix and the development of an aggressive prostate cancer phenotype.

Extracellular vesicles (EVs) secreted by PCa cells also represent a contributory factor to the TME heterogeneity, which can directly modulate the function of neighboring cells (**Figure 3**). EVs can reprogram the inflammatory response of NCAFs and immune cells to induce tumorigenesis and metastasis (Mezzasoma et al. 2019). A better comprehension of the multidimensional complexity in PCa, which arises from the interactions of the tumor cells with the CAFs, NCAFs and their EVs in the TME is essential to improve the management of Pca.

10.5 Extracellular Vesicles

EVs have gained significant attention in PCa research for their role in actively mediating tumor progression and as biomarkers. The guidelines from the International Society of Extracellular Vesicles (ISEV2018) classify EVs primarily based on their size and

biogenesis. Small EVs, often called exosomes, typically range from 50 nm to 150 nm, while larger EV populations, such as microvesicles, range between 100 – 1000 nm and apoptotic bodies (500 – 2000 nm) (Théry et al. 2018). Tumor-derived EVs are released into the TME and are circulated in biological fluids like blood and urine, carrying proteins, lipids, DNA and various species of RNA that closely represent the molecular profile of the cells from where they originate (Tang et al. 2025). Since they are easily accessible through minimally invasive routes, EVs are an excellent tool for use as a liquid biopsy for early detection, monitoring and stratification of CRPC. Therefore, understanding EV biogenesis, cargo specificity and functional impact may unlock new strategies for targeted intervention in PCa.

10.5.1 Biogenesis of Extracellular Vesicles

Apoptotic bodies originate during programmed cell death when the plasma membrane protrudes outwards and encapsulates the cellular fragments further cleared by phagocytosis, generally without participating in further intercellular signaling (Elmore 2007). In contrast, exosomes and microvesicle formation are tightly regulated processes involving distinct molecular mechanisms (Hurley 2015). Microvesicles arise through outward budding of the plasma membrane (Cocucci and Meldolesi 2015), whereas exosomes originate from the endosomal system (Gao et al. 2021). The exosomal biogenesis begins with an inward budding of the endosomal membrane that generates the intraluminal vesicles (ILVs) within the multivesicular bodies (MVBs). These MVBs fuse with the plasma membrane to release the ILVs into the extracellular space as exosomes. (Li et al. 2024; Lu et al. 2023) (see **Figure 4)**. Key proteins involved in the maturation and secretion of exosomes include the Rab family GTPases, particularly Rab27a and Rab31. Rab27a facilitates the docking of MVBs and Rab31 promotes the secretion of exosomes by facilitating ILV formation. (Wei et al. 2021; Zhang et al. 2022). SNARE proteins also facilitate the release of ILVs into the extracellular space as exosomes by fusion of MVBs with the plasma membrane (Hong 2005).

The biogenesis of exosomes can occur via ECSRT-dependent and ESCRT-independent mechanisms. The selection of cargo and ILVs formation is frequently mediated by endosomal sorting complex required for transport (ESCRT) machinery (Datta et al. 2018). ESCRT-0 binds to ubiquitinated transmembrane protein and recruits ECSRT-I via its adaptor protein TSG10 (Baietti et al. 2012). ESCRT-I activation leads to the recruitment of

ESCRT-II, which contains ALG-2-interacting protein X (ALIX) and together these initiate ESCRT-III assembly. ESCRT-III recruits deubiquitylating enzymes (DUBs) and removes ubiquitin from the cargo proteins facilitating their incorporation into the ILVs. Once the ILVs are formed, the ESCRT complexes are disassembled by the ATPase Vps4, allowing the recycling of components. (Hurley 2015). In case of ESCRT-independent mechanism, the lipid raft microdomains enriched in ceramides and tetraspanins such as CD9, CD63 and CD81, as well as proteins like syntenin are regulated by SHP2 phosphatase (Zhang et al. 2021). Recent research also shows that lipid droplets may be involved in the biogenesis of small EVs, suggesting metabolic intersections that influence their production (Genard et al. 2022).

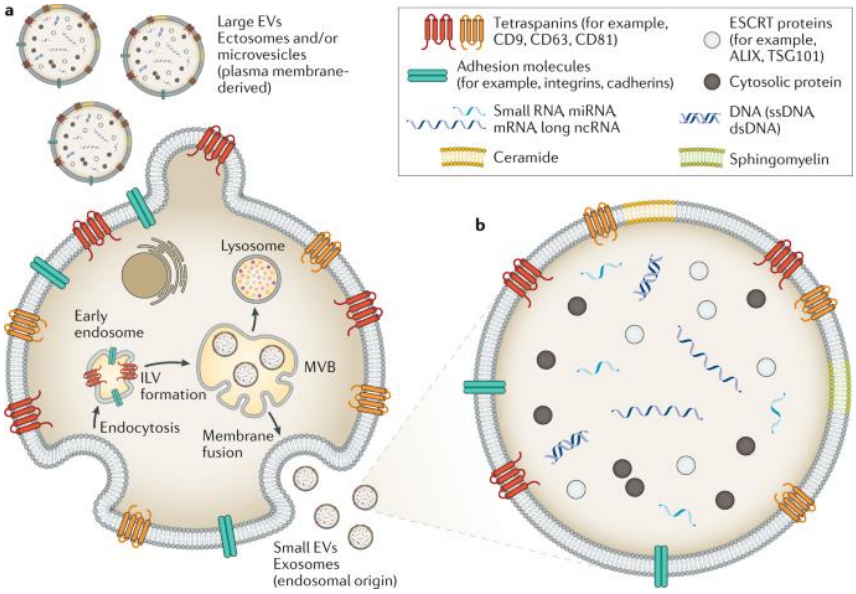

Figure 4: Biogenesis and classification of extracellular vesicles (EVs) (Linxweiler and Junker 2020)

(a) EVs are classified into larger ectosomes or microvesicles, derived from the plasma membrane and small EVs (exosomes) originating from the endosomal system. Exosomes form from the early endosomal membrane's inward budding, leading to the generation of intraluminal vesicles (ILVs) within the multivesicular bodies (MVBs). Fusion of the MVBs with the plasma membrane releases the ILVs into the extracellular space as exosomes. (b) Exosomes are carriers of cargo made up of biomolecules, including tetraspanins, adhesion molecules, ESCRT proteins, ceramides, sphingomyelin, cytosolic proteins, nucleic acids and DNA, which reflect their cellular origin and functional roles in intercellular communication.

Drawing on the review by Linxweiler et al. on urological cancers reveals a broader significance of EVs, where they emphasize that EVs enriched in various biomolecules are active players in the tumor progression, metastasis and drug resistance in PCa. (Linxweiler and Junker 2020)

10.5.2 Exosomes in Prostate Tumor Microenvironment

Intercellular communication depends on EVs, membrane-enclosed particles released into the extracellular space by all cell types. They are crucial in transporting various molecular components, including proteins, lipids and microRNAs (miRNAs), and substantially affect cellular activity in numerous circumstances, notably in cancer biology (Valadi et al. 2007). In recent times, the function of EVs in cancer biology has garnered much attention, especially concerning the development of cancers like PCa.

Exosomes, one of the subsets of EVs, also described as small vesicles, originate from the endosomal system, specifically from MVBs (O'Brien et al. 2020; Witwer and Théry 2019). They are known to mediate the intricate interactions that occur between CAFs, NCAFs and PCa cells themselves (Zheng et al. 2018). Empirical evidence suggests that EVs originating from PCa cells can modulate CAF activity, leading to modifications in the TME that promote cancer cell proliferation and dissemination (Dorai et al., 2018). Additionally, exosomes help PCa cells to evade the immune surveillance by reducing the capacity of the immune system to identify and eradicate cancerous cells, thereby inhibiting T cell activity and downregulating immune checkpoints (Lundholm et al. 2014). This immune modulation makes treating advanced PCa extremely difficult, suggesting new therapeutic approaches may be possible by focusing on exosomal pathways. CAFs and tumor cells interact in a complex way, and as the tumor grows, the balance of signals sent and received by exosomes may change, which could also change the immune environment surrounding the tumor (Wu et al. 2020; Zheng et al. 2018).

Wu et al claim that exosomal communication through exchange of miRNAs can orchestrate a favorable niche for PCa cells to thrive in harsh environments (**Figure 3**). This exchange can further regulate the genome by affecting the expression of genes related to drug resistance, proliferation, metastasis and apoptosis (Wu et al. 2020). Furthermore, exosomes have been found to contain genetic signatures and tumor-associated proteins that are essential biomarkers linked to PCa for diagnosis and follow-up (Li et al. 2017). For instance, exosomes from patients with PCa have been found to contain proteins such as ephrinA2 and PSA, which have often been used as biomarkers for the identification and evaluation of cancer progression (Li et al. 2018).To sum up, EVs, particularly exosomes, have a complex role in the dynamics of PCa progression, influencing tumor growth, immunological evasion and treatment responses significantly impacting CAFs and tumor

cells. Therefore, it is important to thoroughly understand exosomal functions as they may reveal clues and further improve research and clinical outcomes.

10.5.3 Exosomes in Prostate Cancer Metastasis

Beyond their direct interactions with tumor cells, exosomes have systemic effects that prime distant sites for metastasis. Exosomes from tumors have been shown in recent research to alter distant organs, such as bone and lymph nodes, to make them more susceptible to metastatic colonization. For instance, exosomes can promote vascularization and remodel the ECM in target organs, which can start the development of a pre-metastatic niche (Nogués et al. 2018). Preconditioning can promote tumor cell adhesion and extravasation, two crucial stages in the metastatic process. In particular, exosomes may promote lymphangiogenesis, or the development of new lymphatic vessels, which is essential for tumor cell dissemination through lymphatic channels (Nogués et al. 2018). Exosomes' delivery of pro-lymphangiogenic factors enables cancer cells that have spread to use the lymphatic system for metastasis, making disease management and treatment results even more challenging. Furthermore, target organ endothelium and circulating tumor cells (CTCs) can interact thanks to particular integrins and growth factors on exosomes, facilitating CTC extravasation and seeding (Zhang and Yu 2019; Liu et al. 2021).

Exosomes not only aid in metastases but also contribute to immune evasion. Exosomal cargo can be used by tumors to alter immune cell responses, suppressing cytotoxic immune responses that would normally target metastatic cells. For example, it has been demonstrated that immunosuppressive molecules found in tumor-derived exosomes prevent the activation of natural killer (NK) cells and cause the polarization of regulatory T cells (Ramteke et al. 2015). This immune evasion strategy is particularly pertinent in metastasis because it enables cancer cells to live and multiply in distant organs. Additionally, hypoxic conditions commonly found in tumors can also influence exosome composition and promote metastatic activity via hypoxic stress-secreted exosomes, thereby increasing invasiveness and stemness of PCa cells and facilitating their metastatic progression (Ramteke et al. 2015). Exosomal proteins, including metalloproteinases (MMPs), can degrade many ECM proteins, allowing tumor cells to migrate through the matrix barriers that typically prevent this movement (Zhang and Yu 2019). This remodeling not only helps the primary tumor, but it also helps establish secondary tumors in distant locations.

According to current research, the kind and setting of exosomal cargo can significantly impact how likely it is to spread. As per Nogués et al., cancer cells can transform nearby or distant cell types that support cancer proliferation while selectively packaging miRNAs or proteins that enhance their invasive characteristics (Nogués et al. 2018). Overall, exosomes play a complex role in the metastasis of PCa through several mechanisms that go beyond interactions in the TME. These vesicles stimulate the formation of pre-metastatic niches, drive ECM remodeling, create an immunosuppressive environment, and facilitate communication between tumor cells and distant organs. The growing knowledge of the various functions of exosomes in metastasis highlights the possibility that they could be important targets for therapeutic intervention in PCa and other cancers.

10.5.4 Role of Exosomal miRNAs in Prostate Cancer

Given the intricacy of intercellular communication within the TME, exosomal miRNAs have been identified as critical elements in the development and metastasis of PCa (Zhang and Yu 2019). These small, non-coding RNA molecules contained in exosomes, have a significant regulatory impact on recipient cells' gene expression, supporting numerous carcinogenic processes. MiRNAs are in general extremely dependable biomarkers and modulators of tumor biology because of their exceptional stability due to their short size and also within exosomes, because of their lipid bilayer defending against RNases (Melo et al. 2014; Salehi and Sharifi 2018). Exosomal miRNAs are believed to promote angiogenesis, enable replicative immortality, and evade growth suppressors in PCa, all of which are important characteristics of cancer (Zhang and Yu 2019). PCa cells' exosomes frequently contain high concentrations of miRNAs, such as miR-21 and miR-375, which have been linked to promoting carcinogenic pathways (Huang et al. 2015; Melo et al. 2014). MiR-21 has the potential to be both a biomarker and a therapeutic target, as evidenced by its strong correlation with tumor progression, poor prognosis, and treatment resistance (Melo et al. 2014). Circulating exosome analysis has shown that these miRNAs can affect recipient tumor cell behavior, supporting processes such as EMT, which is crucial for metastases (Huang et al. 2015).

Additionally, by transfering immunomodulatory miRNAs, tumor-derived exosomes have been demonstrated to suppress anti-tumor T-cell responses, thereby inducing immune

tolerance (Fabbri et al. 2012). Moreover, exosomes derived from PCa can carry miRNA cargo that changes their phenotype and accelerates the growth of tumors in the surrounding stroma, especially CAFs. MiR-21, for instance, has been demonstrated to alter fibroblast behavior, creating a pro-tumorigenic environment that facilitates the migration and proliferation of cancer cells (Melo et al. 2014; Salehi and Sharifi 2018). Another study by Zhou et al. showed that miR-105 enhances vascular permeability via endothelial disruption, thereby promoting tumor metastases (Zhou et al. 2014). Considering the pathways that exosomal miRNAs activate during metastasis is equally compelling. In 2014, Singh et al. showed that exosomal transfer of miR-10b enhances the migratory and invasion capability of metastatic cells through targeted regulation of specific genes (Singh et al. 2014). PCa is thought to function through similar mechanisms to breast cancer, opening a potential for therapeutically targeting particular exosomal miRNAs to lessen migratory and invasive behavior.

Furthermore, exosomal miRNA profiles, for example, have been found to correlate with the severity of PCa, offering potential prognostic indicators and early diagnostic tools (Huang et al. 2015). These miRNAs are good candidates for non-invasive liquid biopsy techniques because of their exceptional stability and persistent presence in biological fluids. Although the role of exosomal miRNAs in PCa displays potential for therapeutic targets and diagnostics, standardization of isolation procedures, quantification techniques and validation of results across various populations continues to be difficult (Salehi and Sharifi 2018). To turn these discoveries into practical clinical applications, future studies that clarify the precise pathways and mechanisms these miRNAs alter in the context of PCa are essential.

11 HYPOTHESIS AND AIM OF THE STUDY

Many recent studies have increasingly focused on the tumor stroma, which surrounds the tumor cells and constitutes the so-called TME (Quail and Joyce 2013). In particular, CAFs and the small vesicles they release (exosomes) are known as part of the tumor-promoting mechanisms (Luo et al. 2013). CAFs differ from normal fibroblasts in their gene expression (Webber et al. 2016). A study by Josson and colleagues showed that CAFs and NCAFs also differ in their miRNA expression (Josson et al. 2015). These miRNAs, as well as mRNAs and other non-coding RNAs (ncRNAs), are packaged into exosomes (Sato-Kuwabara et al. 2015), which are then taken up by neighboring cells or distant cells and can subsequently modulate the recipient cells. This biological regulatory mechanism plays an important role in tumor growth and metastasis and has been identified as a potential biomarker for various cancers, including PCa (Junker et al. 2016).

Based on these findings, our group previously investigated the effects of primary patient-derived prostate fibroblasts (CAFs, NCAFs and benign prostatic hyperplasia-associated fibroblasts (BPHFs)) on tumor progression in an orthotopic xenograft model (Linxweiler et al. 2020). In this study, we characterized the primary fibroblasts by immunofluorescence staining. While all fibroblasts were positive for vimentin and negative for pan-CK, only CAFs showed positive staining for α-SMA as a marker of fibroblast activation. Orthotopic co-injection of fibroblasts and tumor cells showed different effects in LuCaP136 and LNCaP cells. When LuCaP136 was co-injected with CAFs, a larger tumor volume was measured compared to NCAFs and BPHFs. In LNCaP xenografts, however, all fibroblasts, i.e., CAFs, NCAFs and BPHFs, resulted in a larger tumor volume compared to the co-injection of LNCaPs alone.

Based on the above results, we are now interested in investigating the effect of the same four patient-derived CAF and NCAF pairs and their exosomes used in the in vivo studies on functional aspects of prostate tumor cells in vitro and vice versa. Therefore, the aim of the present work is divided into three main objectives.

1. Studying the influence of patient-derived CAF and NCAF pairs on the viability, proliferation and migration of two PCa cell lines, LNCaP and LNCaP C4-2.

2. Characterization of exosomes from prostate fibroblasts and studying their effect on PCa.
3. Studying the miRNA expression patterns of the prostate fibroblasts for a potential epigenetic role of the prostate fibroblasts and their exosomes.
4. Characterization of exosomes from PCa cell lines and studying their effect on the prostate fibroblasts and hTERT foreskin fibroblasts.

Many studies have investigated the effects of exosomes secreted by PCa cells on the tumor stroma. However, to date, no studies have addressed the role of exosomes from CAFs in the development, progression and metastasis of PCa. The work presented here aims to characterize fibroblasts and their exosomes and to investigate their role in important tumor-associated processes such as viability, proliferation and migration of PCa cells. In addition, the specific miRNA spectrum of CAFs will be investigated in comparison to NCAFs and their exosomes. These findings should contribute to a better understanding of the complexity of tumor development and progression and lead to the development of new diagnostic and therapeutic approaches.

12 MATERIALS

12.1 Patient Samples

CAFs and NCAFs were derived from patient tissues after radical prostatectomy at our department prior to starting of the project. These cells were stored in liquid nitrogen (LN_2) until further use. Written informed consent was obtained from all patients.

12.2 Cell lines

The in-vitro experiments were performed using four different patient-derived fibroblast pairs (CAFs and NCAFs), two immortalized prostate epithelial cell lines (LNCaP [ATCC-CRL-1740] and LNCaP C4-2 [ATCC-CRL-3314]), and hTERT-immortalized foreskin fibroblasts (hTERT).

Table 1. Cell lines used

Cell lines	Name in Databank	Patient Data	Origin	Cell type	Cell details
NCAF1/ CAF1	PNF27/ PTF52	• Male • 48 years	• Human PCa • Gleason Score: 7a	Fibroblasts	Primary Cells
NCAF2/ CAF2	PNF13/ PTF14	• Male • 65 years	• Human PCa • Gleason Score: 7a	Fibroblasts	Primary Cells
NCAF3/ CAF3	PNF26/ PTF51	• Male • 52 years	• Human PCa • Gleason Score: 9	Fibroblasts	Primary Cells
NCAF4/ CAF4	PNF55/ PTF75	• Male • 62 years	• Human PCa • Gleason Score: 7b	Fibroblasts	Primary Cells
hTERT	hTERT	• Male • neonate	Human Foreskin cell lines derived from BJ cell line	Fibroblasts	Immortalized Cells
LNCaP	LNCaP	• Male • 50 years	Human PCa cell lines from metastasis of left supraclavicular lymph node	Epithelial cells	• Immortalized Cells • Androgen-dependent
LNCaP C4-2	LNCaP C4-2	• Male • 50 years	Human PCa LNCaP cell subcutaneous xenograft tumor of castrated mouse	Epithelial like cells	• Immortalized Cell lines • Androgen-independent

12.3 Medium, reagents, and chemicals

Table 2. List of medium, reagents, chemicals and enzymes used	
Medium/Reagents/Chemicals/ Enzymes	**Manufacturer**
Aphidicolin	Sigma-Aldrich Corporation, USA
Bromophenol Blue	Serva Electrophoresis GmbH, Germany
BSA	Serva Electrophoresis GmbH, Germany
CHAPS	Sigma-Aldrich Corporation, USA
Disinfection Incidin Plus	Ecolab Inc, USA
DMEM, 4.5 g Glucose	Gibco Life Technologies, USA
DMSO	Sigma-Aldrich Corporation, USA
DPBS	Sigma-Aldrich Corporation, USA
DTT	Serva Electrophoresis GmbH, Germany
FCS	Sigma-Aldrich Corporation, USA
Glutaraldehyde	Merck KgaA, Germany
Glycine	Sigma-Aldrich Corporation, USA
H_2SO_4	Bernd Kraft GmbH, Germany
Laemmli Buffer	Serva Electrophoresis GmbH, Germany
Methanol (100%)	Merck KgaA, Germany
Milk Powder	Serva Electrophoresis GmbH, Germany
NaCl	Sigma-Aldrich Corporation, USA
PFA	Sigma-Aldrich Corporation, USA
PI Mix	Serva Electrophoresis GmbH, Germany
Qiazol lysis solution	Qiagen N.V., Netherlands
RiboLock RNase Inhibitor	Thermo Fischer Scientific Inc, USA
RNase One Ribonuclease	Promega GmbH, Germany
RNAseZap	Sigma-Aldrich Corporation, USA
RPMI, 2 g Glucose	Gibco Life Technologies, USA
Premixed Electrophoresis Running Buffer (10x)	Bio- Rad Laboratories GmbH, Germany
Triple Color Protein Standard II	Serva Electrophoresis GmbH, Germany
Tris Buffer	Serva Electrophoresis GmbH, Germany
Triton X-100	Sigma-Aldrich Corporation, USA
Trypan Blue Solution	Sigma-Aldrich Corporation, USA
Trypsin-EDTA Solution	Sigma-Aldrich Corporation, USA
Tween 20	Sigma-Aldrich Corporation, USA
Uranyl acetate	Merck KgaA, Germany
Wash Buffer 1 and 2	Agilent Technologies, Germany

12.4 Antibodies and Primers

Table 3. List of Antibodies and Primers used	
Antibodies	**Manufacturer**
α-SMA	Cell Signaling Technology Europe B.V, Netherlands
Alix	New England Biolabs GmbH, Germany
Calreticulin	Cell Signaling Technology Europe B.V, Netherlands
CD9	Cell Signaling Technology Europe B.V, Netherlands
CD63	Abcam plc, UK
CD81	Abcam plc, UK
CD147	Abcam plc, UK
EpCAM	Cell Signaling Technology Europe B.V, Netherlands
GAPDH	Cell Signaling Technology Europe B.V, Netherlands
GM130	Cell Signaling Technology Europe B.V, Netherlands
PSMA	Abcam plc, UK
Primers	**Manufacturer**
miR-10b-5p	Thermo Fischer Scientific Inc, USA
miR-148b-3p	Thermo Fischer Scientific Inc, USA
miR-191-5p	Thermo Fischer Scientific Inc, USA
miR-210-3p	Thermo Fischer Scientific Inc, USA
miR-223-3p	Thermo Fischer Scientific Inc, USA
miR-361-5p	Thermo Fischer Scientific Inc, USA
RNU48	Thermo Fischer Scientific Inc, USA

12.5 Kits

Table 4. List of kits used	
Kit	**Manufacturer**
BrdU colorimetric proliferation assay kit	Roche Diagnostics Deutschland GmbH, Germany
miRNA Complete Labeling and Hyb Kit	Agilent Technologies, Germany
miRNA Spike-In Kit	Agilent Technologies, Germany
Pierce™ BCA Protein Assay Kit	Thermo Fischer Scientific Inc, USA
Pierce™ ECL substrates for high-sensitivity western blot detection	Thermo Fischer Scientific Inc, USA
RNAeasy Mini Kit	Qiagen N.V., Netherlands
TaqMan microRNA RT Kit	Thermo Fischer Scientific Inc, USA
WST-1 Assay Kit	Roche Diagnostics Deutschland GmbH, Germany

12.6 Buffers and Solutions

Table 5. List of Buffers and Solutions		
Buffers/Solutions	**Reagents**	**Concentration/Volume**
BSA Blocking Solution	BSA	5% (m/v)
	TBS-Tween	1x
Lysis Buffer	Tris	50 mM
pH = 7.6	NaCl	150 mM
	Triton X-100	1 % (v/v)
	CHAPS	1 % (v/v)
	SDS	0.1 % (v/v)
	Protease-Inhibitor (PI) Mix	1x
Milk Blocking Solution	Milk Powder	5% (m/v)
	TBS-Tween	1x
Premixed Electrophoresis Running	Tris	25 mM
Buffer (10x)	Glycine	192 mM
	SDS	0.1%
Sample Buffer (6x) (reduced)	Tris	0.5 M
pH =6.8	Glycine	30% (v/v)
	SDS	10% (m/v)
	Dithiotriol (DTT)	600 mM
	Bromophenol Blue	One spatula tip
Sample Buffer (6x) (unreduced)	Tris	0.5 M
pH =6.8	Glycine	30% (v/v)
	SDS	10% (m/v)
	Bromophenol Blue	One spatula tip
TBS-Tween (10x)	Tris	248 mM
pH = 7.6	NaCl	1.37 M
	Tween 20	1% (v/v)
Transfer Buffer (10x)	Tris	48 mM
	Glycine	39 mM
	Methanol	15% (v/v)
	SDS	0.01% (m/v)

12.7 Consumables

Table 6. List of consumables used

Consumable	Format	Manufacturer
BioTrace PVDF Membrane	0.45 µm	PALL GmbH, Germany
Cell counting slides	-	Logos Biosystems, Aligned Genetics Inc, South Korea
Cell culture flasks	25; 75; 175 cm^2	Corning Incorporated, USA
Cell culture plates	6; 24; 96 wells	Corning Incorporated, USA
Cell culture triple flasks	300 cm^2	• Corning Incorporated, USA • Thermo Fischer Scientific Inc, USA
Centrifuge tubes; conical bottom	15; 50 ml	Sarstedt AG & Co., Germany
Centrifuge tubes; round bottom	15 ml	Sarstedt AG & Co., Germany
CIM plates	8 µm pore size	Agilent Technologies, Germany
Cryotubes	2 ml	Greiner Bio-One International GmbH, Austria
Culture Tubes	15 ml	Thermo Fischer Scientific Inc, USA
DNA/RNA low-bind reaction tubes	0.5; 1.5; 2; 5 ml	Eppendorf SE, Germany
Mini-Protean® TGX Stain-free™ Precast Protein Gels	10%; 12 wells; 20 µl V	Bio- Rad Laboratories GmbH, Germany
Mechanical Pipettes	-	Eppendorf SE, Germany
Pasteur Pipettes, Borosilicate Glass	-	Carl Roth GmbH +Co. KG, Germany
Pipette Tips	-	Eppendorf SE, Germany
Reaction Tubes	0.5; 1; 2; 5 ml	Eppendorf SE, Germany
Serological Pipettes	1; 2; 5; 10; 25 ml	Sarstedt AG & Co., Germany
Serological Pipette Gun	-	Eppendorf SE, Germany
Stericup Quick Release Vaccum Filtration System	0.22 µm pore	Sigma-Aldrich Corporation, USA
Transwell inserts	24-well; 0.4 µm 6-well; 0.4 µm	Corning Incorporated, USA
Transwell inserts FluoroBlok	24 well; 8 µm	Corning Incorporated, USA
Ultracentrifugation Tubes, reusable	25 ml	Beckman Coulter Inc, USA
Whatman® paper	-	Serva Electrophoresis GmbH, Germany

12.8 Devices

Table 7. List of devices used

Device	Manufacturer
Axiovert S100 Light Microscope	Carl Zeiss Microscopy GmbH, Germany
Biometra Uno II thermocycler	Analytik Jena, Germany
Centrifuge 5804 R	Eppendorf SE, Germany
Chemostar ECL & Fluorescence Imager	Intas Science Imaging Instruments GmbH, Germany
DNA Microarray Scanner G2565BA	Agilent Technologies, Germany
Electrophoresis Chamber	Bio- Rad Laboratories GmbH, Germany
FEI Tecnai 13 Transmission Electron Microscope	FEI Company, Thermo Fischer Scientific Inc, USA
Heatblock	Eppendorf SE, Germany
Incubator	Thermo Fischer Scientific Inc, USA
Infinite F200 pro microplate reader	Tecan Group Ltd., Switzerland
LightCycler 480 II	Roche Diagnostics Deutschland GmbH, Germany
LUNA-II Automated Cell Counter	Logos Biosystems, Aligned Genetics Inc, South Korea
NanoDrop ND-1000	PeqLab Biotechnology GmbH
NanoSight LM10	Malvern Panalytica, UK
Optima XPN-100 Ultracentrifuge with type 40 Ti rotor	Beckman Coulter Inc, USA
Shaker	Bio-Rad Laboratories GmbH, Germany
Trans-Blot SD Semidry Transfer Chamber	Bio-Rad Laboratories GmbH, Germany
Vacuum Centrifuge	Martin Christ Gefriertrocknungsanlagen GmbH, Germany
xCELLIGENCE RTCA DP System	Agilent Technologies, Germany

12.9 Softwares

Table 8. List of software used	
Software Name	**Manufacturer**
BioRender Illustration Maker	BioRender, Canada
Feature Extraction	Agilent Technologies, Germany
GraphPad Prism software	GraphPad Software, LLC, USA
ImageJ	Wayne Rasband, 1987, USA
INTAS Image Analyzer	Intas Science Imaging Instruments GmbH, Germany
LightCycler 480 II software	Roche Diagnostics Deutschland GmbH, Germany
NTA 3.2	Malvern Panalytica, UK
RTCA Software	Agilent Technologies, Germany
TEM Software	FEI Company, Thermo Fischer Scientific Inc, USA
Qlucore Omics Explorer 3.2	Qlucore Bioinformatics, Sweden

13 METHODS

13.1 Cell Culture

13.1.1 Preservation and Storage of Cells

The cells grown in respective cell culture flasks [Corning Incorporated, USA] were detached and then cryopreserved. The detachment of cells was achieved by aspirating the respective cell culture medium and washing the cells with Dulbecco´s Phosphate Buffered Saline (DPBS) buffer [Sigma-Aldrich Corporation, USA]. Then, depending on size of the cell culture flasks, different volumes of trypsin-EDTA (25 cm^2 = 1 ml; 75 cm^2 = 2 ml; 175 cm^2 = 5 ml; 500 cm^2 = 20 ml) [Sigma-Aldrich Corporation, USA] were added and incubated in the incubator [Thermo Fischer Scientific Inc, USA] at 37°C and 5% (v/v) CO_2 for 4 - 5 min (PCa cell lines) and 9 - 10 min (fibroblasts). The detachment was confirmed by viewing under an Axiovert S100 light microscope [Carl Zeiss Microscopy GmbH, Germany]. The detached and separated cells were transferred to a round-bottom culture tube [Sarstedt AG & Co., Germany] and centrifuged in a 5804 R centrifuge [Eppendorf SE, Germany] at 1100 rpm for 3 min. The supernatant was then discarded and the cells were resuspended in a mixture of 10% dimethyl sulfoxide (DMSO) [Sigma-Aldrich Corporation, USA] and 30% fetal calf serum (FCS) [Sigma-Aldrich Corporation, USA] containing Dulbecco´s Modified Eagle Medium (DMEM) (V = 2 ml) [Gibco Life Technologies, USA]. This suspension was pipetted into a 2 ml cryotube [Greiner Bio-One International GmbH, Austria] and immediately frozen at -80°C or LN_2 at -196°C for long-term storage.

13.1.2 Thawing and Culturing of Cells

To culture the cells, they were taken out from the biobank and thawed quickly in a controlled manner by resuspending the frozen cells in 2 ml of cell line-specific medium containing 10% FCS. The cell suspension was transferred to a round-bottom culture tube and centrifuged at 1100 rpm for 3 min. The DMSO-containing supernatant was discarded entirely, and the cell pellet was resuspended in the desired volume of respective complete medium and transferred to a new 25 cm^2 or 75 cm^2 cell culture flask and cultivated in the incubator at 37 °C and 5% (v/v) CO_2. CAFs, NCAFs and hTERT cell lines were cultivated

in DMEM medium, and LNCaP and LNCaP C4-2 cell lines in Roswell Park Memorial Institute-1640-Medium (RPMI) [Gibco Life Technologies, USA]. The next day, a media change was performed. In the following days, the medium was changed every two to three days, depending on the speed of cell division and metabolism.

13.1.3 Subcultivation

Subculturing of used CAFs, NCAFs and hTERT cells occurred at 90 - 100% confluence of the culture flask (1:4 - 1:6 dilution). For PCa cell lines, subculturing was performed at 85 - 90% confluence of the culture flask (1:15 - 1:20 dilution) to synchronize the exponential growth phase with the fibroblasts to further perform cell-based assays. Detachment of cells was achieved as described in the section **13.1.1**. The enzyme reaction was inhibited by adding the respective FCS-containing medium according to the required dilution (25 cm^2 = 4 ml; 75 cm^2 = 8 ml; 175 cm^2 = 15 ml; 500 cm^2 = 30 ml). The rescued cells were centrifuged at 1100 rpm for 3 min. After centrifugation, the supernatant was discarded, and cell pellets were resuspended in the desired volume of respective complete medium (with 10% FCS) and transferred to a new cell culture flask and cultured further in the incubator at 37°C and 5% (v/v) CO_2.

13.1.4 Cell Counting and Seeding

For in-vitro studies, a specific number of cells was required for seeding. For this, the cells were detached, centrifuged, and resuspended as described in section **13.1.3**. After resuspension, 10 µl of the cell suspension was mixed with 10 µl of trypan blue solution [Sigma-Aldrich Corporation, USA] (1:1 dilution). 10 µl from the above mixture was added to a cell counting slide [Logos Biosystems, Aligned Genetics Inc, South Korea] and counted. The volume of cell suspension required to seed specific cell numbers was determined using the automated cell counter LUNA II [Logos Biosystems, Aligned Genetics Inc, South Korea].

13.1.5 Cell Lysis

For biochemical analysis of protein expression in cells, the cells had to be pelleted, the cell membrane degraded and lysed. For this, the cells were cultivated, detached, and

centrifuged as described in section **13.1.3**. After centrifugation, the cell pellet was incubated in 2 ml lysis buffer (see **Table 5**) for 30 min on ice. Further, the lysed cell suspension was centrifuged at 20,000 g for 5 min at 4°C. The supernatant or clear lysates were then transferred to new reaction tubes [Eppendorf SE, Germany] and stored at -80°C until further use.

13.2 Isolation of Exosomes

13.2.1 Production of Exosome-free Medium

The experiments used complete medium and cell-specific medium with 10% exosome-deficient FCS (ED-FCS). In addition to growth factors, hormones and nutrients, FCS also contains exosomes. These exosomes can induce a shift in the results; therefore, they must be removed. The regular FCS was therefore centrifuged at 200,000 g for at least 18 hours at 4°C in an Optima XPN-100 ultracentrifuge with a type 40 Ti rotor [Beckman Coulter Inc, USA] to produce ED-FCS. The supernatant was sterile filtered using a 0.22 µm filter Stericup [Sigma-Aldrich Corporation, USA] and aliquoted and stored at -20°C until further use.

13.2.2 Isolation of Exosomes from Cell Culture

Before the isolation of exosomes, the cells were cultivated in 300 cm^2 cell culture flasks under 80 ml per flask of respective complete media to obtain enough exosomes. When the cells reached a confluence of 40 – 50 % for PCa cell lines and 70 - 80% for fibroblasts, the medium was aspirated, and the cells were washed 3x with 20 ml DPBS for each flask. The medium was then switched to the respective 10% ED-FCS-containing medium and incubated for 72 hours at 37°C and 5% CO_2. After incubation, the conditioned medium (CM) rich in exosomes, was collected in 50 ml centrifuge tubes [Sarstedt AG & Co., Germany]. The CM also contains other components such as cells and cell debris, apoptotic bodies and larger EVs, which must be removed before exosomes are isolated. Therefore, the CM was first differentially centrifuged at 2,000 g for 20 min at 4°C. The supernatant was transferred to new 50 ml centrifuge tubes and centrifuged at 15,000 g for 30 mins at 4°C. (see **Figure 5**)

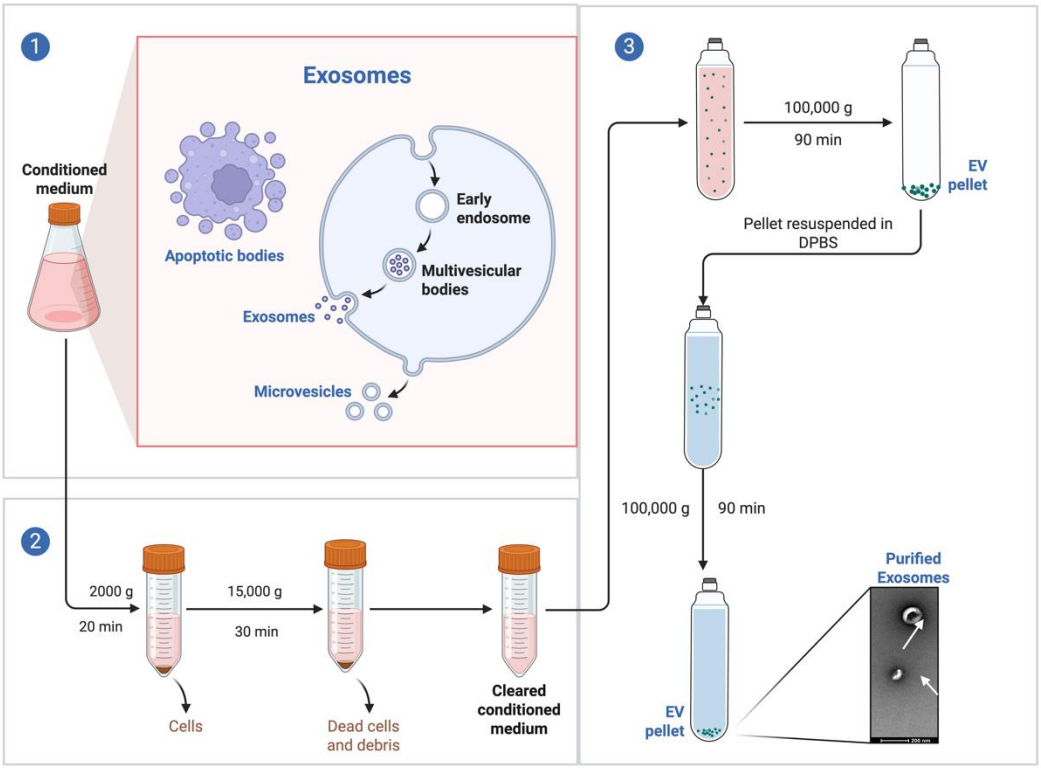

Figure 5: Steps in the isolation of exosomes by ultracentrifugation (UC) [Image created using (BioRender n.d.)]

(1). *Exosomes are produced within the cells via the endosomal pathway, involving early endosomes and multivesicular bodies, which are released into the extracellular space along with other vesicles. (2). Illustrates the* steps involved in differential centrifugation to remove the cells and debris. (3). represents the steps involved in ultracentrifugation to obtain purified exosomes.

The supernatant was collected after centrifugation and transferred to 25 ml ultracentrifugation tubes [Beckman Coulter Inc, USA] to isolate exosomes by ultracentrifugation (UC). UC was performed in an Optima XPN-100 ultracentrifuge with a 40 Ti rotor. The CM was centrifuged at 100,000 g for 90 mins at 4°C. The supernatant was discarded, and the pellet was dissolved in 1 ml DPBS per ultracentrifuge tube. The dissolved pellets were pooled, and the final volume was made up to 25 ml with DPBS and centrifuged again at 100,000 g for 90 mins at 4°C. The pellet was dissolved in 100 µl DPBS for nanoparticle tracking analysis (NTA) and ribonucleic acid (RNA) isolation, in 100 µl 4% Paraformaldehyde (PFA)-DPBS for transmission electron microscopy (TEM), in 100 µl HEPES buffer to use exosomes as treatment for cells or in 70 µl lysis buffer with PI (see **Table 5**) for western blot (WB). The samples in DPBS or 4% PFA-DPBS were stored at 4°C, and the lysed samples were stored at -80°C until further use.

13.3 Characterization of Cells and their Exosomes

To determine the size and quantity of the isolated exosomes, the samples resuspended in DPBS were analyzed using NTA. For analyzing the size and morphology, the samples resuspended in 4% PFA-PBS were imaged using TEM. SDS-polyacrylamide gel electrophoresis (SDS-PAGE) was performed to separate the proteins, followed by WB to determine the expression of proteins in cells and their exosomes.

13.3.1 Nanoparticle Tracking Analysis

NanoSight LM10 [Malvern Panalytica, UK] was used to quantify and determine the size of the isolated exosomes. NTA uses Brownian motion and the laws of dynamic light scattering to determine the size and number of particles in a solution. Therefore, the particles suspended in DPBS are illuminated with a laser beam (approximately 50 μm wide), and the scattered light is then visualized by a microscope (see **Figure 6**) and recorded in real-time. The image was then processed by an in-built software that tracked the trajectories of each of the particles to calculate the hydrodynamic diameter and concentration. This method allows for the accurate quantification of the particles within the range of ~30 – 150 nm, providing key information on the physical characteristics of the isolated exosomes.

Particle size was determined using the Stokes-Einstein equation, which combines Stoke law (describing the drag force on spherical particles of radius r) with Einstein's relation from the kinetic theory of gases. The resulting Stokes-Einstein equation is as follows:

$$D = \frac{k_B T}{6\pi\eta r}$$

where D is the diffusion coefficient, k_B is the Boltzmann constant, T is the absolute temperature, η is the fluid's dynamic viscosity, and r is the hydrodynamic radius of the particle.

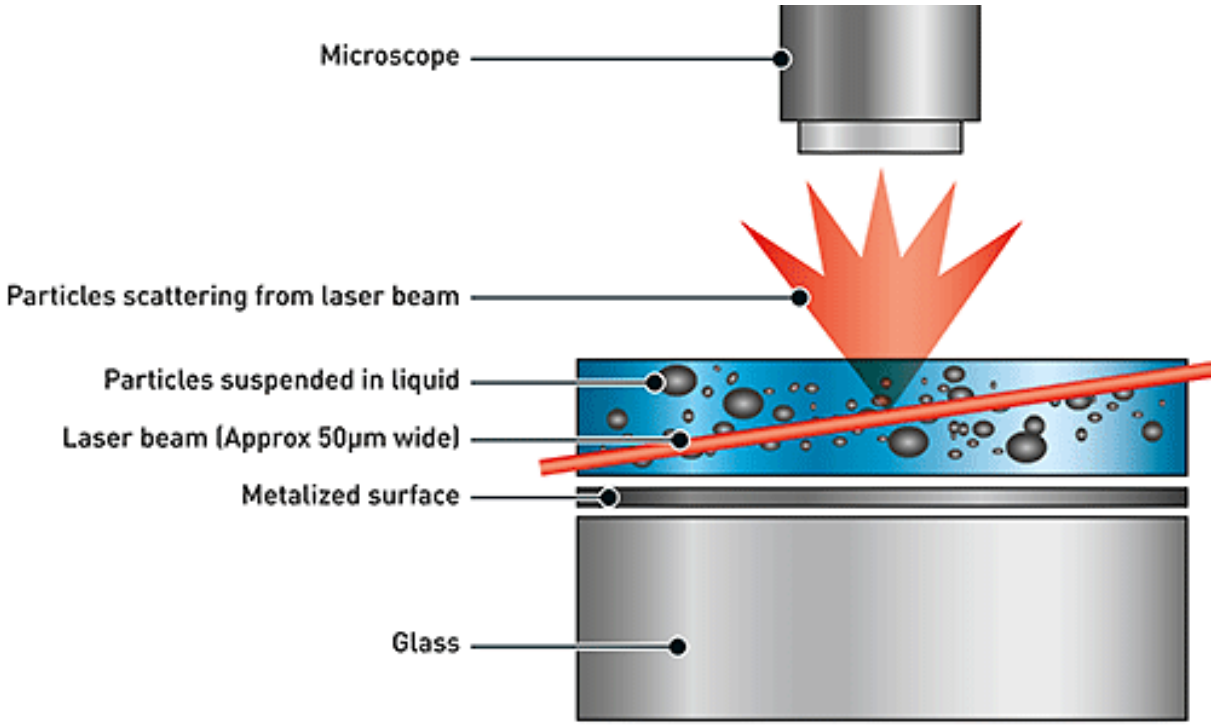

Figure 6: Principle of Nanoparticle Tracking Analysis (NTA)(Nanopartikel-Tracking-Analyse (NTA) n.d.)

Exosomes suspended in liquid are illuminated by a laser beam, causing the light to scatter. A microscope then captures the scattered light, and the Brownian motion of an individual particle is tracked. Using the Stokes–Einstein equation, exosome size and concentration can be then determined.

To achieve a suitable distribution of particles, 100 µl of the isolated exosomes from CAF and NCAF pairs, and PCa cells in DPBS was diluted 1:100, 1:500 and 1:1000 and pipetted onto the measuring chamber one after the other. The protocol was based on the manufacturer's specifications for measuring particles in aqueous solution, considering the specific refractive index of DPBS. The measurements of three biological replicates, each containing 2-3 videos with a duration of 30 s per sample, were recorded and evaluated using NTA 3.2 software [Malvern Panalytica, UK] to determine the size of particles.

13.3.2 Transmission Electron Microscopy

To analyze the size and morphology of the isolated exosomes, the samples were examined by imaging with a transmission electron microscope and its corresponding software. The samples were first fixed in 100 µl 4% PFA-DPBS after ultracentrifugation. 20 µl of the above sample was placed on a parafilm for 1 min, and a carbon-coated copper grid was placed on the drop of sample and incubated for 30 mins. Following the incubation, the

samples were washed three times with distilled water and subsequently fixed with 1% Glutaraldehyde [Merck KgaA, Germany] for 5 mins. Further, the grid was washed thrice with distilled water and stained with 1% uranyl acetate (pH 7) [Merck KgaA, Germany] for 1 min. After 10-15 min, the imaging was performed at 100 kV using a FEI Tecnai 13 TEM [FEI Company, Thermo Fischer Scientific Inc, USA] and its corresponding TEM software.

13.3.3 Protein separation using SDS –PAGE

Cells and their exosomes were analyzed using SDS-PAGE followed by WB to determine the expression of proteins. SDS-PAGE was used for protein separation, the most common method in analytical protein biochemistry (Laemmli 1970). Electrophoresis separates proteins based on size, shape, and charge, wherein molecules move through a gel matrix with their specific velocity. The used gel matrix comprises polyacrylamide gel, which acts as a size-selective sieve driven by an electric field generated throughout the matrix. Proteins are amphoteric compounds that are either charged positively or negatively, depending on their amino acid residues. Because of these different residues, each protein has its isoelectric point (pI). At the beginning, proteins have no net charge. Since electrophoresis is running at a constant pH, each protein in a mixture has its own positive or negative charge and characteristics in velocity. Because all proteins in a sample must run in the same direction towards the cathode, proteins are forced to be negatively charged. This is ensured by adding SDS to the sample buffer. Thus, SDS masks proteins by coating the amino acid residues with negatively charged detergent micelles (Weber and Osborn 1969).

In this work, the Laemmli buffering system was used. 10% Mini-Protean® TGX Stain-freeTM Precast Protein Gels [Bio-Rad Laboratories GmbH, Germany] were clamped between two chambers filled with 1x premixed running buffer solution [Bio-Rad Laboratories GmbH, Germany] in an electrophoresis chamber [Bio-Rad Laboratories GmbH, Germany] during the electrophoresis process. Due to the addition of SDS and heating, the denatured proteins could be separated by their specific Stokes radius (= hydrodynamic radius) based on an electric field applied to the polyacrylamide gel. Resolving gels used in this work were 10% (w/v) concentrated with a 12-lane comb. The wells were filled with 15-20 µl of cell or exosome lysate containing 1x Laemmli buffer [Serva Electrophoresis GmbH, Germany], and empty lanes were filled with 3 µl of Triple Color

Protein Standard II [Serva Electrophoresis GmbH, Germany] for consistency in running front.

The cells were harvested and lysed as described in section **13.1.3** and section **13.1.5** respectively. The protein concentration of the lysed cells and their exosomes (as described in section **13.2.2**) was determined using PierceTM Bicinchoninic Acid (BCA) assay kit [Thermo Fischer Scientific Inc, USA] according to the manufacturer's instructions. Between 1 and 20 µg of protein per sample can be loaded into the pocket of a polyacrylamide gel. The amount of protein used varied depending on the total protein concentration available in the sample, the expression of the protein under investigation and the specificity of the antibodies. The yield of exosomes was often very low, so that the samples had to be used as efficiently as possible. In addition, the expression of specific proteins could be so low that a higher amount of protein had to be used to detect them. It turned out that a quantity of 3-5 µg of protein per pocket was sufficient in most cases. Alternatively, increasing the concentration of primary and secondary antibodies would also have been possible. A protein standard, Triple Color Protein Standard II [Serva Electrophoresis GmbH, Germany] with defined size specifications in kilodaltons (kDa) was loaded into a gel pocket to assign a molecular weight to the protein bands.

Before electrophoresis, the reduced proteins were thermally denatured at 80°C for 5 minutes in a thermoblock [Eppendorf SE, Germany]. Gel electrophoresis was performed for 45 minutes at 25 mA, 200 V, 20 W. The negatively charged, denatured proteins migrated along the electric field through the 10% polyacrylamide gel toward the anode and separated according to size.

13.3.4 Western Blotting

After protein separation, depending on their specific molecular weight, using SDS-gel electrophoresis, proteins were transferred and detected on a solid support membrane made of chemically inert substances. This method, called "Western Blot", was established by Georg Stark in 1979 at Stanford University and relies on the principle of electro-mobility, which also drives the migration of proteins through gel matrix during electrophoresis (Renart, Reiser, and Stark 1979). Proteins were immobilized at their respective migration position in the gel and transferred onto a membrane, on which proteins could be detected by binding specific antibodies later on (Burnette 1981). Therefore, the proteins embedded in

the three-dimensional gel matrix were transferred to a membrane using semidry transfer method and an electric field.

The polyacrylamide gel, a BioTrace polyvinylidene difluoride (PVDF) membrane [PALL GmbH, Germany] and two electrodes were assembled like a sandwich, and proteins were transferred from the gel to the membrane. The most important step in this process is a uniform transfer across the whole gel to ensure a uniform transfer efficiency. The PVDF membrane with a pore size of 0.45 µm was used. This membrane type has a high binding capacity, which also leads to a higher background, but it has good mechanical strength. PVDF membranes are highly hydrophobic and must be activated by rinsing with 100 % (v/v) methanol (MeOH) [Merck KgaA, Germany] for 15 sec. After MeOH activation, the membrane has to be washed with purified water. All used utensils, like membrane, gel and Whatman® papers [Serva Electrophoresis GmbH, Germany], were equilibrated for at least 10 min in transfer buffer before they were packed like a sandwich and placed in Trans-Blot SD Semidry Transfer Chamber [Bio-Rad Laboratories GmbH, Germany]. Semidry blotting was performed at 100 mA, 200 V, 250 W at room temperature (RT) for 60 mins.

Table 9. Primary antibodies used for WB

Antibodies	Origin	Molecular Weight	Conditions	Dilution	Blocking /Ab Dilution Solution
α-SMA	Rabbit	42 kDa	reduced	1:500	5% BSA in TBS-T
Alix	Mouse	95 kDa	reduced	1:1000	5% Milk in TBS-T
Calreticulin	Rabbit	55 kDa	reduced	1:1000	5% BSA in TBS-T
CD9	Rabbit	22/24/35 kDa	reduced	1:1000	5% BSA in TBS-T
CD63	Rabbit	35-63 kDa	reduced	1:1000	5% Milk in TBS-T
CD81	Mouse	22/24 kDa	reduced	1:1000	5% BSA in TBS-T
CD147	Rabbit	50 kDa	reduced	1:1000	5% BSA in TBS-T
EpCAM	Rabbit	40 kDa	reduced	1:1000	5% Milk in TBS-T
GAPDH	Rabbit	37 kDa	reduced	1:1000	5% Milk in TBS-T
GM130	Rabbit	130 kDa	reduced	1:1000	5% BSA in TBS-T
PSMA	Mouse	100 kDa	reduced	1:1000	5% BSA in TBS-T
Syntenin	Rabbit	32 kDa	reduced	1:1000	5% BSA in TBS-T

After the transfer, proteins of interest could be detected and localized using target-specific antibodies. Before antibody detection could start, the membrane had to be prepared to prevent non-specific interactions. In this step, spaces on the membrane which were not occupied by proteins had to be blocked. For this purpose, the membrane was cut depending

on the characteristic of the antibody and the protein being detected and incubated in 5% (w/v) milk- Tris-buffered saline with Tween 20 (TBS-T) solution or 5% (w/v) bovine serum albumin (BSA) TBS-T (see **Table 9**) at RT for 60 min under constant agitation on a shaker [Bio-Rad Laboratories GmbH, Germany]. After the blocking step, to detect the proteins of interest, primary antibodies against exosomes (Alix, CD9, CD63, CD81, Syntenin), prostate cells (PSMA), cellular protein markers (GM130, Calreticulin) and tumor markers (CD147, EpCAM), the membrane was incubated with the primary antibody solution at 4°C overnight, again under constant agitation. The solution consisted of 5% milk-TBST or 5% BSA-TBST with the specific primary antibody in its unique dilution (see **Table 9**).

Table 10. Secondary antibodies used for WB

Antibodies	Dilution	Dilution Solution
Anti-Rabbit-HRP-coupled	1:2000	5% milk- or BSA-TBS-T
Anti-Mouse-HRP-coupled	1:2000	5% milk- or BSA-TBS-T

Following the primary antibody incubation, the membrane was washed to remove remaining unbound antibodies to avoid a strong background. Therefore, the membrane was washed thrice with TBS-T for 5 min each under constant agitation at RT. In the penultimate step, the membrane was incubated with horseradish peroxidase (HRP)-coupled secondary antibodies based on the species of the primary antibody (see **Table 10**) for 60 minutes at RT to visualize the protein. Due to the usage of secondary antibodies, there is an amplification in signal emission, which allows the detection of sparse amounts of proteins. The emitted signal is proportional to the quantity of protein that is detected.

After incubation with secondary antibodies, the membrane was washed thoroughly three times with TBS-T for 5 minutes each on agitation at RT. Chemiluminescent imaging was performed by shortly dipping the membrane in ECL substrates for high-sensitivity western blot detection [Thermo Fischer Scientific Inc, USA]. These were excited using an LED light source. The antibody-specific emission was detected afterwards using a cooled charge-coupled device (CCD) camera combined with emission filters to allow only a well-defined spectrum to reach the collector of the Chemostar ECL & Fluorescence Imager [Intas Science Imaging Instruments GmbH, Germany]. This type of camera collects photons on a chip and translates the collected charge into a digital signal. For protein quantification, GapDH was always used as an internal standard (“housekeeping protein”).

13.4 Co-culture Assays

The interactions between the fibroblasts and the PCa cells were studied using indirect co-culture assays, a standard method to facilitate modelling and investigating the TME role in cancer progression. Multiple methods are available to conduct co-culture assays, and one among them is the direct co-culture, which involves physical contact between different cell types, allowing for intricate cell-cell communications. Another widely used method is the indirect transwell system, where the cells are cultured separately, allowing exchange of only soluble factors like cytokines, EVs or growth factors via their medium. This method helps to stimulate the TME effects on the tumor cells from a distance. Following co-culture, various endpoint assays can be conducted to investigate the regulatory activities initiated by the co-culture conditions, thereby providing insights into the molecular mechanisms of the cells under investigation.

13.4.1 Viability Assay

Along with three technical replicates, all the cellular co-culture and exosomal treatment experiments and assays were analyzed with three biological replicates for each cell line. The cells were harvested and counted before seeding as described in the section **13.1.4**.

13.4.1.1 Cellular Co-culture

For cellular co-culture, at day 0, 15 x 10^3 each of LNCaP and LNCaP C4-2 cells were seeded per well into two 24-well plates [Corning Incorporated, USA] in a mixture of complete medium consisting of DMEM and RPMI in a 1:1 ratio in technical triplicate. After seeding the PCa cells, transwell inserts (6.5 mm, 0.4 µm pore size) [Corning Incorporated, USA] were placed on each of the wells (see **Figure 7**) and 15 x 10^3 of CAFs or NCAFs were seeded in the transwells depending on the plating scheme. Two plates were set up as described above for 2- and 4-day incubation. The plates were incubated in an incubator at 37°C and 5% (v/v) CO_2. After incubation, the transwells with fibroblasts were discarded, and a viability assay was performed for PCa cells on days 2 and 4. The medium was aspirated, and the cells were washed gently once with DPBS, as LNCaP and LNCaP C4-2 cells are loosely adherent. Further, the viability of the cells was measured using the WST-1

assay kit [Roche Diagnostics Deutschland GmbH, Germany] according to the manufacturer's guidelines. The measurement was carried out at a wavelength of 450 nm with a reference wavelength of 620 nm in the Infinite F200 pro microplate reader [Tecan Group Ltd., Switzerland] at two timepoints: 0 h (Blank) and 4 h. PCa cells without co-culture were used as controls.

13.4.1.2 Exosomal Treatment

For exosomal treatment, at day 0, 12 x 10^4 each of LNCaP- and LNCaP C4-2- cells were seeded per well into a 24-well plate in ED-RPMI medium in technical triplicates (see **Figure 7** (2)). The cells were allowed to settle and adhere overnight in an incubator at 37°C and 5% (v/v) CO_2. The following day, 8 µg/ml of CAF- or NCAF-exosomes in ED-RPMI medium was added to each of the wells according to the plating scheme and incubated at 37°C and 5% (v/v) CO_2 for 24 h. After 24 h incubation, the viability assay was performed as described in section **13.4.1.1**.

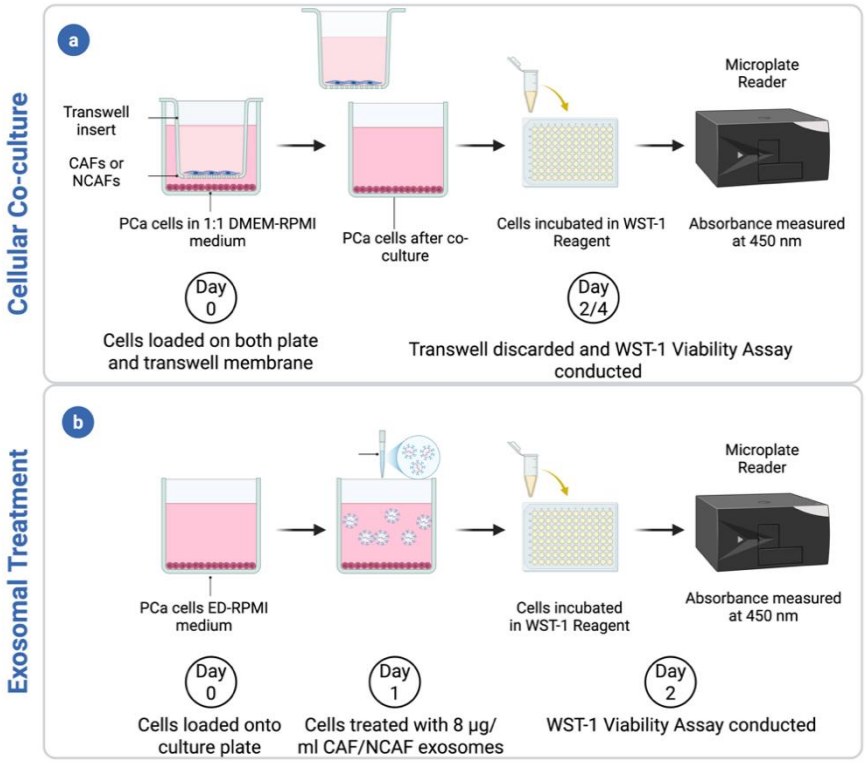

Figure 7: Stepwise illustration of viability assay [Image created using (BioRender n.d.)]

(a). PCa cells were seeded at the bottom with CAFs or NCAFs on the top in transwells. After 2 and 4 days of incubation, the respective culture plates containing PCa cells were used to measure viability (b). PCa cells seeded in exosome-free medium on culture plates were treated with 8 µg/ml of CAF or NCAF exosomes. After incubation for 24 h, the viability of PCa cells was measured.

Exosomal treatment followed by viability assay was also performed for CAF- and NCAF- pairs, where the fibroblasts were treated with PCa exosomes. For this, on day 0, 5 x 10^4 each of CAF- and NCAF- cells were seeded in ED-DMEM medium in 24-well plates and incubated at 37°C and 5% (v/v) CO_2 overnight. On day 1, the fibroblasts were treated with 8 µg/ml of PCa exosomes in ED-DMEM medium and incubated at 37°C and 5% (v/v) CO_2 for 48 h. On day 3, after 48 h incubation, the viability of the fibroblasts was measured as described above. Since primary fibroblasts are known to be very volatile in their behavior owing to their patient-specific characteristics, immortalized hTERT fibroblasts were used as a standard comparison for both cellular and exosomal treatment of fibroblasts. In place of the CAF- or NCAF-cells, 12 x 10^4 hTERT cells were seeded, and the cellular co-culture, exosomal treatment and viability assay were performed as for primary fibroblasts. PCa cells treated with DPBS and self-exosomes in place of CAF- and NCAF- exosomes were used as controls.

13.4.2 Proliferation Assay

The proliferation assay for PCa cells was conducted after cellular co-culture, similar to the viability assay. The LNCaP and LNCaP C4-2 cells were harvested and counted as described in section **13.1.4**. On day 0, 15 x 10^3 each of LNCaP and LNCaP C4-2 cells were seeded per well into two 24-well plates in a mixture of complete medium consisting of DMEM and RPMI in a 1:1 ratio in technical triplicate. Depending on the plating scheme,15 x 10^3 of CAFs or NCAFs were seeded in the transwells. Two plates were set up as described above for 2- and 4-day incubation. The plates were incubated in an incubator at 37°C and 5% (v/v) CO_2. After incubation, the transwells with fibroblasts were discarded, and a proliferation assay was performed for PCa cells on day 2 and day 4 using the Bromodeoxyuridine (BrdU) colorimetric proliferation assay kit [Roche Diagnostics Deutschland GmbH, Germany]. The BrdU labelling solution was diluted with the respective complete medium (1:1000), and 20 µl of it was added per well and incubated for 2h at 37°C and 5% (v/v) CO_2. After incubation, the labelling medium was aspirated and either air dried to store at 4°C for up to a week or the next steps were carried out immediately without drying according to the manufacturer's guidelines. The measurement was carried out at a wavelength of 450 nm with a reference wavelength of 620 nm in the Infinite F200 pro microplate reader within 5 minutes of color development in the last step after adding sulfuric

acid (H_2SO_4) [Bernd Kraft GmbH, Germany]. PCa cells without co-culture were used as controls.

13.4.3 Migration Assay after cellular co-culture

The migration assay for PCa cells after cellular co-culture was performed using two methods: the endpoint assay using the FluoroBlok transwell migration inserts (24-well; 8µm pore size) [Corning Incorporated, USA] and the real-time assay using the xCELLigence RTCA DP system [Agilent Technologies, USA]. Along with two technical replicates, all the cellular co-culture assays were conducted with three biological replicates for each cell line and analyzed.

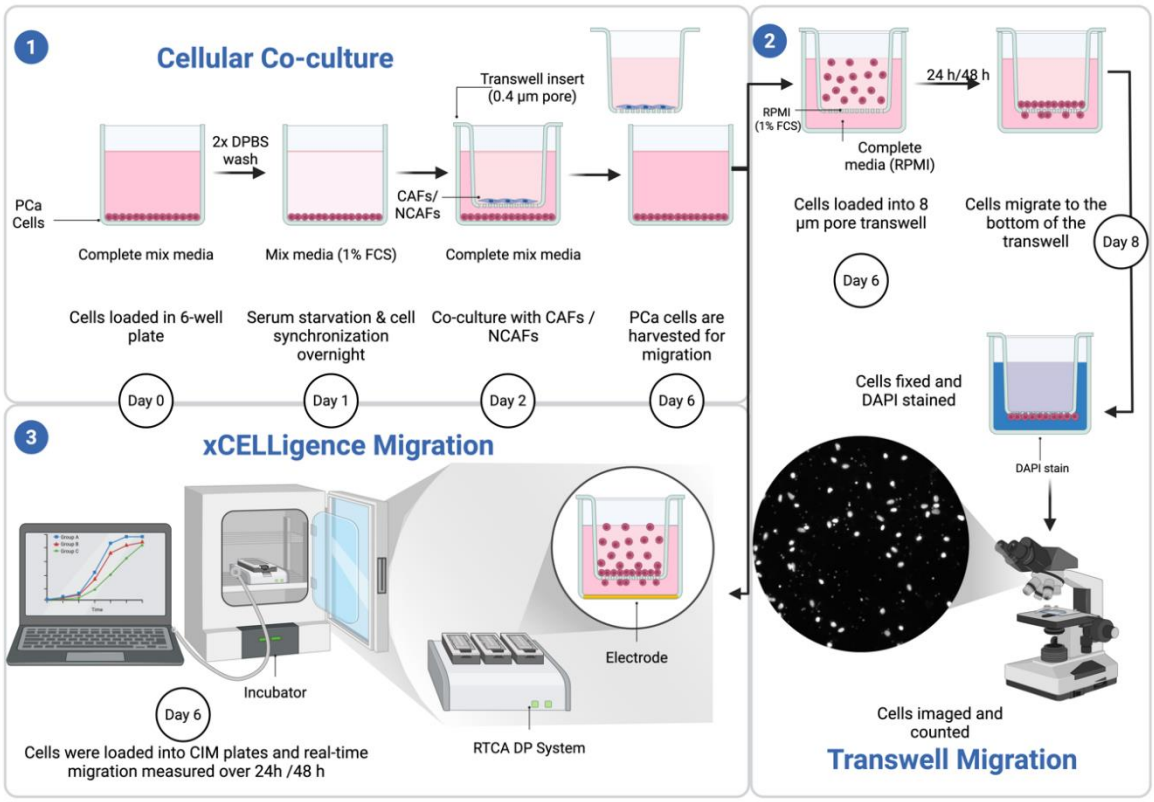

Figure 8: Schematic overview of prostate cancer (PCa) cell migration following co-culture with CAFs and NCAFs (Image created using (BioRender n.d.))

(1). PCa cells were seeded in a 6-well plate and serum-starved overnight in 1% FCS media to synchronize the cell cycle. On Day 2, transwell inserts (0.4µm pore size) containing CAFs or NCAFs were added to establish indirect co-culture. After 4 days, PCa cells were harvested for migration (2). For the transwell migration assay, PCa cells were seeded in 8 µm pore FluoroBlok inserts and allowed to migrate for 24h for LNCaP and 48 h for LNCaP C4-2. On day 8, the migrated cells were fixed, DAPI-stained and visualized under a fluorescence microscope for quantification. (3). In parallel, real-time migration was assessed using the xCELLigence RTCA DP system. Migration of the cells loaded into CIM-plates was monitored over 24h/48 h based on impedance changes across gold electrodes in the lower chamber.

The cells were harvested and counted before seeding as described in the section **13.1.4**. For cellular co-culture, at day 0, 15 x 10^4 LNCaP cells and 9 x 10^4 LNCaP C4-2 cells were seeded per well into a 6-well plate [Corning Incorporated, USA] in a mixture of complete medium consisting of DMEM and RPMI in 1:1 ratio. The next day, on day 1, the cells were washed with DPBS, and a serum-depleted (1%) mix media (DMEM:RPMI) was supplemented to the PCa cells to synchronize the cell cycle overnight. After synchronization of the PCa cells, transwell inserts (24 mm, 0.4 µm pore size) [Corning Incorporated, USA] were placed on each of the wells (see **Figure 8**). 42 x 10^4 of CAFs or NCAFs were added to the transwell for co-culture with LNCaP cells, and 65 x 10^4 of either of the fibroblasts were seeded in the transwell for co-culture with LNCaP C4-2 cells according to the plating scheme. The number of fibroblasts seeded was proportional to the approximate number of PCa cells, considering the growth time of 2 days for PCa cells before co-culture. The cells were co-cultured for 4 days in an incubator at 37°C and 5% (v/v) CO_2.

13.4.3.1 Endpoint Transwell Migration Assay

After the cellular incubation, the transwells with fibroblasts were discarded, and the PCa cells were harvested and counted as described in section **13.1.4**. for endpoint and real-time migration assays in parallel. For the transwell endpoint assay, 8 µg of aphidicolin (which selectively inhibits cell proliferation via DNA polymerase inhibition) per ml, along with complete RPMI media, was added to the lower chamber of a 24-well plate as a chemoattractant in duplicates. 5 x 10^4 PCa cells were loaded into 8 µm pore FluoroBlok transwell inserts [Corning Incorporated, USA]. The plates were incubated for 24h and 48h for LNCaP and LNCaP C4-2, respectively, at 37°C and 5% (v/v) CO_2 to allow the cells to migrate. After migration, the inserts were carefully washed by dipping in DPBS. Then, the inserts were dipped in 1 ml of 100% MeOH for 10 min at -20°C to fix the cells. After fixing, the inserts were washed thrice with DPBS to get rid of excess MeOH and dipped in 1 ml of 4',6-diamidino-2-phenylindole (DAPI) stain (1:1000 dilution with DPBS) for 7 mins in the dark at RT. The excess stain was washed thrice with DPBS, and the inserts were stored in DPBS until visualization by the Eclipse TE2000-S inverted fluorescence microscope [Nikon Corporation, Tokyo, Japan]. PCa cells without co-culture were used as controls.

During microscopy, random fields were chosen and imaged in each insert. The number of cells in each field was counted using ImageJ software [Wayne Rasband, 1987, USA] for accuracy and replicability. The number of migrated cells was calculated by using the formula:

$$Number\ of\ migrated\ cells = \frac{average\ number\ of\ cells\ within\ an\ insert}{area\ of\ the\ microscope\ viewing\ field} \times area\ of\ the\ transwell\ insert$$

Once the number of migrated cells per insert was determined, the percentage migration was calculated using the formula:

$$\%\ migration = \frac{number\ of\ migrated\ cells}{total\ number\ of\ cells\ seeded\ per\ insert} \times 100$$

13.4.3.2 Real-time xCELLigence Assay

In case of real-time assay using the xCELLigence RTCA DP system, the lower chamber of the cellular invasion/ migration (CIM) plate [Agilent Technologies, Germany] was filled with complete RPMI media containing 8 µg/ ml of aphidicolin as a chemoattractant in duplicates. The upper chamber was loaded with 1 x 10^5 PCa cells after cellular co-culture. The assay was set up according to the manufacturer's migration protocol. The CIM plate was placed in the RTCA DP system, and the entire system was placed in an incubator at 37°C and 5% (v/v) CO_2 (see **Figure 8**). Using the RTCA software on the connected computer, the readings were automatically recorded every hour for 24 h for LNCaP cells and 48 h for LNCaP C4-2 cells based on impedance changes across gold electrodes in the lower chamber. After data acquisition, the replicates were averaged to analyze the cell index (CI) curves. Along with the CI curves, the migration rate was analyzed using the slope of the curves during a desired time window to be comparable with the endpoint assays. PCa cells without co-culture were used as controls.

13.4.4 Migration Assay after exosomal treatment

The influence of exosomes from CAFs and NCAF on migration was carried out only for LNCaP C4-2 cells, as the LNCaP cells did not migrate after cellular co-culture.

Therefore, for this study, on day 0, 15 x 10^3 LNCaP C4-2 cells were seeded in complete ED-RPMI medium in a 24-well plate in duplicates. The next day, the complete media was aspirated, and the cells were washed with DPBS gently prior to supplementing the cells with 1% ED-FCS containing RPMI medium overnight for cell synchronization. On day 2, the cells were treated with 8 µg of CAF- and NCAF-exosomes (in HEPES) per ml of complete ED-RPMI medium and incubated at 37°C and 5% (v/v) CO_2 for 24 h. After incubation, the cells were harvested and seeded into the CIM plates for real-time migration assay using the xCELLigence system as described in section **13.4.3.2** using ED-RPMI medium. Along with two technical replicates, all the exosomal treatment experiments and assays were analyzed with three biological replicates for each cell line. PCa cells treated with DPBS and self-exosomes in place of CAF- and NCAF- exosomes were used as controls.

13.5 miRNA Expression Analysis

DNase/RNase-free reaction tubes [Eppendorf SE, Germany] and pipette tips were used for all the miRNA analyses. The working surfaces were cleaned with RNAseZap [Sigma-Aldrich Corporation, USA] to ensure a DNAase/RNAase-free working environment and RNAase contamination was avoided throughout the experiment.

13.5.1 Total RNA isolation from cells and exosomes

To determine the miRNA expression in CAFs and NCAFs and their exosomes, total RNA was isolated using the RNAeasy Mini Kit [Qiagen N.V., Netherlands]

13.5.1.1 RNase Treatment

Along with exosomal RNA, the isolated exosomes may be contaminated with free-circulating RNA. This must be degraded as it can lead to a shift in the miRNA patterns in subsequent expression experiments. It is well known that the exosomal RNAs are protected from degradation by RNase, which means that only the free RNA present is destroyed. The exosomes in DPBS were incubated with 20 U RNase One Ribonuclease [Promega GmbH, Germany] for 30 min at RT. RNase is inactivated by incubating the mixture with 10 U RiboLock RNase Inhibitor [Thermo Scientific] at RT for 10 minutes.

13.5.1.2 Total RNA isolation

The RNase-treated exosomes and their source cells were used for total RNA isolation. The cells and exosomes were lysed with 700 µl Qiazol lysis solution [Qiagen N.V., Netherlands] for 5-30 min at RT (5 min cells; 30 min exosomes). Total RNA isolation was performed according to the manufacturer's protocol. The total RNA was eluted with 15-30 µl RNase-free water. The total RNA concentration and purity were measured using the NanoDrop ND-1000 [PeqLab Biotechnology GmbH].

13.5.2 miRNA Microarray Analysis

This part of the experiment was used to identify specific miRNAs expressed differently between CAF- and NCAF- cells. In addition, miRNAs that are differently expressed in exosomes from CAF- and NCAF- cells were to be identified. Three different CAF-NCAF pairs and their secreted exosomes were used for the analysis. miRNA expression analysis was performed using miRNA Microarrays Version 16 [Agilent Technologies, Germany] and the corresponding miRNA Complete Labeling and Hyb Kit [Agilent Technologies, Germany This version was manufactured according to Sanger and includes 866 human miRNAs and 89 human viral miRNAs. For quality control of the labeling and hybridization reactions, labeling and hybridization spike solutions solutions [Agilent Technologies, Germany] were prepared according to the manufacturer's instructions.

13.5.2.1 miRNA Labeling

For labeling of the miRNA, the samples were first dephosphorylated. For this purpose, 2 µl of sample (total RNA concentration: 50 ng/µl) was transferred to a 1.5 ml reaction vessel and mixed with 0.4 µl calf intestinal alkaline phosphatase (CIP), 0.5 µl 10X CIP buffer, and 1.1 µl labeling spike-in solution. The sample was incubated at 37°C for 30 min to activate the phosphatase. After dephosphorylation, the sample was denatured by adding 2.8 µl of 100% DMSO for 7 minutes at 100°C. The sample was then immediately transferred to an ice bath. In the subsequent labeling reaction, 1 µl of 10X T4 RNA ligase buffer, 3 µl of Cyanine3-pCp, and 0.5 µl of T4 RNA Ligase were added to the denatured sample and, after mixing, incubated at 16°C for 2 h in

the dark. Cyanine3-pCp is a fluorescent dye that binds to the 3' end of the RNA molecule during the labeling reaction binds to the 3' end of the RNA molecule during labeling reaction and labels the RNA regions

13.5.2.2 miRNA Hybridization

After the sample was dried at 50°C for 1 h in the vacuum centrifuge [Martin Christ Gefriertrocknungsanlagen GmbH, Germany], the hybridization reaction was performed. For this purpose, the sample was dissolved in 17 µl RNase-free water and mixed with 1 µl Hyb Spike-In solution [Agilent Technologies, Germany], 4.5 µl 10X GE Blocking Agent, and 22.5 µl 2X Hi-RPM hybridization buffer. The mixed sample was incubated for 5 min at 100°C and 5 min in an ice bath. For hybridization, the entire sample volume was applied to the center of the gasket slides, and the Agilent microarray's active side was placed on top. The microarray was incubated in the Agilent G2545A hybridization oven [Agilent Technologies, Germany] for 20 h at 55°C with a rotation speed of 20 rpm. After 20 h, hybridization was stopped, and the microarrays were transferred to wash buffer 1 (to separate the gasket slide from the actual microarray). This was followed by a washing step in wash buffer 1 and 2 [Agilent Technologies, Germany] at 37°C for 5 min each. After cleaning the microarray, it was scanned with the Agilent Microarray Scanner [Agilent G2565BA, Agilent Technologies, Germany] according to the manufacturer's instructions (see **Table 11**).

Table 11. Scanning instructions for microarray

Scan Settings	Scan Area	Scan Resolution (µm)	Scan Mode	Channel	Green PMT
Format 8 x 60K	61 x 21,6 mm	5	1-Channel	Green	XDR Hi 100% XDR Lo 5%

Data was calculated using the corresponding Feature Extraction software [Agilent Technologies] and evaluated and graphically displayed using the Qlucore Omics Explorer 3.2 software [Qlucore Bioinformatics, Sweden].

13.5.3 Validation of miRNA-expression by qPCR

The miRNAs miR-223-3p, 10b-5p, -210-3p and -148b-3p [Thermo Fischer Scientific Inc, USA] were selected based on the results of microarray analyses and validated using quantitative real-time PCR (qPCR). In addition to these miRNAs, three endogenous controls, the reference miRNA-RNU48, -191-5p and -361-5p were included for all cell and exosomal samples. Specific primers (TaqMan® MicroRNA Assays [Thermo Fischer Scientific Inc, USA] and the TaqMan microRNA RT Kit [Thermo Fischer Scientific Inc, USA] were used to transcribe the miRNA into the corresponding cDNA. For the PCR reaction of the cell culture experiments, 5 µl of sample (total RNA concentration: 20 ng/µl) was added to the reagents in a 200 µl reaction vessel, mixed thoroughly, and incubated on ice for 5 min (**Table 12**). The transcription of miRNA into cDNA was performed for both cellular and exosomal samples using the PCR program (**Table 12**) in the Biometra Uno II thermocycler [Analytik Jena, Germany].

Table 12. Pipetting scheme and PCR program for reverse transcription

Reagents	**Volume (µl) for samples from cells and exosomes**	
100 mM dNTPs (with dTTP)	0.15	
MultiScribe Reverse Transcriptase (50 U/µl)	1	
10X Reverse Transcriptase Buffer	1.5	
RNase Inhibitor	0.19	
RNase-free Water	4.16	
RT-Primer (5X)	3	
PCR program for reverse transcription		
Steps	**Time (min)**	**Temperature (°C)**
Primer hybridization	30	16
Elongation	30	42
Denaturation	5	85

This was followed by qPCR with specific primers [Thermo Fischer Scientific Inc, USA] and fluorescence-labeled TaqMan probes [Thermo Fischer Scientific Inc, USA] using the

TaqMan Gene Expression Master Mix [Thermo Fischer Scientific Inc, USA]. For qPCR, a 10 µl PCR reaction was prepared. For this purpose, 1 µl cDNA was mixed with 0.5 µl TaqMan MicroRNA Assay Primer (20X), 5 µl TaqMan Gene Mastermix, and 3.5 µl nuclease-free water, and pipetted into a well of a 96-well plate. Three technical replicates were applied to each sample. To prevent evaporation, the plate was sealed airtight with a protective film. The plate was then centrifuged at 300 g for 1 min, transferred to the LightCycler 480 II [Roche Diagnostics Deutschland GmbH, Germany], and the PCR program (**Table 13**) was performed.

Table 13. Program for qPCR

Steps	Time (min)	Temperature (°C)	Cycles
Primer Hybridization	30	16	1
Elongation	30	42	45
Denaturation	5	85	

During each PCR cycle, the cDNA is replicated into two identical copies, causing the fluorescence intensity to increase proportionally with the PCR product of each cycle. The intensity is measured after each PCR cycle. The "crossing point" (Ct), which indicates the point at which the fluorescence signal first emerges significantly from the background noise, is used to calculate the expression differences. The Ct values and standard deviation were determined using the LightCycler 480 II software [Roche Diagnostics Deutschland GmbH, Germany]. Two-way ANOVA was performed using the GraphPad Prism software [GraphPad Software, LLC, USA] to calculate statistical significance.

14 RESULTS

14.1 Characterization of cells and their exosomes

To validate the quality of exosomes isolated via UC method from CAFs and NCAFs, the size distribution was determined using NTA, the morphology was characterized using TEM, and the expression of exosome-specific proteins was determined using WB. In the results, it was possible to demonstrate that they exhibit exosome-typical characteristics of shape, size, size distribution, and surface markers. Exosomes belong to the extracellular vesicles and are often referred to in the literature as small extracellular vesicles (sEVs). Subsequent designation of particles as "exosomes" therefore refers to vesicles with a diameter between 30-150 nm, enclosed in a visible lipid bilayer and the presence of specific protein markers.

14.1.1 Particle Size and Concentration Profiling of Exosomes from Primary Prostate Fibroblasts

NTA was performed to assess the size distribution and concentration of the isolated exosomes from three pairs of CAFs and NCAFs derived from PCa tissue from patients after radical prostatectomy. All samples were diluted 1:500 in DPBS before measurements. All samples showed a particle size distribution characteristic of exosomes.

Table 14. Exosome concentration and size distribution

Exosomes from	Dilution in DPBS	Particle Concentration (particle/ml)	Mean Particle Size
NCAF1	1:500	6.91×10^{11}	146.2 nm
CAF1	1:500	1.56×10^{12}	108.9 nm
NCAF2	1:500	3.94×10^{11}	128.3 nm
CAF2	1:500	4.53×10^{11}	135.8 nm
NCAF3	1:500	2.89×10^{11}	138.4 nm
CAF3	1:500	4.88×10^{11}	130. nm

Across all samples, the exosomes concentration ranged from 2.89×10^{11} particles/ml to 1.56×10^{12} particles/ml (**Table 14**). Among the NCAFs, particle concentrations were 6.91×10^{11} particles/ml (NCAF1), 3.94×10^{11} particles/ml (NCAF2) and 2.89×10^{11} particles/ml

(NCAF3). CAF-derived exosomes exhibited concentrations of 1.56 x 10^{12} particles/ml (CAF1), 34.53 x 10^{11} particles/ml (CAF2) and 4.88 x 10^{11} particles/ml (CAF3). CAF1 exosomes had the highest yield in comparison to the lowest yield from NCAF3.

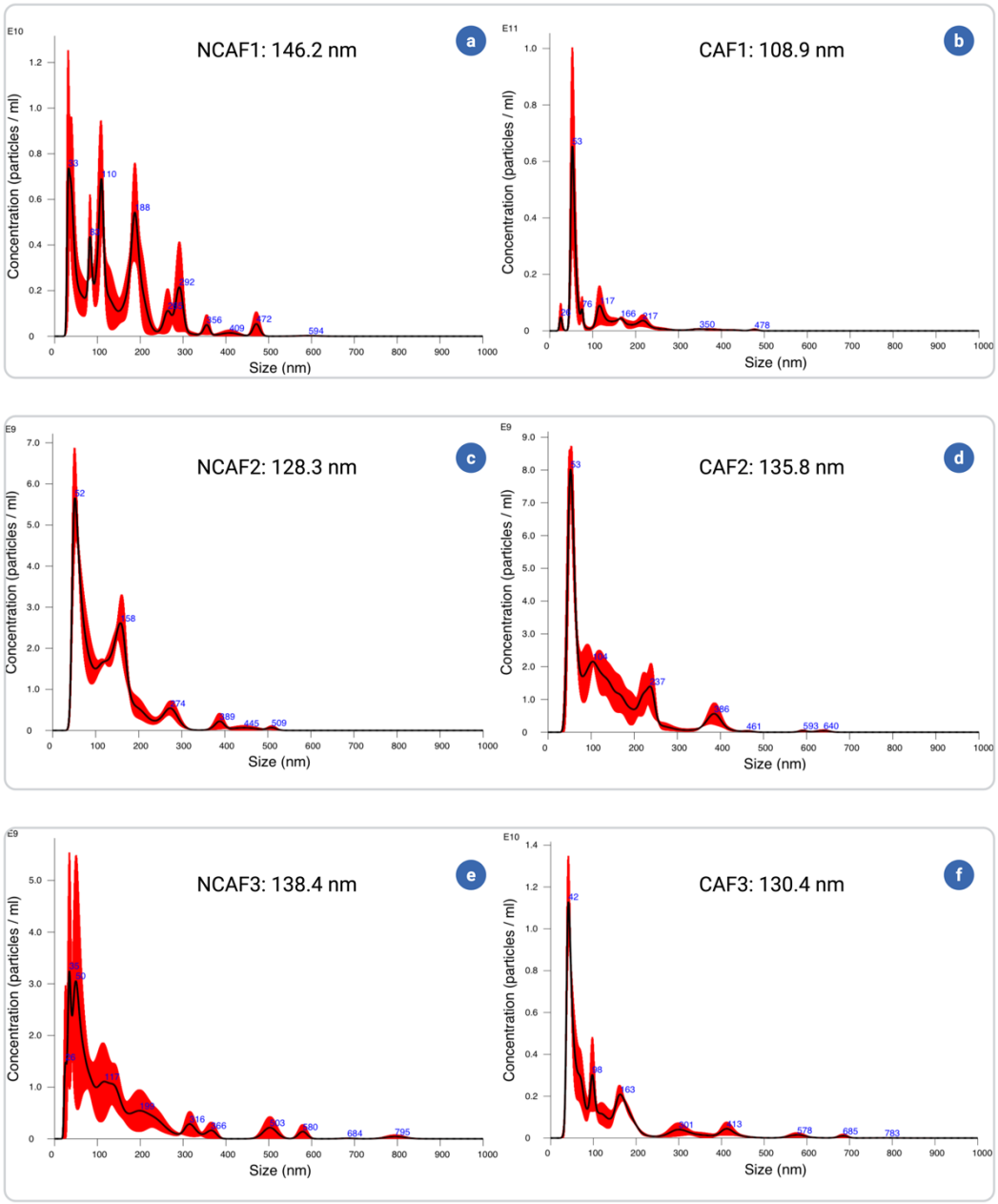

Figure 9: Nanoparticle Tracking Analysis (NTA) of exosomes isolated from prostate fibroblasts

(a,c,e). Size distribution profiles of exosomes derived from three different prostate non-cancer-associated fibroblasts (NCAFs) and (b,d,f). Cancer-associated fibroblasts. The mean sizes of NCAF-derived exosomes were 146.2 nm (NCAF1), 128.3 nm (NCAF2), and 138.4 nm (NCAF3), while those of CAF-derived exosomes were 108.9 nm (CAF1), 135.8 nm (CAF2), and 130.4 nm (CAF3). Each curve represents the mean of three technical replicates (black line) with standard error in red shading.

Overall, NTA revealed a size distribution with a maximum at approximately 100 nm in all three pairs of primary fibroblasts, which aligns well with the accepted size range for exosomes (30-150 nm) as suggested by ISEV2018. (see **Figure 9**). While most of the particles were within this range, occasional larger particles were also observed, which could reflect a minor population of microvesicles or protein aggregates. This brings the mean particle size of exosomes in our samples between 100 and 150 nm (see **Table 14**).

Notably, the size range between CAFs and NCAFs was broadly comparable, confirming the successful enrichment of vesicles consistent with exosomes. The NTA results serve as an important first layer of validation for the identity of the isolated vesicles.

14.1.2 Morphological Analysis of Exosomes from Primary Prostate Fibroblasts

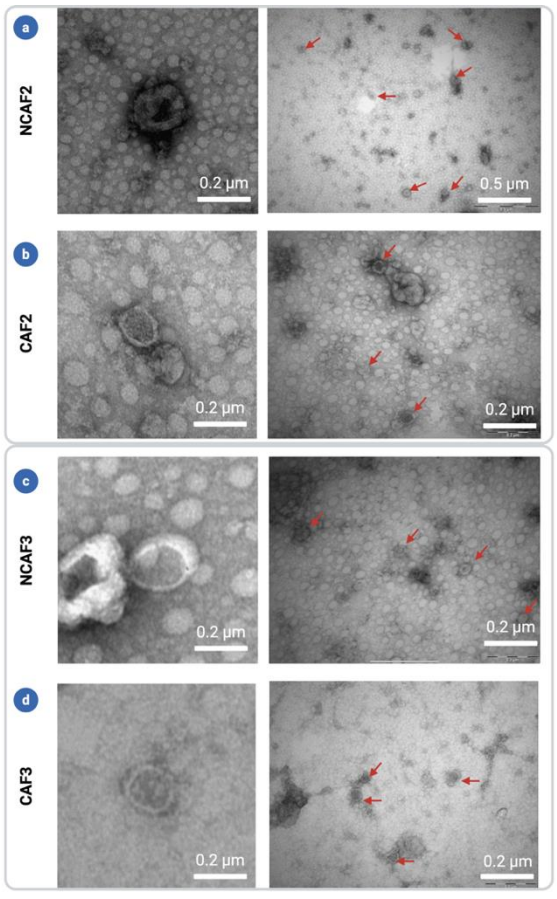

Figure 10: Transmission electron microscopy (TEM) images of exosomes isolated from prostate fibroblasts

TEM images of exosomes derived from two pairs of NCAF (NCAF2 and NCAF3) and CAF (CAF2 and CAF3) samples. The left panel depicts the overall morphology of the isolated exosomes with a cusp-shaped vesicle enclosed in a lipid bilayer and the right panel shows the distribution of individual exosomes or as clusters (indicated by red arrows). Scale bars are indicated on each image.

TEM was performed on two pairs of CAFs and NCAFs to further validate the morphology and vesicular nature of the isolated exosomes. All the samples exhibited an intact membrane with a visible lipid bilayer enclosing a round to cusp-shaped inner structure (see **Figure 10**). Slight differences in the vesicle density and size were observed among the samples, which may reflect biological differences between patient-derived samples.

14.1.3 Profiling of Exosome-Specific Markers in Prostate Fibroblasts-derived Exosomes

To confirm the enrichment of exosomes and assess their purity, western blotting was performed on whole cell lysates and their corresponding exosomes from NCAF1 and CAF1. The exosomes from both fibroblast types showed a clear expression of the exosome markers Alix, Syntenin and CD9. While these proteins were robustly detected in the exosomes, they appeared faint or undetectable in the cellular lysates, confirming the enrichment of exosomes by UC (see **Figure 11**).

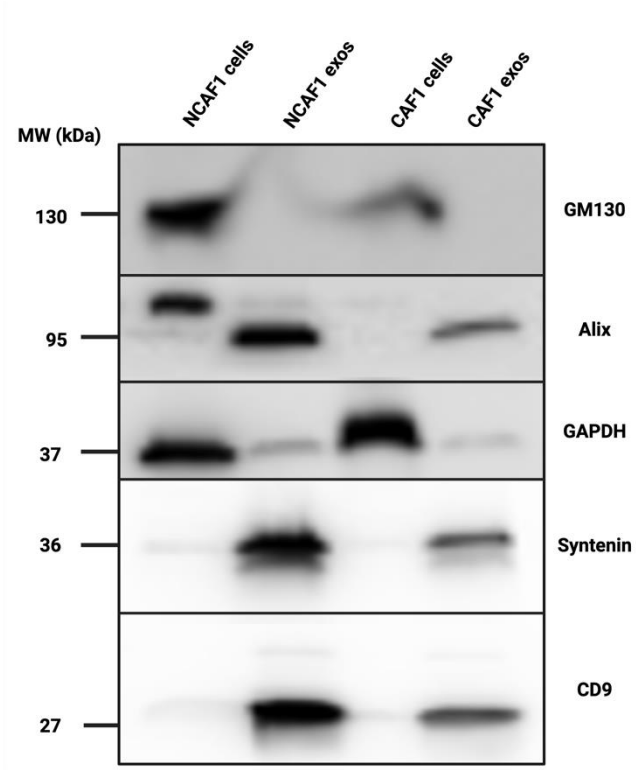

Figure 11: Western blot analysis of exosomal protein markers in prostate fibroblasts

Exosome fractions and their corresponding whole-cell lysates were probed for the exosomal markers Alix, Syntenin and CD9, the Golgi marker GM130 and GAPDH as the housekeeping gene. Alix, Syntenin and CD9 were enriched in exosomes, whereas GM130 was detected only in the cellular lysates, confirming the absence of cellular contamination in exosome fractions. MW: molecular weight (kDa)

The Golgi matrix protein GM130 was used as a negative control for exosomes and was only detected in the whole-cell lysates of both fibroblast types. GAPDH was used as the loading control. This indicates that the exosomal fractions were largely free of cellular components, reflecting an efficient UC-based purified isolation.

14.1.4 Expression Profiling of α-SMA in Prostate Fibroblasts

The expression of α-SMA, a well-established myofibroblast marker, was evaluated in the protein lysates from three pairs of primary prostate fibroblasts by western blotting to assess the activation status of fibroblasts. Protein lysates were prepared from matched NCAFs and CAFs and probed with an anti-α-SMA antibody. GAPDH was used as the loading control.

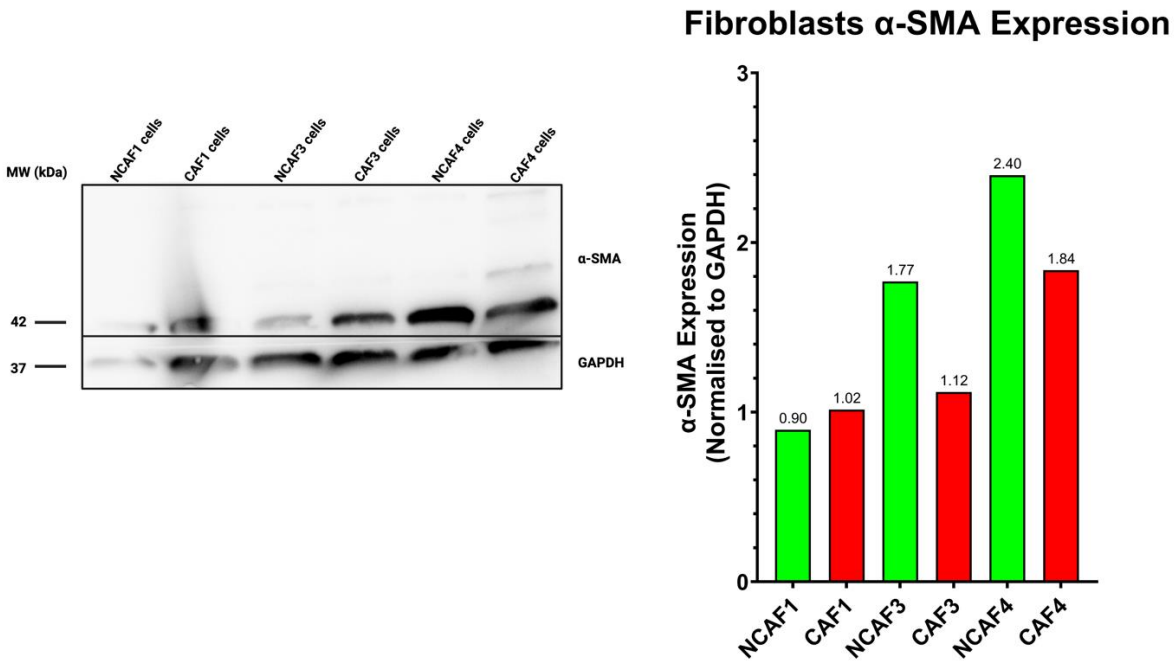

Figure 12: Western blot analysis of α-SMA expression in primary prostate fibroblasts

Protein lysates from normal cancer-associated fibroblasts (NCAF1, NCAF3, NCAF4) and cancer-associated fibroblasts (CAF1, CAF3, CAF4) were probed with an anti-α-SMA antibody (upper row). GAPDH was used as a loading control (lower row). α-SMA was detected in both NCAF and CAF samples, and no consistent patterns of higher expression were observed in CAFs compared to NCAFs; MW: molecular weight (kDa).

As shown in **Figure 12**, α-SMA was expressed in both CAF and NCAF samples at comparable levels. α-SMA was detected in both NCAF and CAF samples, and no consistent patterns of higher expression were observed in CAFs compared to NCAFs. In pair 1, the

expression was similar in both types of fibroblasts. In pair 3 and 4, interestingly the NCAFs had a higher expression pattern compared to CAFs. GAPDH confirmed consistent protein loading across samples.

14.2 Functional assessment of fibroblasts and their exosomes-mediated effects on prostate cancer cells

To better understand the role of patient-derived fibroblasts in modulating PCa cell behavior, we performed a series of functional assays using indirect co-culture and exosome treatments. Indirect co-culture allowed us to study the effects of fibroblast-secreted factors on tumor cells without direct cell-to-cell contact. We first investigated the effect of fibroblast co-culture on three key aspects of PCa cells: viability, proliferation and migration. Both the xCELLigence real-time assay to track dynamic migration kinetics and the endpoint assay to validate the effects were employed for migration. Then, we examined whether fibroblast-derived exosomes could reproduce the changes observed in indirect co-culture. Exosomes isolated from NCAFs and CAFs were tested for their effects on the viability and migration of PCa cells. Together, these functional assays provide insights into the relative contribution of soluble factors and exosomal signaling in modulating PCa cell survival, growth and motility.

14.2.1 Influence of patient-derived fibroblasts in regulating prostate cancer viability

To investigate the influence of patient-derived fibroblasts on the PCa cell survival, viability of LNCaP and LNCaP C4-2 cells after indirect co-culturing with three independent pairs of fibroblasts (NCAFs and CAFs) was assessed. Viability was measured on days 2 and 4.

For pair 1, both NCAF1 and CAF1 enhanced the viability of LNCaP cells with a slight increase observed on day 2 (1.08-fold and 1.14-fold, respectively) and a stronger response by day 4 (1.32-fold and 1.38-fold, respectively) (see **Figure 13.a**). In LNCaP C4-2 cells, the effect was more pronounced, where NCAF1 and CAF1 significantly increased the viability on day 4 (1.50-fold and 1.56-fold, respectively), while a more minor increase was seen at day 2 (1.18-fold and 1.35-fold, respectively) (see **Figure 13.b)**.

In pair 2, both NCAF2 and CAF2 showed a robust stimulatory effect on LNCaP viability. At day 2, NCAF2 increased the viability by 1.28-fold and CAF2 by 1.41-fold, and by day 4, the response was further enhanced by 1.78-fold by NCAF2 and 1.83-fold by CAF2 (see **Figure 13.c)**. In LNCaP C4-2 cells, the most substantial effect was observed on day 2, where NCAF2 and CAF2 increased the viability by 1.42-fold and 1.27-fold, respectively. However, by day 4, this effect diminished, and the viability returned close to control values (see **Figure 13.d)**.

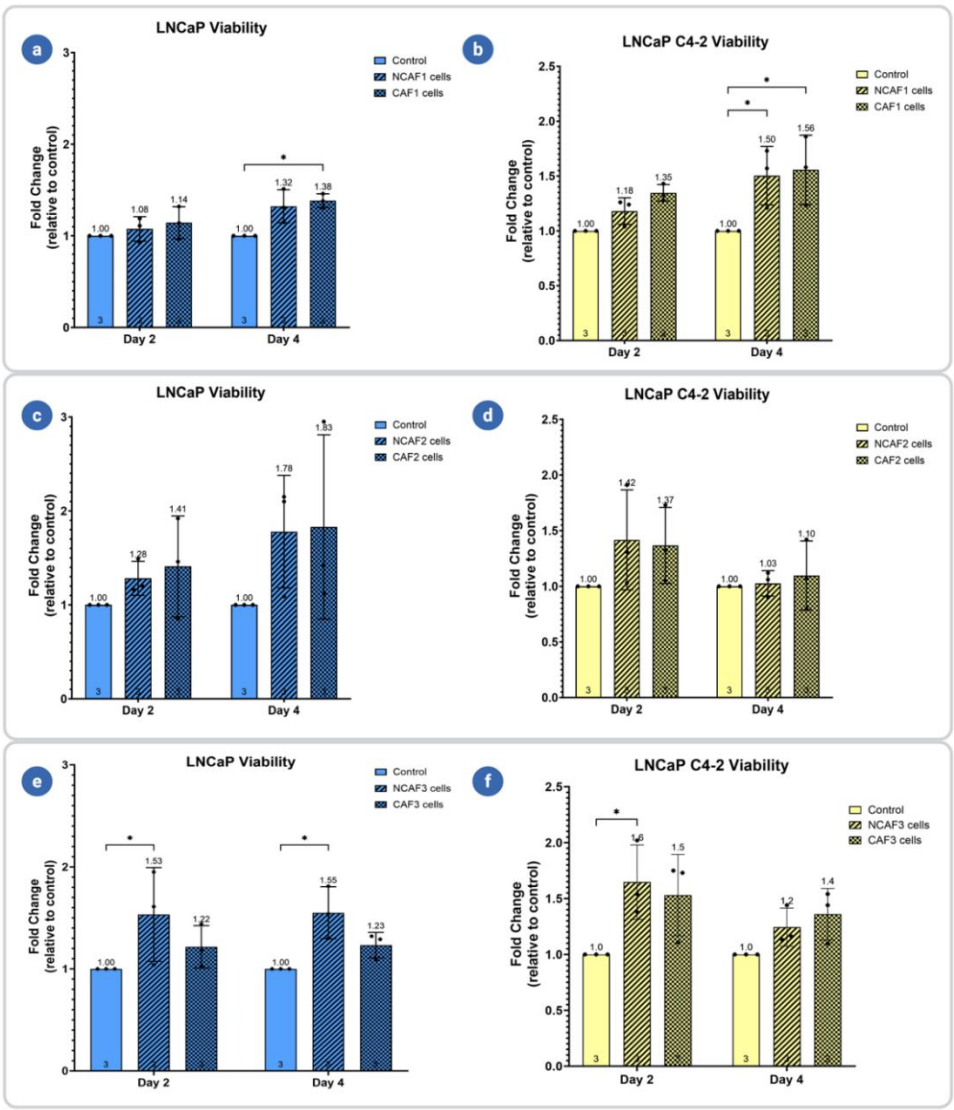

Figure 13: Effect of patient-derived fibroblasts on prostate cancer viability

*(a, b) Pair 1: NCAF1 and CAF1 enhanced viability in both cell lines, with more potent effects on day 4, especially in LNCaP C4-2 cells. (c, d). Pair 2: NCAF2 and CAF2 significantly increased viability in LNCaP cells on days 2 and 4. In LNCaP C4-2 cells, the effect was strong on day 2 but diminished by day 4. (e, f). Pair 3: NCAF3 consistently promoted stronger viability than CAF3 in LNCaP cells, while in LNCaP C4-2 cells, both fibroblast types enhanced viability, with NCAF3 showing a slightly greater effect on day 2. Statistical analysis was performed by two-way ANOVA; *p < 0.05. Data is represented as fold change relative to control ± SD; n=3*

For pair 3, both fibroblast types promoted PCa viability, but the effect was more substantial in NCAFs. In LNCaP cells, NCAF3 increased viability by 1.53-fold on day 2 and 1.55-fold on day 4, while CAF3 induced moderate effects by an increase of 1.22-fold and 1.23-fold on day 2 and day 4, respectively (see **Figure 13.e)**. In LNCaP C4-2 cells, NCAF3 and CAF3 both enhanced the viability on day 2 (1.60-fold and 1.50-fold, respectively), with a more minor but steady effects observed on day 4 (1.20-fold and 1.40-fold, respectively) (see **Figure 13.f)**. Across all three patient-derived fibroblast pairs, fibroblast-induced effects on PCa viability were pair-dependent and varied between NCAFs and CAFs. While CAFs generally exhibited stronger responses in pairs 1 and 2, NCAFs had a slightly greater influence in pair 3. In general, LNCaP C4-2 cells showed higher sensitivity than LNCaP cells, particularly early during co-culture.

14.2.2 Influence of patient-derived fibroblasts in regulating prostate cancer proliferation

To further assess whether the increased viability of PCa cells observed was associated with enhanced proliferation, the proliferation of LNCaP and LNCaP C4-2 cells after co-culture with three patient-derived fibroblast pairs was evaluated. Proliferation was measured on day 2 and day 4 to capture both early and sustained effects.

In pair 1, NCAF1 and CAF1 showed minimal but noticeable influence on LNCaP proliferation, with a slight increase on day 2 (1.17-fold and 1.02-fold, respectively) and further enhancement on day 4 (1.27-fold and 1.18-fold, respectively) was observed (see **Figure 14.a**). In LNCaP C4-2, the stimulatory effect was stronger than in LNCaP cells. On day 2, NCAF1 increased proliferation by 1.55-fold and CAF1 by 1.36-fold, with the effects slightly declining on day 4 (1.25-fold and 1.21-fold, respectively) (see **Figure 14.b**).

In pair 2, both NCAF2 and CAF2 exhibited the strongest proliferative response among all pairs. In LNCaP cells, NCAF2 and CAF2 increased proliferation markedly on day 2 (2.09-fold and 1.68-fold, respectively), which decreased by day 4 to 1.32-fold and 1.21-fold, respectively (see **Figure 14.c**). In LNCaP C4-2 cells, proliferation was also elevated by NCAF2 and CAF2 on day 2 (1.39-fold and 1.28-fold, respectively), but returned to baseline levels by day 4 (1.11-fold and 1.05-fold, respectively) (see **Figure 14.d**).

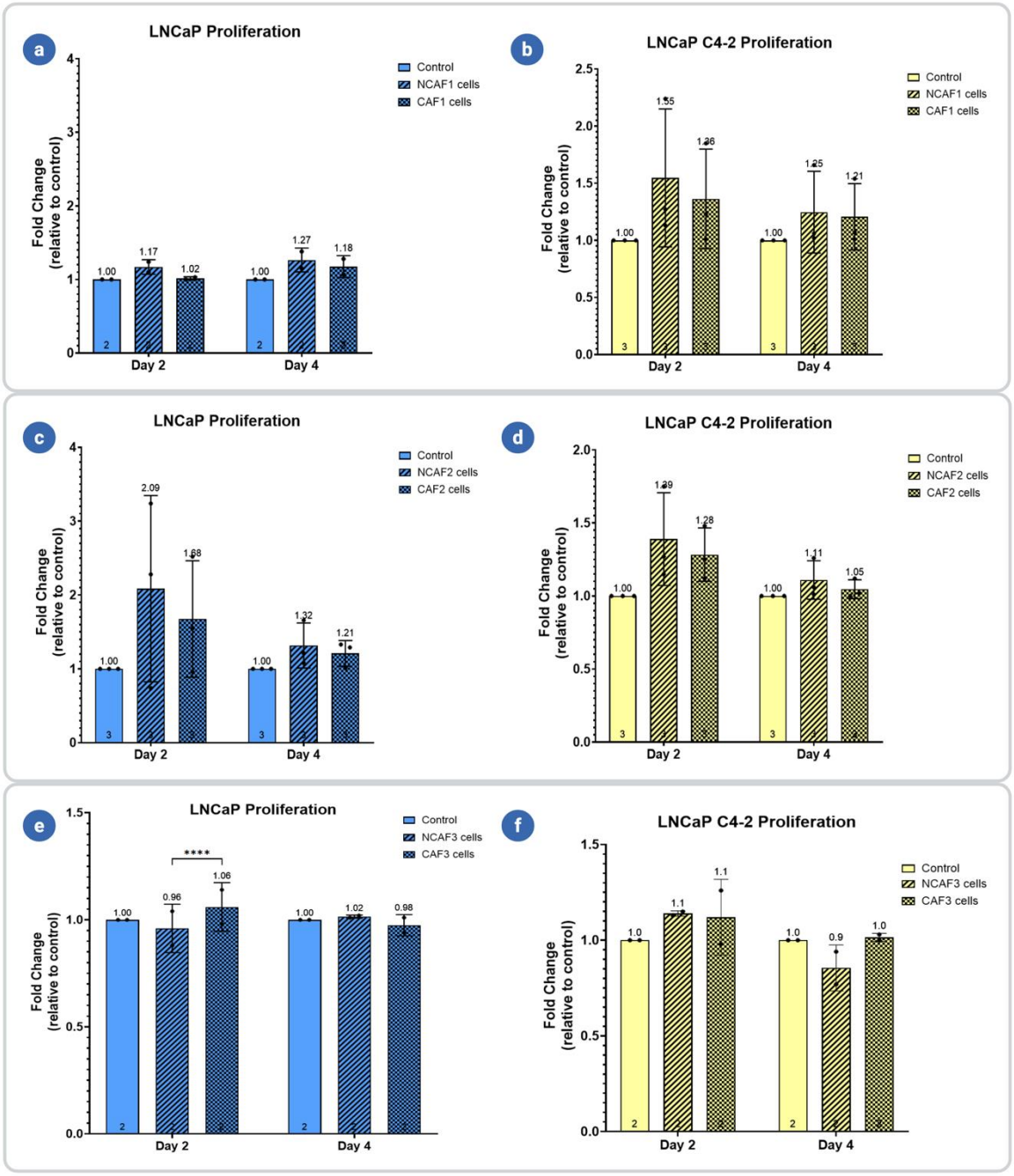

Figure 14: Effect of patient-derived fibroblasts on prostate cancer proliferation.

*(a, b). Pair 1: NCAF1 and CAF1 modestly enhanced LNCaP proliferation, with a stronger and more consistent effect in LNCaP C4-2 cells, particularly at day 2. (c, d). Pair 2: NCAF2 and CAF2 induced the highest proliferation in LNCaP cells on day 2, while the effects on LNCaP C4-2 cells were also significant but declined by day 4. (e, f). Pair 3: NCAF3 and CAF3 had minimal influence on proliferation in both LNCaP and LNCaP C4-2 cells at all timepoints. Statistical analysis was performed by two-way ANOVA; outliers were excluded; *p < 0.05. Data is represented as fold change relative to control ± SD.*

In case of pair 3, NCAF3 and CAF3 had minimal effects on proliferation, with LNCaP cells showing near-baseline levels on day 2 (0.96-fold and 1.06-fold, respectively) and day 4 (1.02-fold and 0.98-fold, respectively) (see **Figure 14.e**). Similarly, LNCaP C4-2

cells exhibited only slight, non-significant changes from NCAF3 and CAF3 on day 2 (1.10-fold for both) and no difference by day 4 (see **Figure 14.f**). Across all three patient-derived fibroblast pairs, the contribution of proliferation varied between pairs. Overall, LNCaP C4-2 cells were more responsive than LNCaP cells and displayed stronger proliferative responses, especially at earlier timepoints.

14.2.3 Influence of patient-derived fibroblasts in regulating prostate cancer motility

In order to determine whether patient-derived fibroblasts influence the migratory potential of PCa cells, migration assays were performed using xCELLigence real-time analysis, and the findings were validated with endpoint transwell migration assays. LNCaP and LNCaP C4-2 cells were indirectly co-cultured with two patient-derived fibroblast pairs. Fibroblasts from pair 2 were excluded from these experiments due to insufficient growth in culture. Interestingly, LNCaP cells did not display any measurable migration in either xCELLigence or endpoint assays under all tested conditions, which is consistent with their less motile phenotype. Therefore, the analysis focused exclusively on the more aggressive LNCaP C4-2 cells.

Real-time assay demonstrated a moderate inhibition of LNCaP C4-2 migration. When co-cultured with NCAF1 and CAF1 fibroblasts, 72% and 86% migration, respectively, were shown, compared to control cells (100%). Among the fibroblasts, CAF1 had a higher migration compared to NCAF1 (see **Figure 15.a**). However, endpoint transwell assays for the same pair revealed a different trend, showing a moderate increase in LNCaP C4-2 migration, reaching 138% with NCAF1 and 144% with CAF1 compared to controls (see **Figure 15.b**). Interestingly, here as well the CAF1 increased migration of LNCaP C4-2 cells compared to NCAF1, similar to real-time assay. Representative microscopic images from transwell inserts show increased cell migration under NCAF1 versus control, and more migration was observed under CAF1 versus NCAF1.

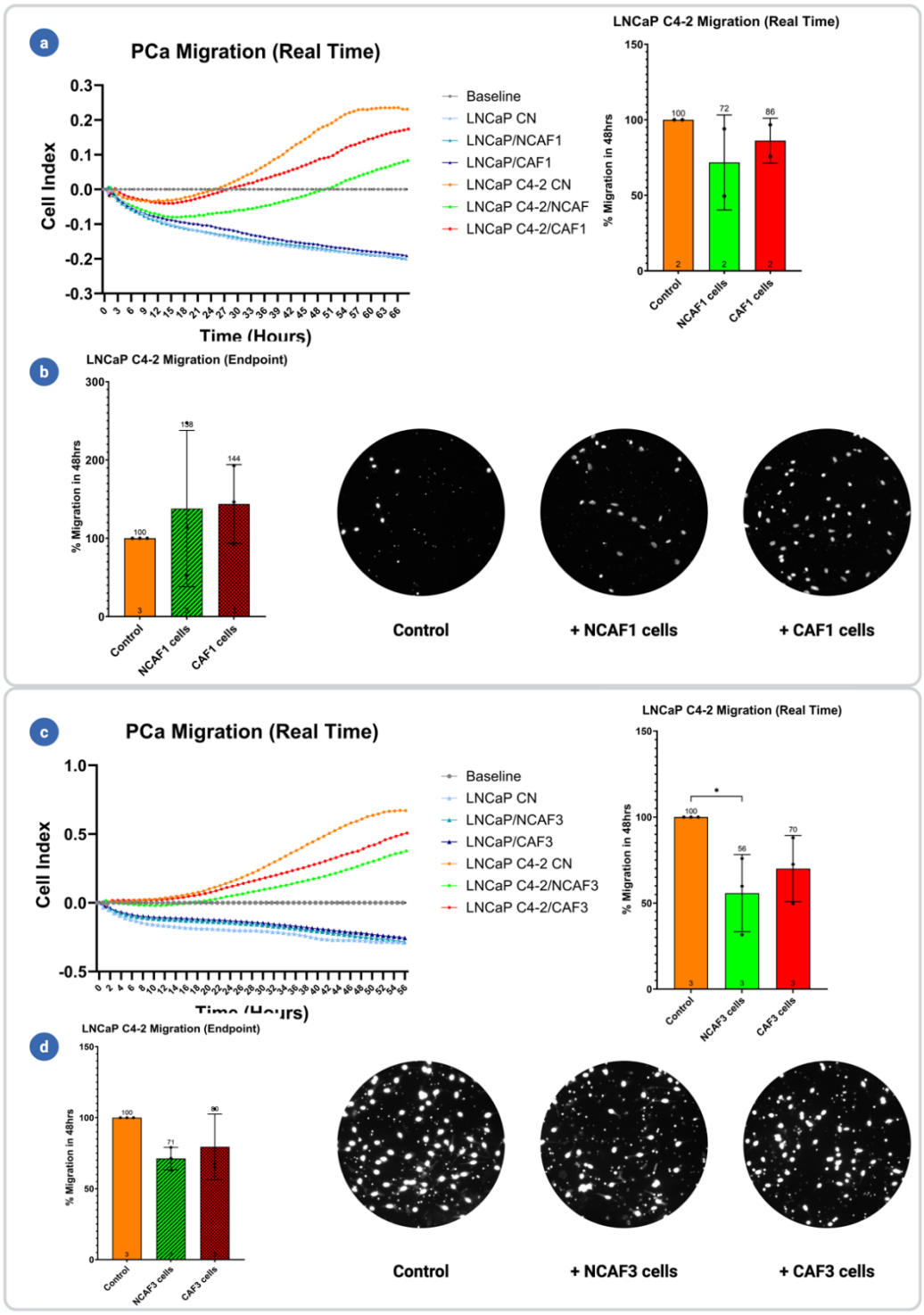

Figure 15: Effect of patient-derived fibroblasts on prostate cancer migration

*(a). Real-time migration of LNCaP and LNCaP C4-2 cells co-cultured with NCAF1 and CAF1 fibroblasts shows reduced migration in LNCaP C4-2 cells (72% NCAF1, 86% CAF1) compared to controls (100%), while LNCaP cells exhibited no migration. (b). Endpoint migration for the same pair showed a moderate increase in LNCaP C4-2 migration (136% NCAF1, 144% CAF1) compared to controls (100%). (c). For NCAF3 and CAF3 fibroblasts, real-time migration on LNCaP C4-2 cells was reduced (56% NCAF3, 70% CAF3) compared to control (100%). (d). Endpoint migration supported this decrease (71% NCAF3, 80% CAF3) compared to controls (100%); Representative images are shown. Statistical analysis was performed by two-way ANOVA; outliers were excluded; *p < 0.05. Data is represented as % migration relative to control ± SD.*

In contrast, fibroblasts from pair 3 consistently reduced migration in both assays. Real-time assay demonstrated a migration of 56% after co-culture with NCAF3 (44% reduction) and 70% migration with CAF3 (30% reduction) versus control (100%) (see **Figure 15.c**). The endpoint assay validated this trend, with migrated cells reduced to 71% with NCAF3 (29% reduction) and 80% with CAF3 (20% reduction) (see **Figure 15.d**). In both real-time and endpoint says, CAF3 resulted in higher migration in LNCaP C4-2 cells compared to NCAF3. Representative microscopic images from transwell inserts confirm the results under NCAF3 and CAF3 conditions. Collectively, these data reveal patient-specific heterogeneity in fibroblast-tumor crosstalk. Pair 3 fibroblasts consistently suppress LNCaP C4-2 migration across methods, whereas pair 1 yielded assay-dependent outcomes.

14.2.4 Influence of exosomes derived from patient-derived fibroblasts in regulating prostate cancer viability

To investigate whether secreted EVs, particularly exosomes, mediated the effects observed during the fibroblast-PCa cellular co-culture, we treated both PCa cells with the exosomes isolated from matched pairs of patient-derived NCAFs and CAFs, and their respective self-exosomes. Exosomes were purified by ultracentrifugation, and cell viability was assessed after 24 hours of treatment. Since the NCAF2/CAF2 pair exhibited poor growth and limited viability during culture, exosomes from a fourth pair of patient-derived fibroblasts (NCAF4/CAF4) were used instead.

For LNCaP cells, treatment with NCAF1- and CAF1-derived exosomes resulted in reduced or maintained PCa viability, with fold changes of 0.86 and 0.91, respectively, compared to control and self-exosomes. These effects were less pronounced in exosomal treatment than the corresponding cellular co-culture, where NCAF1 and CAF1 fibroblasts increased viability. Similarly, in LNCaP C4-2 cells, NCAF1 and CAF1 exosomes showed reduced viability (0.85-fold and -0.91-fold, respectively) compared to control. However, NCAF1 and CAF1 exosomes showed no significant effect compared to LNCaP C4-2 self-exosomes (0.89-fold) (see **Figure 16.a**). Interestingly, self-exosomes from both LNCaP C4-2 cells showed similar decrease in viability as CAF1.

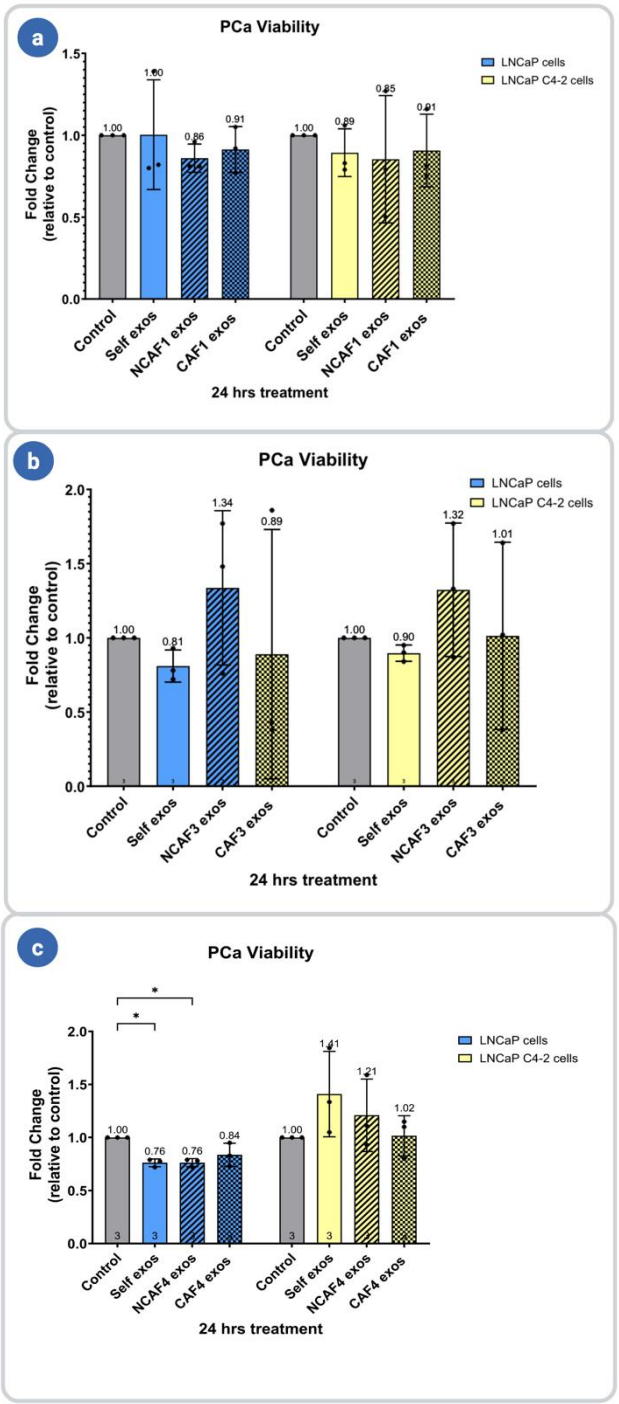

Figure 16: Effect of fibroblast-derived exosomes on prostate cancer viability.

*(a). NCAF1/CAF1, (b). NCAF3/CAF3 and (c). NCAF4/CAF4. Exosomes from PCa cells ("self-exos") were included as controls. Cell viability was measured using the WST assay and expressed as a fold change relative to untreated controls. Statistical analysis was performed by two-way ANOVA; *p < 0.05. Data is represented as % migration relative to control ± SD; n=3.*

Further, in pair 3, the effects observed in co-culture and exosomal treatments partially aligned. NCAF3 exosomes promoted viability by 1.34-fold in LNCaP cells and 1.32-fold in LNCaP C4-2 cells, whereas CAF3 exosomes induced minimal changes, 0.89-

fold in LNCaP and 1.01-fold in LNCaP C4-2 cells (see **Figure 16.b**) compared to control. Notably, in comparison to self-exosomes from both PCa cells, NCAF3 and CAF3 increased viability. These findings indicate that for pair 3, the exosomes derived from fibroblasts likely contribute to the enhanced viability observed in cellular co-cultures where NCAF3 enhanced viability substantially in both PCa cell lines, while CAF3 had a milder effect.

Since pair 2 was unavailable, exosomes from NCAF4 and CAF4 were used. Exosomes derived from the fourth pair of fibroblasts displayed a distinct response. In LNCaP cells, both NCAF4 and CAF4 exosomes significantly reduced the viability by 0.76-fold and 0.84-fold, compared to control. However, in comparison to self-exosomes, CAF4 resulted in increased viability. In contrast, LNCaP C4-2 cells responded differently, showing an increase in viability upon treatment with NCAF4 exosomes (1.21-fold) and CAF4 exosomes did not influence the viability (1.02-fold) compared to control. Interestingly, in comparison to self-exosomes, both NCAF4- and CAF4-exosomes resulted in reduced viability of LNCaP C4-2 (see **Figure 16.c**). Across all fibroblast-derived exosomal treatments, the viability-enhancing effects in cellular co-culture were consistently reproduced in pair 1 with CAF3 resulting in increased viability in both LNCaP and LNCaP C4-2 cells. While pair 1 exosomes aligned closely with co-culture findings, pair 3 exosomes exhibited more variable responses with LNCaP C4-2 cells confirming similar trends and LNCaP cells have the opposite effect.

14.2.5 Influence of exosomes derived from patient-derived fibroblasts in regulating prostate cancer migration

Next, to assess whether fibroblast-derived exosomes influence the migratory behavior of LNCaP C4-2 cells, real-time monitoring with xCELLigence was performed. The effects were compared with cellular co-culture migration data for pairs where both datasets were available, allowing us to distinguish between exosome-mediated and non-exosomal contributions. Treatment with NCAF1 exosomes led to a marked reduction in LNCaP C4-2 migration, lowering it to 55% compared to self-exosomes (101%). In contrast, CAF1 exosomes increased the migration of LNCaP C4-2 cells compared to NCAF1(see **Figure 17.a**). Compared to co-culture data for real-time migration, NCAF1 and CAF1 also reduced migration, and CAF1 increased migration compared to NCAF1 reflecting the cellular trend mediated by exosomes.

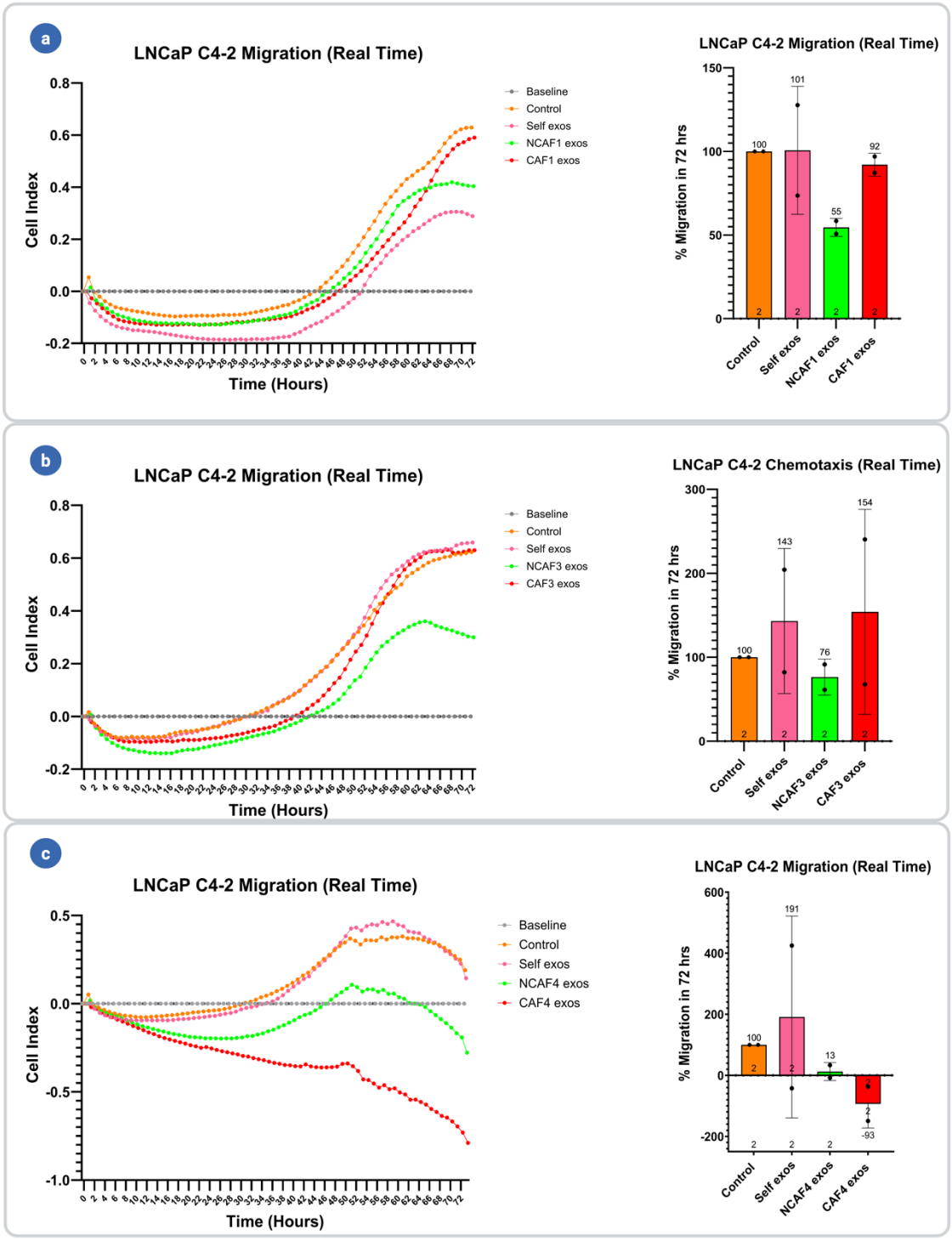

Figure 17:Effect of fibroblast-derived exosomes on prostate cancer migration.

*(a). Pair 1: NCAF1 exosomes reduced migration to 55%, while CAF1 exosomes maintained near-control levels (92%). (b). Pair 3: NCAF3 exosomes reduced migration to 76%, but CAF3 exosomes increased migration to 154%, diverging from co-culture effects. (c). Pair 4: NCAF4 and CAF4 exosomes strongly suppressed migration to 13% and -92%, respectively. Statistical analysis was performed by two-way ANOVA; *p < 0.05. Data is represented as % migration relative to control ± SD; n=2.*

In pair 3, the NCAF3 exosomes led to reduced migration (76%) and CAF3 exosomes led to increased migration (154%) in comparison to self-exosomes (143%) (see **Figure 17.b**). The results from exosomes coordinated with the cellular co-culture data where CAF3 cells also increased migration compared to NCAF3 cells. Exosomes from fibroblasts pair 4 were analyzed independently due to a lack of cellular co-culture data and exhibited a profound inhibitory effect. NCAF4 suppressed migration by 87% and CAF4 completely suppressed the migration of LNCaP C4-2 cells (see **Figure 17.c**). These results indicate that exosomes from pair 4 strongly deliver anti-migratory behavior to LNCaP C4-2 cells. The self-exosomes in case of pair 3 and pair 4 unexpectedly enhanced migration by 43% and 91%, respectively, compared to the control (100%).

These findings confirm our results from cellular co-culture followed by migration for pair 1 and 3. For NCAFs, the inhibitory effects on migration are largely consistent across all pairs.

14.3 Functional assessment of prostate cancer exosomes-mediated effects on patient-derived fibroblast viability

Upon observing the effects of fibroblasts and their exosomes on PCa cell functions, the influence of PCa-derived exosomes on patient-derived fibroblasts was studied, as previous literature has shown promising results. Fibroblasts from three independent patient-derived fibroblast pairs (1, 3 and 4) were treated with exosomes isolated from LNCaP and LNCaP C4-2 cells. Since the results were highly comparable across pairs, the data were analyzed with one outlier replicate excluded from one pair.

Treatment with self-exosomes and LNCaP-derived exosomes consistently reduced fibroblast viability in both NCAFs and CAFs, decreasing it to ~0.88-fold and ~0.76-fold versus control (1). In contrast, LNCaP C4-2-derived exosomes maintained fibroblast viability with values close to controls (~1-1.05-fold). In comparison with self-exosomes, LNCaP exosomes maintained the fibroblasts viability whereas LNCaP C4-2 exosomes increased the viability of both fibroblast types.

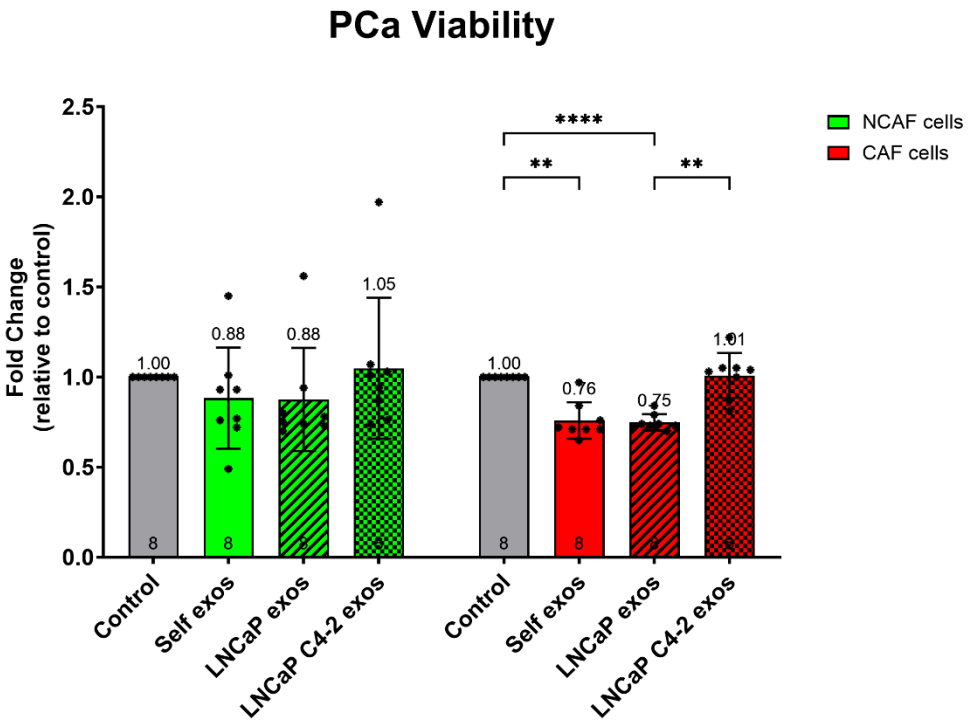

Figure 18: Effect of prostate cancer cells-derived exosomes on patient-derived fibroblast viability.

*Fibroblasts (NCAFs and CAFs) from three patient-derived pairs (1, 3 and 4) were treated for 24 h with exosomes derived from PCa cells and their self-exosomes. Self-exosomes and LNCaP-derived exosomes reduced fibroblast viability in both NCAFs and CAFs (~0.75-fold to ~0.88-fold versus control), whereas LNCaP C4-2-derived exosomes maintained viability (~1-1.05-fold of control). Data were pooled due to comparable responses and one outlier replicate was excluded. Statistical analysis was performed by two-way ANOVA; *p < 0.05, **p < 0.01, ***p < 0.001, ****p < 0.0001. Data is represented as fold change relative to control ± SD; n=8*

These findings indicate that the influence of PCa-derived exosomes on fibroblast viability is cell-line dependent. LNCaP exosomes preserve fibroblast survival, whereas LNCaP C4-2 exosomes largely increase viability.

14.4 Effect of prostate cancer cells and their exosomes on immortalized hTERT foreskin fibroblasts

To determine whether the effects observed with respect to viability of patient-derived NCAFs and CAFs was due to their patient-derived origin, immortalized hTERT foreskin fibroblasts were used as a standardized model system. These cells were selected instead of prostate-derived fibroblasts because they are well-studied and showed consistent growth properties and genetic stability.

As shown in Error! Reference source not found.**a**, cellular co-culture of hTERT fibroblasts with PCa cells for 48 h led to a significant suppression of fibroblast viability compared to untreated controls. Intreasringly, LNCaP cells decreased viability to 0.55-fold on day 2 and 0.58-fold on day 4, while LNCaP C4-2 cells slightly increased viability to 0.62-fold and 0.59-fold respectively.

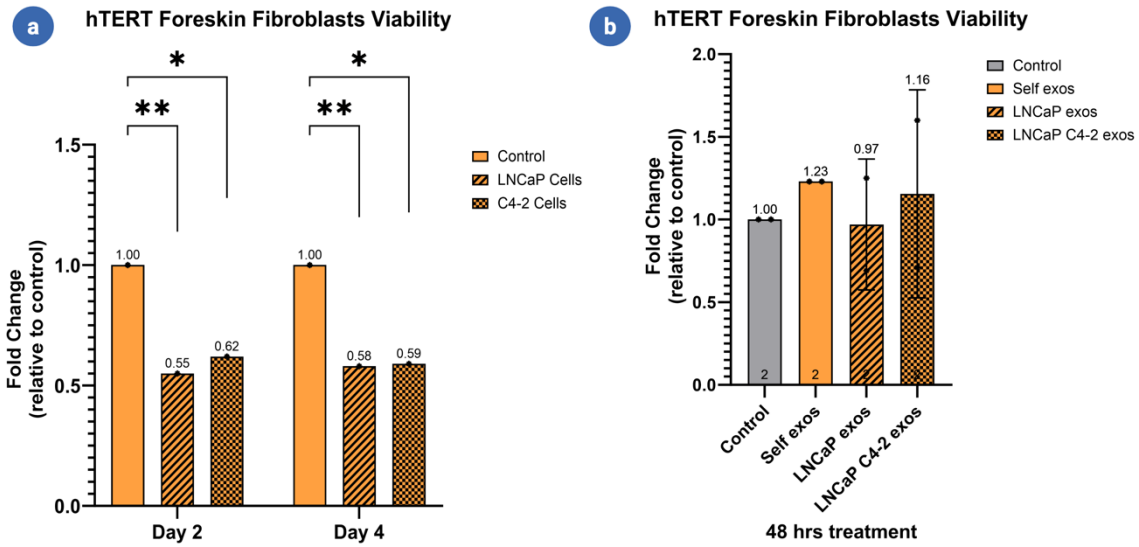

Figure 19: Effect of prostate cancer cells and their exosomes on hTERT fibroblast viability.

*(a). Both LNCaP and LNCaP C4-2 cells significantly suppressed the viability of hTERT fibroblasts; n=1 (b). treatment of hTERT fibroblasts with self-exosomes and PCa-derived exosomes for 48 h shows no significant reduction in viability; n=2. Statistical analysis was performed by two-way ANOVA; *p < 0.05, **p < 0.01. Data is represented as fold change relative to control ± SD.*

Then, the influence of PCa-derived exosomes on hTERT viability was determined as shown in Error! Reference source not found.**b**. Treatment of hTERT fibroblasts with LNCaP- and LNCaP C4-2-derived exosomes for 48 h exhibited preserved viability in the case of LNCaP exosomes (0.97-fold versus control) and an increased viability in the case of LNCaP C4-2 exosomes (1.16-fold versus control). Interestingly, in comparison to self-exosomes, the exosomal experiments were in coordination with the cellular experiments and the LNCaP C4-2 exosomes enhanced the viability of hTERT cells compared to LNCaP exosomes.

14.5 Assessment of α-SMA in hTERT fibroblasts after co-culture with prostate cancer cells

To assess whether the exposure to PCa cells influences the activation of hTERT fibroblast, the α-SMA expression was analyzed using western blotting after 48 h co-culture with LNCaP and LNCaP C4-2 cells. Surprisingly, hTERT fibroblasts exhibited a significant reduction in α-SMA expression after co-culture with both PCa cells.

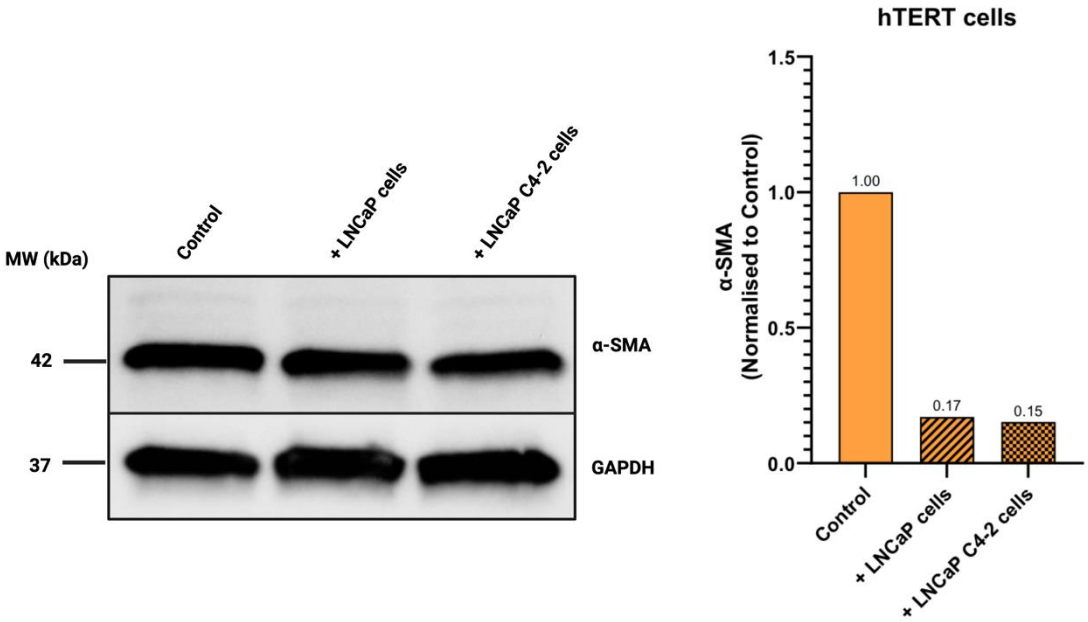

Figure 20: α-SMA expression in hTERT fibroblasts after co-culture with prostate cancer cells.

Western blotting analysis showing α-SMA expression in hTERT fibroblasts after 48 h of indirect co-culture with LNCaP and LNCaP C4-2 cells. Densitometric quantification normalized to control (1.0) revealed a reduction of α-SMA expression level to 0.17 and 0.15 upon co-culture with LNCaP and LNCaP C4-2 cells, respectively. GAPDH was used as the loading control.

Quantification revealed that α-SMA expression decreased to approximately 0.17-fold following co-culture with LNCaP cells and 0.15-fold with LNCaP C4-2 cells compared to untreated controls, where expression was normalized to 1.0.

14.6 Identification and Validation of miRNA Pattern in Patient-derived Prostate Fibroblasts and their exosomes

Global miRNA expression profiling was performed using patient-derived fibroblast pairs and their exosomes to identify the possible miRNAs associated with the activation of

prostate NCAFs and CAFs. A microarray-based screening detected differentially expressed miRNAs between the two fibroblast types. Further to validate the microarray findings, a subset of consistently upregulated miRNAs was selected for qPCR analysis of both cellular and exosomal fractions. The combined approach allows us to confirm the microarray data's reliability and assess their roles in prostate cancer development and progression.

14.6.1 Microarray-Based Identification of Differentially Expressed miRNAs

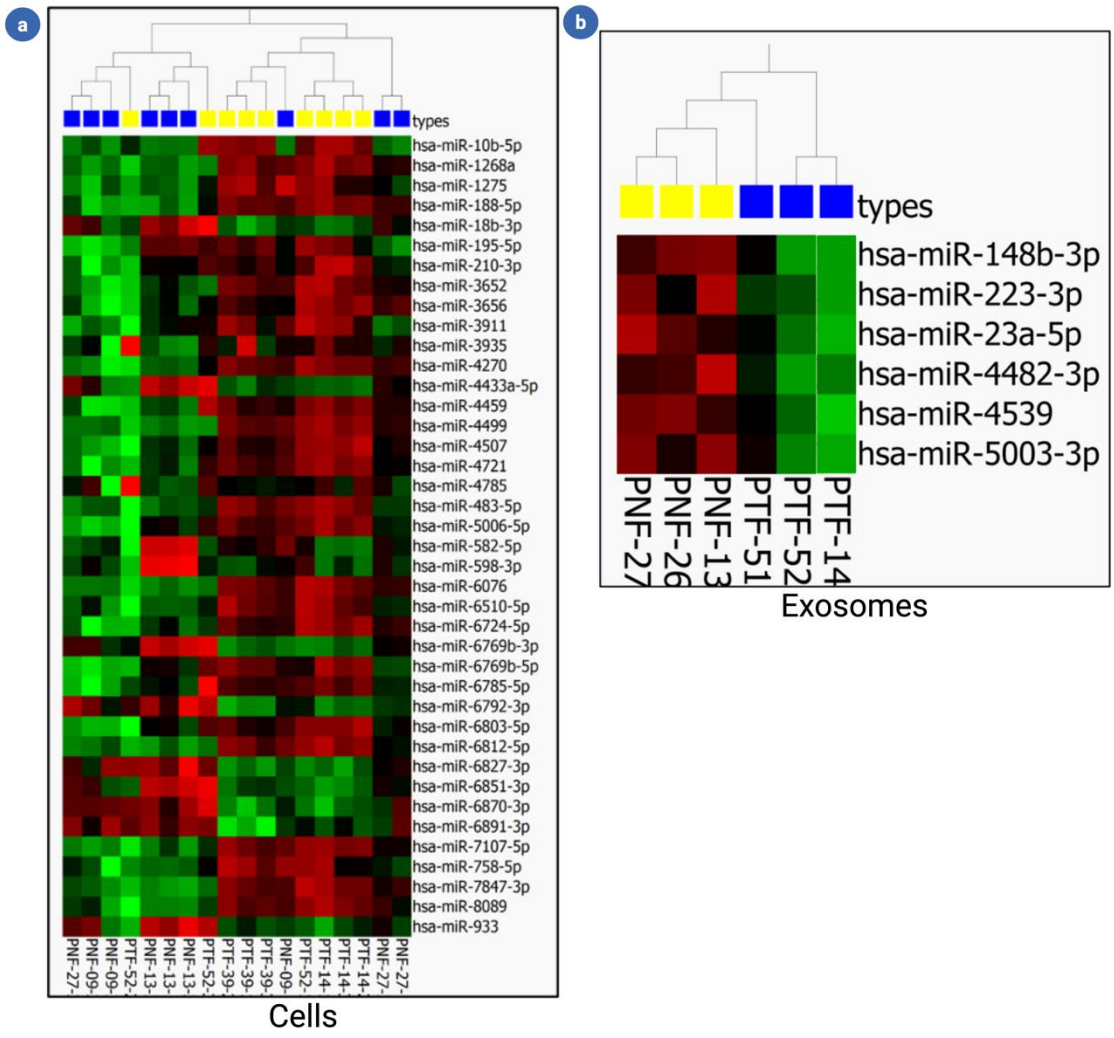

Figure 21: Global microarray profiling of cellular and exosomal miRNAs derived from patient prostate fibroblasts.

(a). Heatmap showing hierarchical clustering of differentially expressed cellular miRNAs in CAFs (PTFs-yellow) versus NCAFs (PNFs-blue). (b). Heatmap of exosomal miRNA expression profiles showing distinct clustering between CAF-derived (PTFs-blue) and NCAF-derived exosomes (PNFs-yellow). Red represents upregulated expression and green indicates downregulation.

Microarray profiling revealed distinct miRNA expression patterns between CAFs and NCAFs in cells and exosomes. 41 miRNAs were identified to be differentially expressed in both NCAFs and CAFs and 6 miRNAs in their exosomes based on their p-values (**Table 15**). Among them, miR-10b-5p and miR-210-3p, upregulated in CAFs, and miR-148b-3p and miR-223-3p, upregulated in CAF-derived exosomes, were selected for further validation by qPCR based on their p-value (**Table 15**) and literature.

Table 15. List of expressed cellular and exosomal miRNAs

Cellular miRNAs	**p-value**
hsa-miR-10b-5p	0.00000001686
hsa-miR-1268a	0.0385
hsa-miR-1275	0.0230
hsa-miR-188-5p	0.0102
hsa-miR-18b-3p	0.0469
hsa-miR-195-5p	0.0297
hsa-miR-210-3p	0.0202
hsa-miR-3652	0.0499
hsa-miR-3656	0.0444
hsa-miR-3911	0.0420
hsa-miR-3935	0.0084
hsa-miR-4270	0.0221
hsa-miR-4433a-5p	0.0351
hsa-miR-4459	0.0086
hsa-miR-4499	0.0462
hsa-miR-4507	0.0471
hsa-miR-4721	0.0109
hsa-miR-4785	0.0476
hsa-miR-483-5p	0.0267
hsa-miR-5006-5p	0.0402
hsa -miR-582-5p	0,0283
hsa-miR-598-3p	0.0229
hsa-miR-6076	0.0309
hsa-miR-6510-5p	0.0392
hsa-miR-6724-5p	0.0320
hsa-miR-6769b-3p	0,0370
hsa-miR-6769b-5p	0.0046
hsa-miR-6785-5p	0.0024
hsa-miR-6792-3p	0.0294
hsa-miR-6803-5p	0.0499
hsa-miR-6812-5p	0.0166

hsa-miR-6827-3p	0.0142
hsa-miR-6851-3p	0.0351
hsa-miR-6870-3p	0.0224
hsa-miR-6891-3p	0.0186
hsa-miR-7107-5p	0.0204
hsa-miR-758-5p	0.0158
hsa-miR-7847-3p	0.0242
hsa-miR-8089	0.0446
hsa-miR-933	0.0363
Exosomal miRNAs	**p-value**
hsa-miR-148b-3p	0.0240
hsa-miR-223-3p	0.0277
hsa-miR-23a-5p	0.0377
hsa-miR-4482-3p	0.0245
hsa-miR-4539	0.0327
hsa-miR-5003-3p	0.0450

14.6.2 Validation of selected upregulated miRNAs

To confirm the findings of microarray, qPCR was performed to validate the selected four miRNAs (miR-10b-5p, miR-223-3p, miR-210-3p and miR-148-3p) that were differentially expressed among cellular and exosomal fractions of NCAFs and CAFs. qPCR analysis was performed using three independent normalization strategies with miR-361-5p, miR-191-5p and RNU48 as reference controls. This ensures the choice of internal control does not influence the expression differences and allows for a consistent confirmation of observed trends.

qPCR analysis confirmed significant and consistent upregulation of miR-10b-5p and miR-210-3p in CAFs compared to NCAFs across all normalization strategies (**Figure 22.** a-c). When normalized to miR-361-5p (**Figure 22.a**), both miRNAs showed statistically significant elevation in CAFs. Similar results were obtained with miR-191-5p (**Figure 22.b**), further supporting their upregulation. Normalization with RNU48 (**Figure 22.c**) again confirmed these trends. The exosomal miRNAs miR-148-3p and miR-223-3p expression patterns could also be confirmed to be upregulated in NCAFs in the cellular fractions. Analysis of exosomal miRNAs revealed that miR-10b-5p and miR-210-3p were also enriched in CAF-derived exosomes compared to NCAF-derived exosomes. When normalized to miR-361-5p (**Figure 22.d**), both miRNAs showed clear enrichment in CAF

exosomes, a pattern, consistently reproduced with miR-191-5p and RNU48. In contrast, miR-210-3p and miR-148b-3p upregulation in NCAF-derived exosomes could not be confirmed in exosomal fraction.

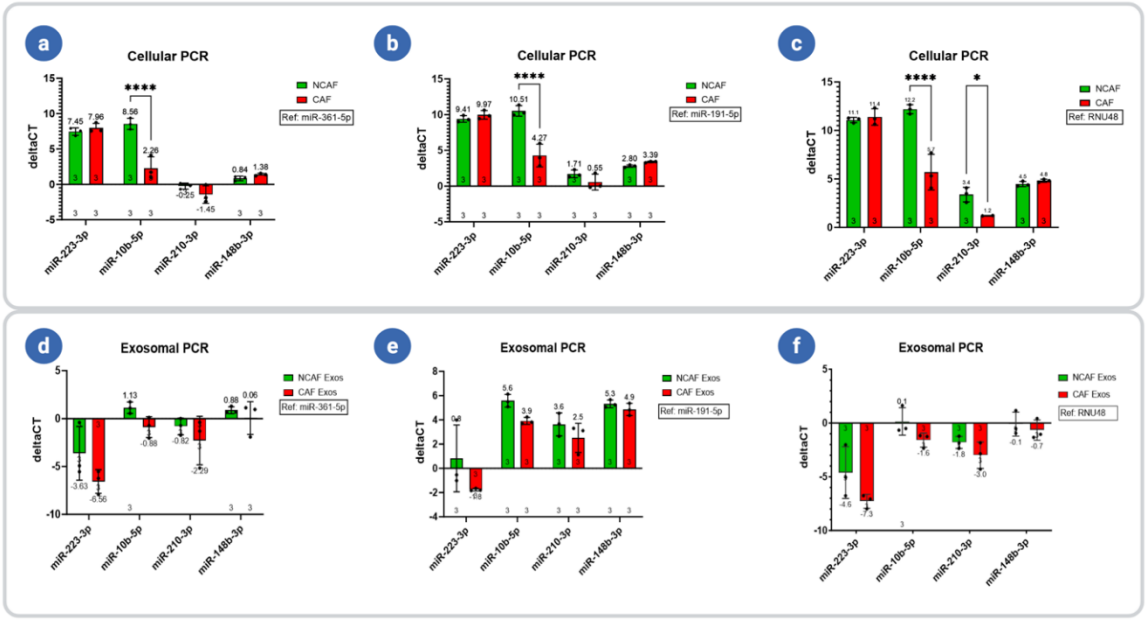

Figure 22: qPCR validation of cellular and exosomal miRNAs from NCAFs and CAFs.

*Expression analysis of miR-223-3p, miR-10b-5p, miR-210-3p and miR-148b-3p in patient-derived fibroblasts and their corresponding exosomes. Results are shown for three different normalization strategies using independent reference controls: (a, d). normalization against miR-361-5p; (b, e). normalization against miR-191-5p; (c, f). normalization against RNU48. Statistical analysis was performed by two-way ANOVA; *p < 0.05, **p < 0.01; ***p < 0.001, ****p < 0.0001. Data is represented as fold change relative to control ± SD.*

15 DISCUSSION

15.1 Exosome Characterization and Compliance with MISEV

Accurate exosome characterization based on the MISEV2018 guidelines (Théry et al. 2018; Welsh et al. 2024) is essential to draw biologically relevant conclusions from the functional experiments. Characterization builds a robust foundation, particularly when working with primary patient-derived fibroblasts, where inter-patient heterogeneity strongly influences secretion patterns and cargo composition. In this study, exosomes were isolated using differential centrifugation following established protocols in our group. This method was chosen for its widespread use and ability to enrich for small EVs while maintaining structural integrity. Potential limitations of UC such as co-isolation of protein aggregates or microvesicles were mitigated through careful sample handling and washing steps. This work used a multi-faceted approach using NTA, TEM and western blot profiling to confirm exosome size, morphology, marker expression and preparation purity across four matched pairs of NCAFs and CAFs

Particle size and concentration were determined using NTA. NTA was performed under standardized conditions, using identical camera settings, detection thresholds and dilution factors to minimize technical variability. Exosomes derived from both fibroblast types were predominantly within the 50-150 nm size range, characteristic of exosomes. However, in some samples, multiple size peaks were observed, most likely reflecting the heterogeneity of vesicular populations. This heterogeneity can result not only from the biological diversity of exosomes but also from technical factors such as vesicle aggregation or differences in refractive index which influence light scattering for NTA. In addition to classical exosomes, smaller microvesicles or distinct subpopulation of exosomes maybe present in the isolates, differing in size and molecular composition appearing as mixed population. Similar findings have been reported in literature and are considered to represent biological diversity of EVs and the methodological limitations of the isolation procedure (Kowal et al. 2016). Additionally, consistent and striking differences were observed in particle concentrations between matched NCAF and CAF pairs. Across all three patient-derived fibroblast pairs, CAF-derived exosomes exhibited higher particle yields than their matched NCAFs, suggesting a conserved CAF-driven secretory phenotype.

To further ensure accuracy, all samples were measured in duplicates and the mean particle concentrations were calculated, reducing variability due to swarm detection or clumping. Interestingly, CAF1-exosomes exhibited highest overall particle yield among all samples, despite originating from a 48-year-old patient with Gleason 7a tumor. While high EV production is often associated with advanced disease, several studies have shown that stromal activation can occur in early and intermediate tumors, driven by tumor-derived paracrine factors rather than tumor grade alone. Signaling pathways, including TGF-β, Wnt5A and IL-6, are known to reprogram fibroblasts into secretory, pro-tumorigenic phenotypes even in intermediate Gleason cases (Nedaeinia et al. 2024; Peng et al. 2023). This exceptionally high CAF1 particle yield may therefore be attributed to early stromal activity, potentially enhanced by biopsy localization effects, as fibroblasts sampled near invasive tumors tend to exhibit stronger secretory behavior due to hypoxia and elevated cytokine exposure (Pacheco-Torres et al. 2024). Additional technical considerations such as slight variations in centrifugation efficiency or pipetting may also influence the absolute particle count although the overall trend remains biologically relevant.

In contrast, CAF3-exosomes derived from a 52-year-old patient with a Gleason 9 tumor displayed moderate exosome yields despite originating from a highly aggressive tumor microenvironment. This suggests that particle concentration does not directly reflect disease severity. Furthermore, CAF2-exosomes from a 65-year-old with Gleason 7a exhibited intermediate particle concentration, supporting patient-specific differences in stromal responses. NTA measurements could be influenced not only by biological variability but also by technical factors. Although standard isolation protocol and measurement parameters were used, variability in sample viscosity, clumping and swarm detection can affect accurate particle counting and size distributions (Tian et al. 2024). Furthermore, NTA relies on light-scattering properties, meaning vesicles with heterogeneous refractive indices, commonly observed in patient-derived exosomes may generate apparent differences in concentration independent of accurate secretion rates (Dragovic et al. 2011). Thus, while the results indicate a genuine CAF-driven increase in exosome output, technical variability may contribute to subtle differences between samples. Taken together, these considerations underline the importance of combining NTA with complementary techniques to achieve reliable characterization.

TEM imaging further validated exosome morphology, showing a well-preserved cup-shaped structure across all samples, indicating intact exosomal preparations. TEM samples were prepared by negatively staining with uranyl acetate and images were captured at multiple magnifications to ensure representative visualization of exosome morphology. Care was taken to avoid grid drying artifacts and excessive electron beam exposure which could lead to vesicle collapse. Despite overall structural similarity, CAF3-exosomes showed slightly irregular surface features across the sample. This difference may reflect an artefact during TEM preparation. Dehydration, staining inconsistencies and grid preparation can induce distortions or structural collapse (Dragovic et al. 2011).

Western blotting assessed canonical exosomal markers (CD63, CD81 and Syntenin) and cellular markers (Calreticulin and GM130). NCAF- and CAF-exosomes showed strong enrichment of exosomal markers and no cellular contamination, confirming a high purity of isolated exosomes. Western blot samples were loaded based on protein content determined by BCA assay to ensure equal loading and multiple exposures were captured to verify signal integrity. Since western blot data are unavailable for other pairs, future work incorporating marker profiling for all pairs would help validate whether particle yield differences observed by NTA are also reflected at the molecular level in protein expression.

15.2 Functional Influence of NCAFs and CAFs on Prostate Cancer Progression

The functional analyses performed in this work demonstrate that CAFs influence PCa cell behavior in a patient-specific and context-dependent manner. By comparing cellular co-culture experiments with exosomal treatments, variable effects on PCa cell viability, proliferation and migration were observed across four patient-derived fibroblast pairs. The mixed responses we observed across fibroblast pairs reflect a three-way dialogue between patient-specific stromal reprogramming, EV cargo and recipient tumor cell biology.

In cellular co-culture, CAF1 enhanced the viability of PCa cells, whereas NCAF1 induced stronger proliferation. Cellular co-culture experiments were performed using transwell inserts to separate fibroblasts and tumor cells while allowing exchange of soluble factors, mimicking paracrine interactions without direct contact. Additionally, all experiments were performed in triplicates or duplicates, and the cells were seeded at standardized numbers to minimize variability arising from differential confluency. Viability

was assessed using WST-1 assay, which reflects mitochondrial activity, while BrdU incorporation assays provided measure of DNA synthesis to directly evaluate proliferation. The survival versus proliferation results from CAFs often being pro-survival and involved in therapy-tolerant signaling like TGF-β, IL-6, PI3-Akt and metabolic support (Madorran et al. 2024). Furthermore, this apparent divergence between survival and proliferation maybe explained by a dual mechanism that define cellular viability, the proliferation rate and the degree of apoptosis. A higher viability can therefore arise either from increased proliferative capacity or from reduced apoptotic activity, depending on the dominant regulatory signals (Hanahan and Weinberg 2011). Thus, the observed increase in viability in the presence of CAF1 may result not only from proliferative effects but also from an attenuation of apoptosis, while NCAF1 predominantly promoted proliferation. Apoptotic contribution to viability could therefore be indirectly inferred from the divergence between viability and proliferation. NCAFs may supply mitogenic factors like FGF and HGF that reflect as BrdU-positive S phase entry (Yu, Wang, and Wang 2022; Zhao et al. 2023). LNCaP cells did not migrate, and an increased migration was observed in LNCaP C4-2 cells after co-culture with CAF1 in both xCELLigence and endpoint assays compared to NCAF1. However, an assay-based discrepancy was observed in this pair in general.

In pair 2, CAF2 enhanced survival, while NCAF2 induced higher proliferation, similar to pair 1. The effects in pair 2 were also partially time dependent, with a reduction in overall viability and proliferation observed on day 4 compared to day 2 in most cases. Time-dependent assay setup were designed to capture both early and late responses, revealing dynamic interactions between fibroblasts and tumor cells that may evolve over several days. Migration assays were not performed for pair 2 due to insufficient growth after cellular viability and proliferation experiments, which also prevented exosome isolation for further experiments.

In the third pair, opposite effects concerning viability and proliferation were observed after cellular co-culture. Here, NCAF3 enhanced viability, whereas both NCAF3 and CAF3 more or less maintained the proliferation of both PCa cells. Pair 3 exhibited consistent pro-migratory effects in both cellular assays. In both xCELLigence and endpoint assays, CAF3 increased migration compared to NCAF3. This suggests that CAF3 is programmed towards metastases-supportive signaling, consistent with its origin from a high-grade tumor with Gleason 9, where tumor-driven hypoxia and TGF-β activation enhance fibroblast

reprogramming (Pacheco-Torres et al. 2024; Shi et al. 2020). Both fibroblast types led to decreased migration of LNCaP C4-2 cells in case of pair 4.

The differences observed across cellular co-culture in this study are likely a combination of biological patient-based heterogeneity and subtle experimental variables. The use of primary patient-derived fibroblasts captures true biological diversity but also introduces variability due to donor age, tumor stage and fibroblast passage number. To mitigate this, all fibroblasts were used at early passages (P3- P15), minimizing senescence-related effects while maintaining functional relevance as much as possible. Indirect fibroblast-tumor co-cultures provide a continuous, bi-directional communication between cells enabling prolonged exposure to soluble factors, ECM remodeling enzymes and juxtracrine signals. Moreover, outcomes can vary between assays; for example, WST-based viability measurements reflect mitochondrial metabolic activity rather than absolute cell numbers. BrdU incorporation measures DNA synthesis, explaining why fibroblasts sometimes enhance metabolic survival without proportionally increasing proliferation. Similarly, discrepancies in migration could partly stem from the methodological differences. xCELLigence real-time impedance captures dynamic migratory events, including early migration, whereas transwell endpoint assays provide a cumulative cell count and may underrepresent subtle, time-dependent phenotypes.

All experiments were carefully controlled for seeding density, serum concentration and incubation times to ensure comparability. Media controls without fibroblasts were included to account for baseline proliferation, viability and migration. The differences between the PCa cell types also play an important role in the observed effects. LNCaP is androgen-dependent and intrinsically poorly migratory, while LNCaP C4-2 cells are derived from LNCaP but are androgen-independent with greater motility and mesenchymal features. This explains the greater effects of fibroblasts on the migration of LNCaP C4-2 cells, and LNCaP often fails to migrate altogether. These differences have been documented earlier and provide a mechanistic backdrop for our work (Ghassemi et al. 2020; Sommer et al. 2022).

15.3 Functional Influence of NCAF- and CAF-Exosomes on Prostate Cancer Progression

The functional analyses performed in this work demonstrate that CAFs-exosomes also influence PCa cell behavior in a patient-specific and context-dependent manner along with cells. While CAFs secreted more exosomes than NCAFs, their functional effects were not directly correlated with particle secretion. This emphasizes that exosome cargo rather than particle numbers are critical for modulating PCa cell behavior. This further highlights that exosome cargo and assay-specific factors are central determinants of their role in PCa progression. Exosomal treatments were performed by isolating exosomes using UC followed by resuspension in PBS. A fixed concentration of exosomes were applied per well in functional assays to maintain comparability. Treatment duration was set at 24-48 h depending on assays. CAF1-exosomes enhanced or maintained PCa viability and migration close to self-exosome levels compared to NCAF1 in exosomal treatments. These findings demonstrate that CAF1's high exosome yield is not inherently linked to pro-migratory or survival behavior without enrichment of cargo required for the downstream signaling. Exosomal viability and migration data are unavailable for pair 2. However, exosomal experiments in pair 3 revealed a contrasting pattern where NCAF3-exosome enhanced viability in both PCa cells compared to CAF3. However, CAF3 had a strong pro-migratory effect on LNCaP C4-2 cells.

This divergence highlights a possible functional specialization between NCAF- and CAF-exosomes. NCAFs likely secrete exosomes enriched in growth-supportive cargo that enhances survival and mitochondrial activity whereas CAF-exosomes appear to carry cargo that promotes EMT and migration. Studies have shown that CAF-derived exosomes from high-grade prostate tumors are enriched in pro-invasive miRNAs such as miR-1290, which activates the GSK3β-catenin pathway to enhance PCa migration and metastasis (Wang et al. 2022). Similarly, under hypoxic TME, CAF-exosomes become enriched with miR-500a-3p, accelerating EMT and metastases through FBxW7/HSF1 pathway modulation (Liu et al. 2024). Pair 4 fibroblast exosomes contributed moderately to PCa viability. CAF4-exosomes slightly enhanced LNCaP viability, whereas NCAF4 enhanced LNCaP C4-2 viability. Interestingly, NCAF4-exosomes mirror patterns seen in NCAF1- and NCAF3-exosomes in consistently reducing migration of LNCaP C4-2 cells, whereas CAF-exosomes possibly require selective cargo programming to become pro-invasive (Urabe et al. 2024).

Exosome isolation, preparation and dosing can also have an effect, particularly in the case of patient-derived exosomes, due to limited yield, which leads to multiple isolations at different cell passages between the different functional experiments. To minimize batch-to-batch variability, all exosome isolations were performed under identical centrifugation speeds, rotors, duration, and storage was standardized at -80 °C until use. A further challenge in this field is that the dosage of exosomes for in-vitro assays is not universally defined but based on various factors like the exosome yield from cell lines, isolation method and available previous literature. Different studies employ varying concentrations leading to outcomes that may differ depending on whether dosing is based on particle number, protein content or volume of conditioned medium. This lack of standardization complicates direct comparisons across studies and may partially account for the heterogeneous results reported in literature. Further, in this context, we did not perform systemic testing of different concentration of exosomes. The main reason being the limited yield of fibroblast-derived exosomes, especially from patient-derived primary fibroblasts. Therefore, testing a broad range of concentrations would have required large amounts of exosomes, which in turn would have risked depleting the available exosomes before functional experiments could be completed. Moreover, primary fibroblasts have a restricted proliferation capacity in culture and prolonged passaging can lead to stagnation, senescence or phenotypic drift. These biological constraints made it necessary to prioritize the use of available exosome preparations for functional assays rather than for extensive dosing trials. In our experiments, the concentration of exosomes was normalized based on total protein content, which is a commonly applied but imperfect standard in the field. Protein based dosing does not always directly reflect the number of vesicles or their functional cargo, as protein levels may also include co-isolated contaminants or reflect differences in vesicle surface protein expression. This can lead to subtle variations in biological readouts since two preparations with equal protein content may still differ in actual vesicle number or functional potency. Nonetheless, protein normalization was used here to ensure comparability across experiments, while recognizing and accepting the limitations.

In our study, we also used self-exosomes, meaning exosomes derived from the same fibroblast population under investigation to serve as an internal control. This approach allows us to differentiate whether functional effects are truly due to crosstalk between fibroblasts and tumor cells or are simply a consequence of the general presence of EVs. It also helps to control for the possibility that very high exosome concentrations could trigger

unspecific stress responses or artifact-like effects in recipient cells, independent of their cellular origin. By including self-exosomes as a reference, the observed changes were ensured to be not merely the result of exosome overload but reflected fibroblast-specific signaling differences. Using self-exosomes therefore provided a baseline for evaluating the specificity of CAF-and NCAF-derived exosome effects on PCa cells. Finally, patient-specific factors, such as tumor Gleason grade, stromal activation status and fibroblast senescence, could influence the functional outcomes independently of assay design. Together, these factors support the observed outcomes across the functional assays arising from an interplay of tumor cell biology, fibroblast heterogeneity, exosome composition and technical limitations rather than representing experimental inconsistencies. In exosomal treatments, a finite and standardized exosome dosage and treatment schedule is maintained, potentially underrepresenting cumulative and continuous effects on PCa cells.

15.4 Reciprocal Effects of Prostate Cancer Cells and their Exosomes on Patient-derived Fibroblasts

This work further aimed to investigate the reciprocal crosstalk between the PCa cells and the fibroblasts. While the previous section focused on how fibroblasts and their exosomes influence PCa cell behavior, it is equally important to understand the opposite, as this bidirectional interaction is a critical driver of tumor progression and therapy resistance (Giannoni et al. 2010). The TME is highly dynamic and evidence demonstrates that cancer cells actively reprogram adjacent fibroblasts by releasing soluble factors, EVs and direct contact- dependent signaling, converting quiescent NCAFs into activated CAFs that support tumor growth, invasion and metastasis (Wu et al. 2023).

To assess the impact of PCa-exosomes on fibroblast behavior, exosomes isolated from both LNCaP, and C4-2 cells were treated on fibroblasts. The results were analyzed collectively since the observed effects were consistent across all tested fibroblasts. Treatment with LNCaP-exosomes maintained fibroblast viability, while LNCaP C4-2 exosomes enhanced fibroblast viability. These differences likely reflect the intrinsic molecular differences between LNCaP and LNCaP C4-2 cells. LNCaP cells represent an androgen-dependent, less aggressive phenotype with a primarily homeostatic and growth-maintaining phenotype. Exosomes released from LNCaP are reported to contain moderate levels of EGFR ligands (Kharmate et al. 2016), integrins such as αvβ3 and αvβ6

(Vlaeminck-Guillem 2018) and miRNAs involved in sustaining metabolic balance without driving excess activation. In contrast, LNCaP C4-2-exosomes, which represent a castration-resistant and more aggressive lineage with a cargo profile enriched in pro-invasive factors that activate fibroblast survival pathways, including PI3K/Akt, STAT3 and MAPK cascades, thereby boosting fibroblast metabolic fitness and enhancing their transition towards CAF-like phenotype. The enhanced CAF survival may reflect a feed-forward signaling loop in which PCa cells maintain the survival and activation factors, thereby sustaining pro-tumorigenic stroma. In contrast, NCAFs, lacking prior activation, may require vigorous or prolonged stimulation to achieve similar levels of responsiveness.

To further validate the findings obtained from patient-derived fibroblasts and minimize biological variability, we used hTERT-immortalized human foreskin fibroblasts as a standard reference model. These fibroblasts are widely used as controls in prostate tumor-stroma interaction studies due to their stable growth, reduced senescence and reproducible responses compared to primary cells (Kogan et al. 2006). In our experiments, hTERT fibroblasts were subjected to both cellular co-culture with PCa cells and treatment with PCa-exosomes to assess viability. Interestingly, PCa cells reduced hTERT viability, whereas PCa-exosomes confirmed the effects observed in primary fibroblast pairs. LNCaP C4-2-exosomes enhanced the viability of hTERT cells compared to LNCaP-exosomes, confirming that the effects were not limited to patient-specific conditions but represent a general stromal response to PCa- exosomes. Additionally, to confirm the fibroblast activation, α-SMA, a well-established marker, was examined in the hTERT fibroblasts after co-culture with PCa-cells. Increased α-SMA reflects the transition of fibroblasts from NCAFs to an activated, myofibroblast-like phenotype, which is commonly induced by cancer-cell-derived signals. In our present work, co-culture with PCa cells led to an unexpected downregulation of α-SMA in hTERT fibroblasts. Several factors could contribute to this finding.

First, the hTERT fibroblasts represent a relatively naïve, non-activated fibroblast population, and respond differently than patient-derived fibroblasts due to their immortalized nature and lack of prior tumor conditioning leading to them being less prone to classical myofibroblastic differentiation. Secondly, the time of treatment in our setup might not have been sufficient to induce a stable α-SMA upregulation, as fibroblast activation is often dynamic and time-dependent process. Thirdly, α-SMA alone may not

fully capture the activation status, since fibroblast activation can involve other phenotypic states including metabolic reprogramming or secretion of paracrine factors without cytoskeletal remodeling. Additional markers such as FAP, PDGFRβ or secreted cytokines like IL-6, CXCL12 could provide a broader view of the activation state. Therefore, PCa cells may reprogram hTERT fibroblasts towards a metabolically supportive, non-contractile state instead of initiating myofibroblastic differentiation.

15.5 miRNA Profiling and Its Potential Role in Prostate Cancer through Cargo Packaging

miRNAs are emerging as key regulators of gene expression that modulate diverse biological processes, including tumorigenesis and TME remodeling. In PCa, the TME comprises a dynamic interplay between tumor cells, NCAFS, CAFs, immune cells and EVs, particularly exosomes. These exosomes act as carriers of miRNAs as cargo, transferring regulatory information between cells and influencing cancer development and progression. The microarray analysis of exosomal miRNAs derived from patient-derived fibroblast pairs revealed a subset of miRNAs that were significantly dysregulated, suggesting a potential regulatory role in fibroblast-PCa communication. Microarray analysis of exosomal miRNAs from patient-derived fibroblast pairs identified a subset of candidates that differed between CAF and NCAF conditions. Therefore, miR-10b-5p, miR-223-3p, miR-210-3p and miR-148b-3p were selected for qPCR validation based on fold-change, p-value and prior involvement in cancer progression.

qPCR revealed two distinct patterns, with miR-10b-5p and miR-210-3p were consistently enriched in CAF cells and their derived exosomes, confirming their cellular microarray expression patterns. Interestingly, their expression was not seen in the exosomes microarray but was still expressed when validated with qPCR. In contrast, upregulation of two miRNAs from exosomal microarray, miR-223-3p and miR-148b-3p, was confirmed at the cellular level but not in exosomal qPCR fractions. This pattern clearly gives two possible outcomes: (i) dual signals, present in cells and loaded into exosomes, (ii) cell-restricted signals, present in cells but not selectively loaded into exosomes. The dual confirmation in both fractions supports a selective miRNA sorting into exosomes model. It highlights that fibroblasts do not uniformly export all dysregulated miRNAs to modulate PCa cell behavior.

Furthermore, technical differences between array and qPCR such as probe chemistry, reverse-transcription efficiency, reference normalization and low RNA input from exosomes can explain discrepancies between the two methods. Contemporary EV guidelines and studies demonstrate that miRNA packaging is regulated, involving RNA-binding proteins (RBPs) and by mechanisms involving YBX1-dependent loading and other RBP-miRNA interactions, which create miRNA cargo loading aligned with cellular state and intended downstream signaling (Shurtleff et al. 2016; Welsh et al. 2024).

Among the validated miRNAs, miR-10b-3p was significantly upregulated in CAFs and their exosomes compared to NCAFs. Functionally, CAF1 and CAF3 cells exhibited strong pro-migratory effects on LNCaP C4-2 cells in this study. Importantly, this phenotype was retained at the exosomal level, with CAF1- and CAF3-exosomes driving migration relative to NCAF-exosomes, linking functional results to exosome-mediated mechanisms. Mechanistically, miR-10b is widely implicated in EMT primarily through regulation of transcription factors like HOXD10, which influence downstream effectors such as RhoC and MMPs to drive migration (Mezlini et al. 2013). Significantly, Shukla and colleagues came up with evidence that miR-10b is directly linked to E-cadherin in a context-dependent manner; in many systems, E-cadherin downregulation appears indirect via EMT regulators rather than direct 3'-UTR target (Shukla et al. 2023). Our data, showing enrichment of miR-10b in CAFs and CAF-exosomes are consistent with a pro-migratory and survival-promoting role, although direct prostate-specific CAF evidence remains limited.

miR-210-3p was also confirmed to be upregulated in both fibroblast cells and their exosomes. miR-210-3p, known as hypoxia-inducing miRNA, is a central regulator of oxygen-sensitive transcription factors and enables adaptation of cells to low-oxygen tumor environments (Andl et al. 2020). In PCa, miR-210 promotes cell survival and proliferation under oxygen-deprived conditions by suppressing apoptotic pathways and enhancing metabolic activity (Qu and Huang 2018; Quero et al. 2011). It is transcriptionally activated by hypoxia-inducible factors (HIFs), which drive tumor adaptation within the hypoxic TME (Huang, Le, and Giaccia 2010). In our experiments, CAF1 and CAF2 cells enhanced PCa cell viability, while CAF1- and CAF3-exosomes maintained survival close to self-exosome levels. Similarly, CAF1- and CAF3-exosomes, derived from high-grade tumor, strongly promoted migration, likely reflecting the synergistic effects of miR-210-mediated hypoxic adaptation and pro-migratory signaling. Furthermore, miR-210 regulates FGFRL1 and other

targets linked to tumor cell survival and angiogenesis (Tsuchiya et al. 2011). Importantly, CAF-derived miR-210, delivered through exosomes, has been shown to remodel the microenvironment by creating niches supportive of tumor progression (Andersen et al. 2016). These mechanisms are consistent with our findings that CAF-exosomes enriched in miR-210 possibly contribute to enhanced survival and invasion in PCa cells, particularly in advanced tumors like pair 3.

In this work, qPCR data revealed a contrasting expression pattern of miR-223-3p between CAFs and their exosomes. miR-223-3p was upregulated in CAF-derived exosomes but downregulated within CAF cells. Functionally, CAF1- and CAF3- exosomes promoted LNCaP C4-2 migration, while NCAF exosomes generally reduced migration, suggesting that miR-223 from CAFs may contribute to a pro-invasive signaling axis. Literature supports a dual role of miR-223 in PCa. Kurozumi et al. demonstrated that miR-223-3p acts as a tumor suppressive miRNA, targeting integrin subunits ITGA3 and ITGB1, which regulate adhesion and migration (Kurozumi et al. 2016). Conversely, its selective enrichment in CAF exosomes indicates a potential differential packaging and delivery to PCA cells, where miR-223 could modulate adhesion-related signaling pathways. Ren et al. highlighted that miR-223 influences apoptotic control and cell survival in other cancer contexts. This suggests that exosomal miR-223 from CAFs may act on PCa cells to subtly adjust survival and invasion dynamics (Ren et al. 2019). Taken together, these findings indicate a compartment-specific functional specialization. Intracellular depletion of miR-223 may enhance CAF activation, while its exosomal release may enable bidirectional communication with tumor cells, tuning migration and TME adaptation.

Further, the fourth miRNA, miR-148b-3p, was enriched in NCAFs cells and in CAF-exosomes, indicating a cargo-specific regulatory mechanism. Because these are relative measurements between matched patient-derived samples, we cannot directly claim absolute upregulation or downregulation. Therefore, it can be described as relative enrichment. This dual expression pattern suggests that NCAFs retain miR-148b intracellularly for stromal regulation, whereas CAFs preferentially package miR-148b into their exosomes, potentially influencing PCa cell behavior. Functionally, CAF1- and CAF3-exosomes promoted LNCaP C4-2 migration, which aligns with evidence that suggests that miR-148b participates in pathways controlling proliferation, apoptosis and cell-matrix signaling in breast cancer (Du et al. 2020). In contrast, the strong upregulation of miR-148b within NCAFs suggests a

distinct role in fibroblast-intrinsic regulation, likely contributing to ECM remodeling and stromal homeostasis. Given that NCAF exosomes were less enriched in miR-148b and correlated with reduced migration in the functional assay, it is plausible that NCAFs preferentially retain miR-148b intracellularly to sustain their non-activated phenotype, while CAFs actively export miR-148b into exosomes to modify tumor cell responses.

Overall, CAFs strategically package oncogenic miRNAs such as miR-10b, miR-223, miR-210 and miR-148b into exosomes to enhance PCa cell migration, survival and tumor progression. In contrast, NCAFs preferentially maintain intracellular miR-223 and miR-148b expression, supporting a more quiescent fibroblast phenotype and producing exosomes less enriched in pro-invasive cargo. However, further validation of these miRNAs in the context of PCa is crucial to confirm their roles.

16 FUTURE PROSPECTS AND CLINICAL RELEVANCE

This study provides novel insights into the role of patient-derived fibroblasts and their possible exosome-mediated miRNA cargo in modulating PCa progression. However, several unanswered questions remain regarding the precise molecular mechanisms underlying the PCa-stromal communication and how these findings can be translated into clinical applications. To gain further mechanistic understanding, future experiments should aim to comprehensively characterize the cargo of fibroblast-derived exosomes. While miR-10b, miR-210, mir-223 and miR-148b were validated, small RNA sequencing and proteomic profiling could reveal additional signaling molecules influencing tumor-fibroblast interactions in the TME. These analyses could identify novel pathways regulating viability, proliferation, invasion and therapy resistance in PCa cells.

An important step forward would involve functional blocking studies using miRNA inhibitors (anatgomiRs) or mimics to directly validate the mentioned miRNAs' contribution to the observed effects on viability, proliferation, migration and tumor-promoting behaviors. Since the data in this study suggest that CAF-exosomes can strongly influence survival and motility, additional apoptosis-focused studies are needed to clarify whether these effects arise from suppression of programmed cell death or adaptation. Measuring apoptotic markers such as BAX, BCL-2, cleaved caspases and Annexin V in PCa cells after treatment with CAF-exosomes would provide direct insights into survival-promoting mechanisms. Similarly, while this study evaluated fibroblast-driven effects on migration, future work should focus on Matrigel-based invasion assays or 3D spheroid models to assess the ability of CAFs and their exosomes to promote ECM penetration. Such work would distinguish between effects on simple migration versus actual invasion. Combining these invasion studies with downstream pathways could further reveal whether miR-10b and miR-210 enrichment in CAF-exosomes drives EMT and metastatic dissemination. To extend this mechanistic understanding, pathway-focused studies using western blotting, qPCR and phosphor-protein profiling after fibroblast-exosomes treatment could confirm activation of key regulators linked to EMT, such as E-cadherin, N-cadherin and vimentin, apoptosis, such as caspases and BCL-2, and hypoxia-driven signaling regulators, such as HIF1α, VEGF and FGFRL1. Advanced methods such as single-cell RNA sequencing could also capture inter-patient heterogeneity in NCAF and CAF pairs and identify subpopulations of fibroblasts

with distinct functional roles. Integrating CRISPR-mediated knockout or activation strategies targeting specific miRNAs or downstream targets could provide evidence for the observed phenotypes.

From a translational perspective, miR-10b and miR-210 in CAF-exosomes offers strong potential for developing non-invasive biomarkers for aggressive PCa. Exosomal miRNAs could be monitored in plasma and urine liquid biopsy, enabling early detection and prediction of disease progression. Elevated exosomal miR-10b and miR-210 may hold a prognostic value, correlating with higher Gleason scores, increased metastatic potential and poorer patient outcomes. Therapeutically, targeting these miRNAs using locked nucleic acid (LNA) inhibitors or antagomiRs could suppress CAF-driven pro-tumor signaling. Conversely, NCAF-derived exosomes could be engineered as carriers of tumor-suppressive miRNAs, such as miR-223, to counteract CAF-induced invasion. Pharmacological inhibition of exosome biogenesis, such as, using GW4869 or other small molecule inhibitors, could also be tested to disrupt fibroblast-mediated tumor-stroma communication. Finally, the strong patient-specific variability observed in this study highlights the importance of a personalized medical approach. Since the Gleason score, tumor grade and fibroblast activation state influence miRNA packaging and exosomal effects, integrating molecular profiling of patient fibroblasts with clinical data could improve patient stratification and guide tailored therapies. Together, these future studies will enable a more comprehensive understanding of CAF-driven PCa progression and support the development of novel diagnostic tools and targeted therapies.

17 LIMITATIONS

While this study provides important insights into the role of patient-derived fibroblasts and their exosomes in PCA progression, several limitations must be acknowledged. Firstly, the analysis was performed using only four fibroblast pairs, of which two pairs could not be used for all experiments, limiting the ability to generalize the findings across broader patient populations. Although consistent patterns were observed, larger cohorts are necessary to validate the trends and account for patient heterogeneity. This study also faced challenges with incomplete experimental coverage due to the primary fibroblasts' limited growth over passages. For example, functional exosome experiments could not be performed for pair 2 due to insufficient survival, leading to missing data for specific assays and restricting cross-patient comparisons.

Technical variability represents another limitation. Exosome isolation yields varied significantly across patient samples, affecting the use of exosomes from a single isolation in functional experiments, potentially introducing noise into viability, proliferation and migration outcomes. Although standard protocols were used, patient-specific differences in fibroblast secretion rates and passage-related changes may have influenced the data. Moreover, this study focused primarily on a small subset of miRNAs identified from microarray profiling. While the miRNAs were validated, other regulatory cargoes, including protein, long non-coding RNAs and metabolites, were not fully explored but may play an equally significant role in modulating PCa behavior.

Finally, the in vitro co-culture and exosomal treatment systems used here cannot fully replicate the complexity of in vivo TME, where dynamic interactions between immune cells, endothelial cells and ECM components influence tumor progression. Future studies using advanced 3D organoid models, patient-derived xenografts or microfluidic tumor-on-chip systems would provide more physiologically relevant insights into fibroblast-driven PCa signaling. These limitations emphasize the need for comprehensive, multi-dimensional studies to validate and extend the findings presented here.

18 BIBLIOGRAPHY

Abate-Shen, Cory, and Michael M. Shen. 2000. ‘Molecular Genetics of Prostate Cancer’. Genes & Development 14(19):2410–34. doi:10.1101/gad.819500.

Agoulnik, Irina U., Ajula Vaid, William E. Bingman, Halime Erdeme, Anna Frolov, Carolyn L. Smith, Gustavo Ayala, Michael M. Ittmann, and Nancy L. Weigel. 2005. ‘Role of SRC-1 in the Promotion of Prostate Cancer Cell Growth and Tumor Progression’. Cancer Research 65(17):7959–67. doi:10.1158/0008-5472.CAN-04-3541.

Andersen, Sigve, Elin Richardsen, Line Moi, Tom Donnem, Yngve Nordby, Nora Ness, Marte Eilertsen Holman, Roy M. Bremnes, and Lill-Tove Busund. 2016. ‘Fibroblast miR-210 Overexpression Is Independently Associated with Clinical Failure in Prostate Cancer – a Multicenter (in Situ Hybridization) Study’. Scientific Reports 6(1):36573. doi:10.1038/srep36573.

Andl, Thomas, Kavya Ganapathy, Alexia Bossan, and Ratna Chakrabarti. 2020. ‘MicroRNAs as Guardians of the Prostate: Those Who Stand before Cancer. What Do We Really Know about the Role of microRNAs in Prostate Biology?’ International Journal of Molecular Sciences 21(13):4796. doi:10.3390/ijms21134796.

Baietti, Maria Francesca, Zhe Zhang, Eva Mortier, Aurélie Melchior, Gisèle Degeest, Annelies Geeraerts, Ylva Ivarsson, Fabienne Depoortere, Christien Coomans, Elke Vermeiren, Pascale Zimmermann, and Guido David. 2012. ‘Syndecan–Syntenin–ALIX Regulates the Biogenesis of Exosomes’. Nature Cell Biology 14(7):677–85. doi:10.1038/ncb2502.

Barcellos-de-Souza, Pedro, Giuseppina Comito, Coral Pons-Segura, Maria Letizia Taddei, Valentina Gori, Valentina Becherucci, Franco Bambi, Francesca Margheri, Anna Laurenzana, Mario Del Rosso, and Paola Chiarugi. 2016. ‘Mesenchymal Stem Cells Are Recruited and Activated into Carcinoma-Associated Fibroblasts by Prostate Cancer Microenvironment-Derived TGF-B1’. Stem Cells 34(10):2536–47. doi:10.1002/stem.2412.

Barfeld, Stefan J., Alfonso Urbanucci, Harri M. Itkonen, Ladan Fazli, Jessica L. Hicks, Bernd Thiede, Paul S. Rennie, Srinivasan Yegnasubramanian, Angelo M. DeMarzo, and Ian G. Mills. 2017. 'C-Myc Antagonises the Transcriptional Activity of the Androgen Receptor in Prostate Cancer Affecting Key Gene Networks'. EBioMedicine 18:83–93. doi:10.1016/j.ebiom.2017.04.006.

Bergman, J., and M. S. Litwin. 2012. 'Quality of Life in Men Undergoing Active Surveillance for Localized Prostate Cancer'. JNCI Monographs 2012(45):242–49. doi:10.1093/jncimonographs/lgs026.

BioRender. n.d. Retrieved 23 July 2025. https://app.biorender.com/illustrations/687a220c0728b2cec3e758f3.

Bjurlin, Marc A., H. Ballentine Carter, Paul Schellhammer, Michael S. Cookson, Leonard G. Gomella, Dean Troyer, Thomas M. Wheeler, Steven Schlossberg, David F. Penson, and Samir S. Taneja. 2013. 'Optimization of Initial Prostate Biopsy in Clinical Practice: Sampling, Labeling and Specimen Processing'. Journal of Urology 189(6):2039–46. doi:10.1016/j.juro.2013.02.072.

Boutros, Paul C., Michael Fraser, Nicholas J. Harding, Richard De Borja, Dominique Trudel, Emilie Lalonde, Alice Meng, Pablo H. Hennings-Yeomans, Andrew McPherson, Veronica Y. Sabelnykova, Amin Zia, Natalie S. Fox, Julie Livingstone, Yu-Jia Shiah, Jianxin Wang, Timothy A. Beck, Cherry L. Have, Taryne Chong, Michelle Sam, Jeremy Johns, Lee Timms, Nicholas Buchner, Ada Wong, John D. Watson, Trent T. Simmons, Christine P'ng, Gaetano Zafarana, Francis Nguyen, Xuemei Luo, Kenneth C. Chu, Stephenie D. Prokopec, Jenna Sykes, Alan Dal Pra, Alejandro Berlin, Andrew Brown, Michelle A. Chan-Seng-Yue, Fouad Yousif, Robert E. Denroche, Lauren C. Chong, Gregory M. Chen, Esther Jung, Clement Fung, Maud H. W. Starmans, Hanbo Chen, Shaylan K. Govind, James Hawley, Alister D'Costa, Melania Pintilie, Daryl Waggott, Faraz Hach, Philippe Lambin, Lakshmi B. Muthuswamy, Colin Cooper, Rosalind Eeles, David Neal, Bernard Tetu, Cenk Sahinalp, Lincoln D. Stein, Neil Fleshner, Sohrab P. Shah, Colin C. Collins, Thomas J. Hudson, John D. McPherson, Theodorus Van Der Kwast, and Robert G. Bristow. 2015. 'Spatial Genomic Heterogeneity within Localized, Multifocal Prostate Cancer'. Nature Genetics 47(7):736–45. doi:10.1038/ng.3315.

Bray, Freddie, Mathieu Laversanne, Hyuna Sung, Jacques Ferlay, Rebecca L. Siegel, Isabelle Soerjomataram, and Ahmedin Jemal. 2024. 'Global Cancer Statistics 2022: GLOBOCAN Estimates of Incidence and Mortality Worldwide for 36 Cancers in 185 Countries'. CA: A Cancer Journal for Clinicians 74(3):229–63. doi:10.3322/caac.21834.

Burnette, W. Neal. 1981. '"Western Blotting": Electrophoretic Transfer of Proteins from Sodium Dodecyl Sulfate-Polyacrylamide Gels to Unmodified Nitrocellulose and Radiographic Detection with Antibody and Radioiodinated Protein A'. Analytical Biochemistry 112(2):195–203. doi:10.1016/0003-2697(81)90281-5.

Cancer WHO. n.d. Retrieved 27 June 2025. https://www.who.int/news-room/fact-sheets/detail/cancer.

Chen, Liwei, Songshu Meng, Hai Wang, Purva Bali, Wenlong Bai, Benyi Li, Peter Atadja, Kapil N. Bhalla, and Jie Wu. 2005. 'Chemical Ablation of Androgen Receptor in Prostate Cancer Cells by the Histone Deacetylase Inhibitor LAQ824'. Molecular Cancer Therapeutics 4(9):1311–19. doi:10.1158/1535-7163.MCT-04-0287.

Chen, Rui, Shancheng Ren, Ming Kwong Yiu, Ng Chi Fai, Wai Sam Cheng, Lap Hong Ian, Seiji Naito, Tadashi Matsuda, Elijah Kehinde, Ali Kural, Jason Yichun Chiu, Rainy Umbas, Qiang Wei, Xiaolei Shi, Liqun Zhou, Jian Huang, Yiran Huang, Liping Xie, Lulin Ma, Changjun Yin, Danfeng Xu, Kexin Xu, Zhangqun Ye, Chunxiao Liu, Dingwei Ye, Xin Gao, Qiang Fu, Jianquan Hou, Jianlin Yuan, Dalin He, Tiejun Pan, Qiang Ding, Fengshuo Jin, Benkang Shi, Gongxian Wang, Xiuheng Liu, Dongwen Wang, Zhoujun Shen, Xiangbo Kong, Wanhai Xu, Yaoliang Deng, Haibo Xia, Alexa N. Cohen, Xu Gao, Chuanliang Xu, and Yinghao Sun. 2014. 'Prostate Cancer in Asia: A Collaborative Report'. Asian Journal of Urology 1(1):15–29. doi:10.1016/j.ajur.2014.08.007.

Ciatto, S., M. Zappa, R. Bonardi, and G. Gervasi. 2000. 'Prostate Cancer Screening: The Problem of Overdiagnosis and Lessons to Be Learned from Breast Cancer Screening'. European Journal of Cancer 36(11):1347–50. doi:10.1016/S0959-8049(00)00119-2.

Cocucci, Emanuele, and Jacopo Meldolesi. 2015. ‘Ectosomes and Exosomes: Shedding the Confusion between Extracellular Vesicles’. Trends in Cell Biology 25(6):364–72. doi:10.1016/j.tcb.2015.01.004.

Datta, Amrita, Hogyoung Kim, Lauren McGee, Adedoyin E. Johnson, Sudha Talwar, Juan Marugan, Noel Southall, Xin Hu, Madhu Lal, Debasis Mondal, Marc Ferrer, and Asim B. Abdel-Mageed. 2018. ‘High-Throughput Screening Identified Selective Inhibitors of Exosome Biogenesis and Secretion: A Drug Repurposing Strategy for Advanced Cancer’. Scientific Reports 8(1):8161. doi:10.1038/s41598-018-26411-7.

Decker, Keith F., Dali Zheng, Yuhong He, Tamara Bowman, John R. Edwards, and Li Jia. 2012. ‘Persistent Androgen Receptor-Mediated Transcription in Castration-Resistant Prostate Cancer under Androgen-Deprived Conditions’. Nucleic Acids Research 40(21):10765–79. doi:10.1093/nar/gks888.

Ding, Chen, Jiange Wang, Jie Wang, Jiqiang Niu, Zhikai Xiahou, Zhou Sun, Zhenzhen Zhao, and Dongyang Zeng. 2025. ‘Heterogeneity of Cancer-Associated Fibroblast Subpopulations in Prostate Cancer: Implications for Prognosis and Immunotherapy’. Translational Oncology 52:102255. doi:10.1016/j.tranon.2024.102255.

Dong, Yan, Haitao Zhang, Allen C. Gao, James R. Marshall, and Clement Ip. 2005. ‘Androgen Receptor Signaling Intensity Is a Key Factor in Determining the Sensitivity of Prostate Cancer Cells to Selenium Inhibition of Growth and Cancer-Specific Biomarkers’. Molecular Cancer Therapeutics 4(7):1047–55. doi:10.1158/1535-7163.MCT-05-0124.

Dragovic, Rebecca A., Christopher Gardiner, Alexandra S. Brooks, Dionne S. Tannetta, David J. P. Ferguson, Patrick Hole, Bob Carr, Christopher W. G. Redman, Adrian L. Harris, Peter J. Dobson, Paul Harrison, and Ian L. Sargent. 2011. ‘Sizing and Phenotyping of Cellular Vesicles Using Nanoparticle Tracking Analysis’. Nanomedicine: Nanotechnology, Biology and Medicine 7(6):780–88. doi:10.1016/j.nano.2011.04.003.

Du, Ye, Na Wei, Ruolin Ma, Shuheng Jiang, and Dong Song. 2020. ‘A miR-210-3p Regulon That Controls the Warburg Effect by Modulating HIF-1α and P53 Activity in Triple-

Negative Breast Cancer'. Cell Death & Disease 11(9):731. doi:10.1038/s41419-020-02952-6.

Elmore, Susan. 2007. 'Apoptosis: A Review of Programmed Cell Death'. Toxicologic Pathology 35(4):495–516. doi:10.1080/01926230701320337.

Fabbri, Muller, Alessio Paone, Federica Calore, Roberta Galli, Eugenio Gaudio, Ramasamy Santhanam, Francesca Lovat, Paolo Fadda, Charlene Mao, Gerard J. Nuovo, Nicola Zanesi, Melissa Crawford, Gulcin H. Ozer, Dorothee Wernicke, Hansjuerg Alder, Michael A. Caligiuri, Patrick Nana-Sinkam, Danilo Perrotti, and Carlo M. Croce. 2012. 'MicroRNAs Bind to Toll-like Receptors to Induce Prometastatic Inflammatory Response'. Proceedings of the National Academy of Sciences 109(31). doi:10.1073/pnas.1209414109.

Finne, Patrik, Mahdi Fallah, Matti Hakama, Stefano Ciatto, Jonas Hugosson, Harry De Koning, Sue Moss, Vera Nelen, and Anssi Auvinen. 2010. 'Lead-Time in the European Randomised Study of Screening for Prostate Cancer'. European Journal of Cancer 46(17):3102–8. doi:10.1016/j.ejca.2010.09.034.

Fong, Ka-wing, Jonathan C. Zhao, Jung Kim, Shangze Li, Yeqing A. Yang, Bing Song, Laure Rittie, Ming Hu, Ximing Yang, Bernard Perbal, and Jindan Yu. 2017. 'Polycomb-Mediated Disruption of an Androgen Receptor Feedback Loop Drives Castration-Resistant Prostate Cancer'. Cancer Research 77(2):412–22. doi:10.1158/0008-5472.CAN-16-1949.

Francis, Jeffrey C., and Amanda Swain. 2018. 'Prostate Organogenesis'. Cold Spring Harbor Perspectives in Medicine 8(7):a030353. doi:10.1101/cshperspect.a030353.

Gallagher, David J., Angel M. Cronin, Matthew I. Milowsky, Michael J. Morris, Jasmine Bhatia, Peter T. Scardino, James A. Eastham, Kenneth Offit, and Mark E. Robson. 2012. 'Germline BRCA Mutation Does Not Prevent Response to Taxane-based Therapy for the Treatment of Castration-resistant Prostate Cancer'. BJU International 109(5):713–19. doi:10.1111/j.1464-410X.2011.10292.x.

Gao, Yanan, You Qin, Chao Wan, Yajie Sun, Jingshu Meng, Jing Huang, Yan Hu, Honglin Jin, and Kunyu Yang. 2021. 'Small Extracellular Vesicles: A Novel Avenue for

Cancer Management'. Frontiers in Oncology 11:638357. doi:10.3389/fonc.2021.638357.

Genard, Géraldine C., Luca Tirinato, Francesca Pagliari, Jessica Da Silva, Alessandro Giammona, Fatema Alquraish, Marie Bordas, Maria Grazia Marafioti, Simone Di Franco, Jeannette Janssen, Daniel Garcia-Calderón, Rachel Hanley, Clelia Nistico, Yoshinori Fukasawa, Torsten Müller, Jeroen Krijgsveld, Matilde Todaro, Francesco Saverio Costanzo, Giorgio Stassi, Michelle Nessling, Karsten Richter, Kendra K. Maass, Carlo Liberale, and Joao Seco. 2022. 'Lipid Droplets Fuel Small Extracellular Vesicle Biogenesis'.

Ghassemi, Parham, Koran S. Harris, Xiang Ren, Brittni M. Foster, Carl D. Langefeld, Bethany A. Kerr, and Masoud Agah. 2020. 'Comparative Study of Prostate Cancer Biophysical and Migratory Characteristics via Iterative Mechanoelectrical Properties (iMEP) and Standard Migration Assays'. Sensors and Actuators B: Chemical 321:128522. doi:10.1016/j.snb.2020.128522.

Giannoni, Elisa, Francesca Bianchini, Lorenzo Masieri, Sergio Serni, Eugenio Torre, Lido Calorini, and Paola Chiarugi. 2010a. 'Reciprocal Activation of Prostate Cancer Cells and Cancer-Associated Fibroblasts Stimulates Epithelial-Mesenchymal Transition and Cancer Stemness'. Cancer Research 70(17):6945–56. doi:10.1158/0008-5472.CAN-10-0785.

Giannoni, Elisa, Francesca Bianchini, Lorenzo Masieri, Sergio Serni, Eugenio Torre, Lido Calorini, and Paola Chiarugi. 2010b. 'Reciprocal Activation of Prostate Cancer Cells and Cancer-Associated Fibroblasts Stimulates Epithelial-Mesenchymal Transition and Cancer Stemness'. Cancer Research 70(17):6945–56. doi:10.1158/0008-5472.CAN-10-0785.

Guo, Jin-Jin, Ying-Jie Li, and Lu-Lu Xin. 2015. 'Tangeretin Prevents Prostate Cancer Cell Proliferation and Induces Apoptosis via Activation of Notch Signalling and Regulating the Androgen Receptor (AR) Pathway and the Phosphoinositide 3-Kinase (PI3k)/Akt/mTOR Pathways'. Bangladesh Journal of Pharmacology 10(4):937. doi:10.3329/bjp.v10i4.23699.

Guo, Zhiyong, Xi Yang, Feng Sun, Richeng Jiang, Douglas E. Linn, Hege Chen, Hegang Chen, Xiangtian Kong, Jonathan Melamed, Clifford G. Tepper, Hsing-Jien Kung, Angela M. H. Brodie, Joanne Edwards, and Yun Qiu. 2009. 'A Novel Androgen Receptor Splice Variant Is Up-Regulated during Prostate Cancer Progression and Promotes Androgen Depletion–Resistant Growth'. Cancer Research 69(6):2305–13. doi:10.1158/0008-5472.CAN-08-3795.

Haffner, Michael C., Timothy Mosbruger, David M. Esopi, Helen Fedor, Christopher M. Heaphy, David A. Walker, Nkosi Adejola, Meltem GÃ¼rel, Jessica Hicks, Alan K. Meeker, Marc K. Halushka, Jonathan W. Simons, William B. Isaacs, Angelo M. De Marzo, William G. Nelson, and Srinivasan Yegnasubramanian. 2013. 'Tracking the Clonal Origin of Lethal Prostate Cancer'. Journal of Clinical Investigation 123(11):4918–22. doi:10.1172/JCI70354.

Han, Zhaodong, Rujun Mo, Shanghua Cai, Yuanfa Feng, Zhenfeng Tang, Jianheng Ye, Ren Liu, Zhiduan Cai, Xuejin Zhu, Yulin Deng, Zhihao Zou, Yongding Wu, Zhouda Cai, Yuxiang Liang, and Weide Zhong. 2022. 'Differential Expression of E2F Transcription Factors and Their Functional and Prognostic Roles in Human Prostate Cancer'. Frontiers in Cell and Developmental Biology 10:831329. doi:10.3389/fcell.2022.831329.

Hanahan, Douglas, and Robert A. Weinberg. 2011. 'Hallmarks of Cancer: The Next Generation'. Cell 144(5):646–74. doi:10.1016/j.cell.2011.02.013.

Hong, Wanjin. 2005. 'SNAREs and Traffic'. Biochimica et Biophysica Acta (BBA) - Molecular Cell Research 1744(2):120–44. doi:10.1016/j.bbamcr.2005.03.014.

Hoofring, Alan. 2007. Prostate and Nearby Organs.

Huang, Xiaoyi, Tiezheng Yuan, Meihua Liang, Meijun Du, Shu Xia, Rachel Dittmar, Dian Wang, William See, Brian A. Costello, Fernando Quevedo, Winston Tan, Debashis Nandy, Graham H. Bevan, Sherri Longenbach, Zhifu Sun, Yan Lu, Tao Wang, Stephen N. Thibodeau, Lisa Boardman, Manish Kohli, and Liang Wang. 2015. 'Exosomal miR-1290 and miR-375 as Prognostic Markers in Castration-Resistant Prostate Cancer'. European Urology 67(1):33–41. doi:10.1016/j.eururo.2014.07.035.

Huang, Xin, Quynh-Thu Le, and Amato J. Giaccia. 2010. 'MiR-210 – Micromanager of the Hypoxia Pathway'. Trends in Molecular Medicine 16(5):230–37. doi:10.1016/j.molmed.2010.03.004.

Hurley, James H. 2015. 'ESCRT s Are Everywhere'. The EMBO Journal 34(19):2398–2407. doi:10.15252/embj.201592484.

Ito, Kazuto. 2014. 'Prostate Cancer in Asian Men'. Nature Reviews Urology 11(4):197–212. doi:10.1038/nrurol.2014.42.

Josson, S., M. Gururajan, S. Y. Sung, P. Hu, C. Shao, H. E. Zhau, C. Liu, J. Lichterman, P. Duan, Q. Li, A. Rogatko, E. M. Posadas, C. L. Haga, and L. W. K. Chung. 2015. 'Stromal Fibroblast-Derived miR-409 Promotes Epithelial-to-Mesenchymal Transition and Prostate Tumorigenesis'. Oncogene 34(21):2690–99. doi:10.1038/onc.2014.212.

Junker, Kerstin, Joana Heinzelmann, Carla Beckham, Takahiro Ochiya, and Guido Jenster. 2016. 'Extracellular Vesicles and Their Role in Urologic Malignancies'. European Urology 70(2):323–31. doi:10.1016/j.eururo.2016.02.046.

Kakehi, Yoshiyuki, Mikio Sugimoto, Rikiya Taoka, and the committee for establishment of the evidenced-based clinical practice guideline for prostate cancer of the Japanese Urological Association. 2017. 'Evidenced-based Clinical Practice Guideline for Prostate Cancer (Summary: Japanese Urological Association, 2016 Edition)'. International Journal of Urology 24(9):648–66. doi:10.1111/iju.13380.

Kharmate, Geetanjali, Elham Hosseini-Beheshti, Josselin Caradec, Mei Yieng Chin, and Emma S. Tomlinson Guns. 2016. 'Correction: Epidermal Growth Factor Receptor in Prostate Cancer Derived Exosomes'. PLOS ONE 11(6):e0157392. doi:10.1371/journal.pone.0157392.

Kogan, Ira, Naomi Goldfinger, Michael Milyavsky, Merav Cohen, Igor Shats, Gabriele Dobler, Helmut Klocker, Bohdan Wasylyk, Maureen Voller, Tilly Aalders, Jack A. Schalken, Moshe Oren, and Varda Rotter. 2006. 'hTERT-Immortalized Prostate Epithelial and Stromal-Derived Cells: An Authentic In Vitro Model for Differentiation and Carcinogenesis'. Cancer Research 66(7):3531–40. doi:10.1158/0008-5472.CAN-05-2183.

Kohaar, Indu, Gyorgy Petrovics, and Shiv Srivastava. 2019. ‘A Rich Array of Prostate Cancer Molecular Biomarkers: Opportunities and Challenges’. International Journal of Molecular Sciences 20(8):1813. doi:10.3390/ijms20081813.

Kowal, Joanna, Guillaume Arras, Marina Colombo, Mabel Jouve, Jakob Paul Morath, Bjarke Primdal-Bengtson, Florent Dingli, Damarys Loew, Mercedes Tkach, and Clotilde Théry. 2016. ‘Proteomic Comparison Defines Novel Markers to Characterize Heterogeneous Populations of Extracellular Vesicle Subtypes’. Proceedings of the National Academy of Sciences 113(8). doi:10.1073/pnas.1521230113.

Kurozumi, Akira, Yusuke Goto, Ryosuke Matsushita, Ichiro Fukumoto, Mayuko Kato, Rika Nishikawa, Shinichi Sakamoto, Hideki Enokida, Masayuki Nakagawa, Tomohiko Ichikawa, and Naohiko Seki. 2016. ‘Tumor-suppressive Micro RNA -223 Inhibits Cancer Cell Migration and Invasion by Targeting ITGA 3/ ITGB 1 Signaling in Prostate Cancer’. Cancer Science 107(1):84–94. doi:10.1111/cas.12842.

Laemmli, U. K. 1970. ‘Cleavage of Structural Proteins during the Assembly of the Head of Bacteriophage T4’. Nature 227(5259):680–85. doi:10.1038/227680a0.

Li, Aichun, Tianbao Zhang, Min Zheng, Yanning Liu, and Zhi Chen. 2017. ‘Exosomal Proteins as Potential Markers of Tumor Diagnosis’. Journal of Hematology & Oncology 10(1):175. doi:10.1186/s13045-017-0542-8.

Li, Dejun, Yujun Gao, Chong Wang, and Lianghai Hu. 2024. ‘Proteomic and Phosphoproteomic Profiling of Urinary Small Extracellular Vesicles in Hepatocellular Carcinoma’. The Analyst 149(17):4378–87. doi:10.1039/D4AN00660G.

Li, Peng, Xin Yu, Kai Ge, Jonathan Melamed, Robert G. Roeder, and Zhengxin Wang. 2002. ‘Heterogeneous Expression and Functions of Androgen Receptor Co-Factors in Primary Prostate Cancer’. The American Journal of Pathology 161(4):1467–74. doi:10.1016/S0002-9440(10)64422-7.

Li, Shibao, Yao Zhao, Wenbai Chen, Lingyu Yin, Jie Zhu, Haoliang Zhang, Chenchen Cai, Pengpeng Li, Lingyan Huang, and Ping Ma. 2018. ‘Exosomal ephrinA2 Derived

from Serum as a Potential Biomarker for Prostate Cancer'. Journal of Cancer 9(15):2659–65. doi:10.7150/jca.25201.

Linxweiler, Johannes, Turkan Hajili, Christina Körbel, Carolina Berchem, Philip Zeuschner, Andreas Müller, Michael Stöckle, Michael D. Menger, Kerstin Junker, and Matthias Saar. 2020. 'Cancer-Associated Fibroblasts Stimulate Primary Tumor Growth and Metastatic Spread in an Orthotopic Prostate Cancer Xenograft Model'. Scientific Reports 10(1). doi:10.1038/s41598-020-69424-x.

Linxweiler, Johannes, and Kerstin Junker. 2020. 'Extracellular Vesicles in Urological Malignancies: An Update'. Nature Reviews Urology 17(1):11–27. doi:10.1038/s41585-019-0261-8.

Liu, Yang, Ke Shi, Yong Chen, Xianrui Wu, Zheng Chen, Ke Cao, Yongguang Tao, Xiang Chen, Junlin Liao, and Jianda Zhou. 2021. 'Exosomes and Their Role in Cancer Progression'. Frontiers in Oncology 11. doi:10.3389/fonc.2021.639159.

Liu, Zhanliang, Zhemin Lin, Mingxin Jiang, Guangyi Zhu, Tianyu Xiong, Fang Cao, Yun Cui, and Y. N. Niu. 2024. 'Cancer-Associated Fibroblast Exosomes Promote Prostate Cancer Metastasis through miR-500a-3p/FBXW7/HSF1 Axis under Hypoxic Microenvironment'. Cancer Gene Therapy 31(5):698–709. doi:10.1038/s41417-024-00742-2.

Lopez, Sandra M., Alexander I. Agoulnik, Manqi Zhang, Leif E. Peterson, Egla Suarez, Gregory A. Gandarillas, Anna Frolov, Rile Li, Kimal Rajapakshe, Christian Coarfa, Michael M. Ittmann, Nancy L. Weigel, and Irina U. Agoulnik. 2016. 'Nuclear Receptor Corepressor 1 Expression and Output Declines with Prostate Cancer Progression'. Clinical Cancer Research 22(15):3937–49. doi:10.1158/1078-0432.CCR-15-1983.

Lu, Yun, Liru Zhao, Jiaqi Mao, Wen Liu, Wensheng Ma, and Bingjiao Zhao. 2023. 'Rab27a-Mediated Extracellular Vesicle Secretion Contributes to Osteogenesis in Periodontal Ligament-Bone Niche Communication'. Scientific Reports 13(1):8479. doi:10.1038/s41598-023-35172-x.

Lundholm, Marie, Mona Schröder, Olga Nagaeva, Vladimir Baranov, Anders Widmark, Lucia Mincheva-Nilsson, and Pernilla Wikström. 2014. 'Prostate Tumor-Derived

Exosomes Down-Regulate NKG2D Expression on Natural Killer Cells and CD8+ T Cells: Mechanism of Immune Evasion' edited by P. Busson. PLoS ONE 9(9):e108925. doi:10.1371/journal.pone.0108925.

Luo, Yong, Ling Lan, Yong-Guang Jiang, Jia-Hui Zhao, Ming-Chuan Li, Neng-Bao Wei, and Yun-Hua Lin. 2013. 'Epithelial-Mesenchymal Transition and Migration of Prostate Cancer Stem Cells Is Driven by Cancer-Associated Fibroblasts in an HIF-1α/β-Catenin-Dependent Pathway'. Molecules and Cells 36(2):138–44. doi:10.1007/s10059-013-0096-8.

Madorran, Eneko, Miha Ambrož, Jure Knez, and Monika Sobočan. 2024. 'An Overview of the Current State of Cell Viability Assessment Methods Using OECD Classification'. International Journal of Molecular Sciences 26(1):220. doi:10.3390/ijms26010220.

McNeal, John E. 1981. 'The Zonal Anatomy of the Prostate'. The Prostate 2(1):35–49. doi:10.1002/pros.2990020105.

Melo, Sonia A., Hikaru Sugimoto, Joyce T. O'Connell, Noritoshi Kato, Alberto Villanueva, August Vidal, Le Qiu, Edward Vitkin, Lev T. Perelman, Carlos A. Melo, Anthony Lucci, Cristina Ivan, George A. Calin, and Raghu Kalluri. 2014. 'Cancer Exosomes Perform Cell-Independent MicroRNA Biogenesis and Promote Tumorigenesis'. Cancer Cell 26(5):707–21. doi:10.1016/j.ccell.2014.09.005.

Mezlini, Aziz M., Bo Wang, Amit Deshwar, Quaid Morris, and Anna Goldenberg. 2013. 'Identifying Cancer Specific Functionally Relevant miRNAs from Gene Expression and miRNA-to-Gene Networks Using Regularized Regression' edited by X.-Y. Guan. PLoS ONE 8(10):e73168. doi:10.1371/journal.pone.0073168.

Mezzasoma, Letizia, Egidia Costanzi, Paolo Scarpelli, Vincenzo Nicola Talesa, and Ilaria Bellezza. 2019. 'Extracellular Vesicles from Human Advanced-Stage Prostate Cancer Cells Modify the Inflammatory Response of Microenvironment-Residing Cells'. Cancers 11(9):1276. doi:10.3390/cancers11091276.

Mohler, James L., Christopher W. Gregory, O. Harris Ford, Desok Kim, Catharina M. Weaver, Peter Petrusz, Elizabeth M. Wilson, and Frank S. French. 2004. 'The

Androgen Axis in Recurrent Prostate Cancer'. Clinical Cancer Research 10(2):440–48. doi:10.1158/1078-0432.CCR-1146-03.

Mostaghel, Elahe A., Brett T. Marck, Stephen R. Plymate, Robert L. Vessella, Stephen Balk, Alvin M. Matsumoto, Peter S. Nelson, and R. Bruce Montgomery. 2011. 'Resistance to CYP17A1 Inhibition with Abiraterone in Castration-Resistant Prostate Cancer: Induction of Steroidogenesis and Androgen Receptor Splice Variants'. Clinical Cancer Research 17(18):5913–25. doi:10.1158/1078-0432.CCR-11-0728.

Nadiminty, Nagalakshmi, Ramakumar Tummala, Chengfei Liu, Wei Lou, Christopher P. Evans, and Allen C. Gao. 2015. 'NF-κB2/P52:C-Myc:hnRNPA1 Pathway Regulates Expression of Androgen Receptor Splice Variants and Enzalutamide Sensitivity in Prostate Cancer'. Molecular Cancer Therapeutics 14(8):1884–95. doi:10.1158/1535-7163.MCT-14-1057.

Nadiminty, Nagalakshmi, Ramakumar Tummala, Chengfei Liu, Joy Yang, Wei Lou, Christopher P. Evans, and Allen C. Gao. 2013. 'NF-κB2/P52 Induces Resistance to Enzalutamide in Prostate Cancer: Role of Androgen Receptor and Its Variants'. Molecular Cancer Therapeutics 12(8):1629–37. doi:10.1158/1535-7163.MCT-13-0027.

Nanopartikel-Tracking-Analyse (NTA). n.d. Retrieved 21 July 2025. https://www.malvernpanalytical.com/de/products/technology/light-scattering/nanoparticle-tracking-analysis.

Natani, Sirisha, Maresha Ramakrishna, Teja Nallavolu, and Ramesh Ummanni. 2023. 'MicroRNA-147b Induces Neuroendocrine Differentiation of Prostate Cancer Cells by Targeting Ribosomal Protein RPS15A'. The Prostate 83(10):936–49. doi:10.1002/pros.24535.

Nedaeinia, Reza, Simin Najafgholian, Rasoul Salehi, Mohammad Goli, Maryam Ranjbar, Hamid Nickho, Shaghayegh Haghjooy Javanmard, Gordon A. Ferns, and Mostafa Manian. 2024. 'The Role of Cancer-Associated Fibroblasts and Exosomal miRNAs-Mediated Intercellular Communication in the Tumor Microenvironment and the Biology of Carcinogenesis: A Systematic Review'. Cell Death Discovery 10(1):380. doi:10.1038/s41420-024-02146-5.

Nogués, Laura, Alberto Benito-Martin, Marta Hergueta-Redondo, and Héctor Peinado. 2018. 'The Influence of Tumour-Derived Extracellular Vesicles on Local and Distal Metastatic Dissemination'. Molecular Aspects of Medicine 60:15–26. doi:10.1016/j.mam.2017.11.012.

O'Brien, Killian, Koen Breyne, Stefano Ughetto, Louise C. Laurent, and Xandra O. Breakefield. 2020. 'RNA Delivery by Extracellular Vesicles in Mammalian Cells and Its Applications'. Nature Reviews Molecular Cell Biology 21(10):585–606. doi:10.1038/s41580-020-0251-y.

Pacheco-Torres, Jesus, Raj Kumar Sharma, Yelena Mironchik, Flonne Wildes, W. Nathaniel Brennen, Dmitri Artemov, Balaji Krishnamachary, and Zaver M. Bhujwalla. 2024. 'Prostate Fibroblasts and Prostate Cancer Associated Fibroblasts Exhibit Different Metabolic, Matrix Degradation and PD-L1 Expression Responses to Hypoxia'. Frontiers in Molecular Biosciences 11:1354076. doi:10.3389/fmolb.2024.1354076.

Peng, Zhiwei, Zhiwei Tong, Zihao Ren, Manping Ye, and Kongwang Hu. 2023. 'Cancer-Associated Fibroblasts and Its Derived Exosomes: A New Perspective for Reshaping the Tumor Microenvironment'. Molecular Medicine 29(1):66. doi:10.1186/s10020-023-00665-y.

Qiu, Xintao, Nadia Boufaied, Tarek Hallal, Avery Feit, Anna De Polo, Adrienne M. Luoma, Walaa Alahmadi, Janie Larocque, Giorgia Zadra, Yingtian Xie, Shengqing Gu, Qin Tang, Yi Zhang, Sudeepa Syamala, Ji-Heui Seo, Connor Bell, Edward O'Connor, Yang Liu, Edward M. Schaeffer, R. Jeffrey Karnes, Sheila Weinmann, Elai Davicioni, Colm Morrissey, Paloma Cejas, Leigh Ellis, Massimo Loda, Kai W. Wucherpfennig, Mark M. Pomerantz, Daniel E. Spratt, Eva Corey, Matthew L. Freedman, X. Shirley Liu, Myles Brown, Henry W. Long, and David P. Labbé. 2022. 'MYC Drives Aggressive Prostate Cancer by Disrupting Transcriptional Pause Release at Androgen Receptor Targets'. Nature Communications 13(1):2559. doi:10.1038/s41467-022-30257-z.

Qu, Yuanyuan, Bo Dai, Dingwei Ye, Yunyi Kong, Kun Chang, Zhongwei Jia, Xiaoqun Yang, Hailiang Zhang, Yao Zhu, and Guohai Shi. 2015. 'Constitutively Active AR-V7 Plays an Essential Role in the Development and Progression of Castration-Resistant Prostate Cancer'. Scientific Reports 5(1):7654. doi:10.1038/srep07654.

Qu, Yuejun, and Wenqiang Huang. 2018. 'Effects of microRNA-210 on the Diagnosis and Treatment of Prostate Cancer'. Molecular Medicine Reports. doi:10.3892/mmr.2018.9105.

Quail, Daniela F., and Johanna A. Joyce. 2013. 'Microenvironmental Regulation of Tumor Progression and Metastasis'. Nature Medicine 19(11):1423–37. doi:10.1038/nm.3394.

Quero, Laurent, Ludwig Dubois, Natasja G. Lieuwes, Christophe Hennequin, and Philippe Lambin. 2011. 'miR-210 as a Marker of Chronic Hypoxia, but Not a Therapeutic Target in Prostate Cancer'. Radiotherapy and Oncology 101(1):203–8. doi:10.1016/j.radonc.2011.05.063.

Ramteke, Anand, Harold Ting, Chapla Agarwal, Samiha Mateen, Ranganathan Somasagara, Anowar Hussain, Michael Graner, Barbara Frederick, Rajesh Agarwal, and Gagan Deep. 2015. 'Exosomes Secreted under Hypoxia Enhance Invasiveness and Stemness of Prostate Cancer Cells by Targeting Adherens Junction Molecules: HYPOXIC-EXOSOMES ROLE IN PCA AGGRESSIVENESS'. Molecular Carcinogenesis 54(7):554–65. doi:10.1002/mc.22124.

Rao, Srinivasa, Clare Verrill, Lucia Cerundolo, Nasullah Khalid Alham, Zeynep Kaya, Miriam O'Hanlon, Alicia Hayes, Adam Lambert, Martha James, Iain D. C. Tullis, Jane Niederer, Shelagh Lovell, Altan Omer, Francisco Lopez, Tom Leslie, Francesca Buffa, Richard J. Bryant, Alastair D. Lamb, Boris Vojnovic, David C. Wedge, Ian G. Mills, Dan J. Woodcock, Ian Tomlinson, and Freddie C. Hamdy. 2024. 'Intra-Prostatic Tumour Evolution, Steps in Metastatic Spread and Histogenomic Associations Revealed by Integration of Multi-Region Whole-Genome Sequencing with Histopathological Features'. Genome Medicine 16(1):35. doi:10.1186/s13073-024-01302-x.

Rao, Zhigang, Ziqi He, Yi He, Zonghua Guo, Dongbo Kong, and Jufang Liu. 2017. 'MicroRNA-512-3p Is Upregulated, and Promotes Proliferation and Cell Cycle Progression, in Prostate Cancer Cells'. Molecular Medicine Reports. doi:10.3892/mmr.2017.7844.

Rebello, Richard J., Christoph Oing, Karen E. Knudsen, Stacy Loeb, David C. Johnson, Robert E. Reiter, Silke Gillessen, Theodorus Van Der Kwast, and Robert G. Bristow. 2021. 'Prostate Cancer'. Nature Reviews Disease Primers 7(1):9. doi:10.1038/s41572-020-00243-0.

Ren, Jie, Xiaodan Li, Hao Dong, Longlong Suo, Jun Zhang, Lina Zhang, and Jing Zhang. 2019. 'miR-210-3p Regulates the Proliferation and Apoptosis of Non-small Cell Lung Cancer Cells by Targeting SIN3A'. Experimental and Therapeutic Medicine. doi:10.3892/etm.2019.7867.

Renart, J., J. Reiser, and G. R. Stark. 1979. 'Transfer of Proteins from Gels to Diazobenzyloxymethyl-Paper and Detection with Antisera: A Method for Studying Antibody Specificity and Antigen Structure.' Proceedings of the National Academy of Sciences 76(7):3116–20. doi:10.1073/pnas.76.7.3116.

RKI 2020. n.d.

Salehi, Mahsa, and Mohammadreza Sharifi. 2018. 'Exosomal miRNAs as Novel Cancer Biomarkers: Challenges and Opportunities'. Journal of Cellular Physiology 233(9):6370–80. doi:10.1002/jcp.26481.

Sato-Kuwabara, Yukie, Sonia A. Melo, Fernando A. Soares, and George A. Calin. 2015. 'The Fusion of Two Worlds: Non-Coding RNAs and Extracellular Vesicles - Diagnostic and Therapeutic Implications (Review)'. International Journal of Oncology 46(1):17–27. doi:10.3892/ijo.2014.2712.

Schröder, Fritz H., Jonas Hugosson, Monique J. Roobol, Teuvo L. J. Tammela, Marco Zappa, Vera Nelen, Maciej Kwiatkowski, Marcos Lujan, Liisa Määttänen, Hans Lilja, Louis J. Denis, Franz Recker, Alvaro Paez, Chris H. Bangma, Sigrid Carlsson, Donella Puliti, Arnauld Villers, Xavier Rebillard, Matti Hakama, Ulf-Hakan Stenman, Paula Kujala, Kimmo Taari, Gunnar Aus, Andreas Huber, Theo H. Van Der Kwast, Ron H. N. Van Schaik, Harry J. De Koning, Sue M. Moss, and Anssi Auvinen. 2014. 'Screening and Prostate Cancer Mortality: Results of the European Randomised Study of Screening for Prostate Cancer (ERSPC) at 13 Years of Follow-Up'. The Lancet 384(9959):2027–35. doi:10.1016/S0140-6736(14)60525-0.

Sekhoacha, Mamello, Keamogetswe Riet, Paballo Motloung, Lemohang Gumenku, Ayodeji Adegoke, and Samson Mashele. 2022. 'Prostate Cancer Review: Genetics, Diagnosis, Treatment Options, and Alternative Approaches'. Molecules 27(17):5730. doi:10.3390/molecules27175730.

Seo, W. Y., B. C. Jeong, E. J. Yu, H. J. Kim, S. H. Kim, J. E. Lim, G. Y. Kwon, H. M. Lee, and J. H. Kim. 2013. 'CCAR1 Promotes Chromatin Loading of Androgen Receptor (AR) Transcription Complex by Stabilizing the Association between AR and GATA2'. Nucleic Acids Research 41(18):8526–36. doi:10.1093/nar/gkt644.

Shi, Xueke, Christian D. Young, Hongmei Zhou, and Xiao-Jing Wang. 2020. 'Transforming Growth Factor-β Signaling in Fibrotic Diseases and Cancer-Associated Fibroblasts'. Biomolecules 10(12):1666. doi:10.3390/biom10121666.

Shoag, Jonathan, and ChristopherE Barbieri. 2016. 'Clinical Variability and Molecular Heterogeneity in Prostate Cancer'. Asian Journal of Andrology 18(4):543. doi:10.4103/1008-682X.178852.

Shukla, Kamla Kant, Gautam Choudhary, Shrimanjunath Sankanagoudar, Sanjeev Misra, Jeewan Vishnoi, Puneet Pareek, Kiran Pilla, Sachchida N. Pandey, and Praveen Sharma. 2023. 'Deregulation of miR-10b and miR-21 Correlate with Cancer Stem Cells Expansion through the Apoptotic Pathway in Prostate Cancer'. Asian Pacific Journal of Cancer Prevention 24(6):2105–19. doi:10.31557/APJCP.2023.24.6.2105.

Shurtleff, Matthew J., Morayma M. Temoche-Diaz, Kate V. Karfilis, Sayaka Ri, and Randy Schekman. 2016. 'Y-Box Protein 1 Is Required to Sort microRNAs into Exosomes in Cells and in a Cell-Free Reaction'. eLife 5:e19276. doi:10.7554/eLife.19276.

Singh, Ramesh, Radhika Pochampally, Kounosuke Watabe, Zhaohui Lu, and Yin-Yuan Mo. 2014. 'Exosome-Mediated Transfer of miR-10b Promotes Cell Invasion in Breast Cancer'. Molecular Cancer 13(1). doi:10.1186/1476-4598-13-256.

Sommer, Ulrich, Tiziana Siciliano, Celina Ebersbach, Alicia-Marie K. Beier, Matthias B. Stope, Korinna Jöhrens, Gustavo B. Baretton, Angelika Borkowetz, Christian Thomas, and Holger H. H. Erb. 2022. 'Impact of Androgen Receptor Activity on Prostate-Specific Membrane Antigen Expression in Prostate Cancer Cells'. International Journal of Molecular Sciences 23(3):1046. doi:10.3390/ijms23031046.

Tang, Sijie, Huiying Cheng, Xueyan Zang, Jiawei Tian, Zhongli Ling, Lingling Wang, Wenrong Xu, and Jiajia Jiang. 2025. 'Small Extracellular Vesicles: Crucial Mediators for Prostate Cancer'. Journal of Nanobiotechnology 23(1):230. doi:10.1186/s12951-025-03326-w.

Théry, Clotilde, Kenneth W. Witwer, Elena Aikawa, Maria Jose Alcaraz, Johnathon D. Anderson, Ramaroson Andriantsitohaina, Anna Antoniou, Tanina Arab, Fabienne Archer, Georgia K. Atkin-Smith, D. Craig Ayre, Jean-Marie Bach, Daniel Bachurski, Hossein Baharvand, Leonora Balaj, Shawn Baldacchino, Natalie N. Bauer, Amy A. Baxter, Mary Bebawy, Carla Beckham, Apolonija Bedina Zavec, Abderrahim Benmoussa, Anna C. Berardi, Paolo Bergese, Ewa Bielska, Cherie Blenkiron, Sylwia Bobis-Wozowicz, Eric Boilard, Wilfrid Boireau, Antonella Bongiovanni, Francesc E. Borràs, Steffi Bosch, Chantal M. Boulanger, Xandra Breakefield, Andrew M. Breglio, Meadhbh Á. Brennan, David R. Brigstock, Alain Brisson, Marike Ld Broekman, Jacqueline F. Bromberg, Paulina Bryl-Górecka, Shilpa Buch, Amy H. Buck, Dylan Burger, Sara Busatto, Dominik Buschmann, Benedetta Bussolati, Edit I. Buzás, James Bryan Byrd, Giovanni Camussi, David Rf Carter, Sarah Caruso, Lawrence W. Chamley, Yu-Ting Chang, Chihchen Chen, Shuai Chen, Lesley Cheng, Andrew R. Chin, Aled Clayton, Stefano P. Clerici, Alex Cocks, Emanuele Cocucci, Robert J. Coffey, Anabela Cordeiro-da-Silva, Yvonne Couch, Frank Aw Coumans, Beth Coyle, Rossella Crescitelli, Miria Ferreira Criado, Crislyn D'Souza-Schorey, Saumya Das, Amrita Datta Chaudhuri, Paola De Candia, Eliezer F. De Santana, Olivier De Wever, Hernando A. Del Portillo, Tanguy Demaret, Sarah Deville, Andrew Devitt, Bert Dhondt, Dolores Di Vizio, Lothar C. Dieterich, Vincenza Dolo, Ana Paula Dominguez Rubio, Massimo Dominici, Mauricio R. Dourado, Tom Ap Driedonks, Filipe V. Duarte, Heather M. Duncan, Ramon M. Eichenberger, Karin Ekström, Samir El Andaloussi, Celine Elie-Caille, Uta Erdbrügger, Juan M. Falcón-Pérez, Farah Fatima, Jason E. Fish, Miguel Flores-Bellver, András Försönits, Annie Frelet-Barrand, Fabia Fricke, Gregor Fuhrmann, Susanne Gabrielsson, Ana Gámez-Valero, Chris Gardiner, Kathrin Gärtner, Raphael Gaudin, Yong Song Gho, Bernd Giebel, Caroline Gilbert, Mario Gimona, Ilaria Giusti, Deborah Ci Goberdhan, André Görgens, Sharon M. Gorski, David W. Greening, Julia Christina Gross, Alice Gualerzi, Gopal N. Gupta, Dakota Gustafson, Aase Handberg, Reka A. Haraszti, Paul Harrison, Hargita Hegyesi, An Hendrix, Andrew F. Hill, Fred H. Hochberg,

Karl F. Hoffmann, Beth Holder, Harry Holthofer, Baharak Hosseinkhani, Guoku Hu, Yiyao Huang, Veronica Huber, Stuart Hunt, Ahmed Gamal-Eldin Ibrahim, Tsuneya Ikezu, Jameel M. Inal, Mustafa Isin, Alena Ivanova, Hannah K. Jackson, Soren Jacobsen, Steven M. Jay, Muthuvel Jayachandran, Guido Jenster, Lanzhou Jiang, Suzanne M. Johnson, Jennifer C. Jones, Ambrose Jong, Tijana Jovanovic-Talisman, Stephanie Jung, Raghu Kalluri, Shin-ichi Kano, Sukhbir Kaur, Yumi Kawamura, Evan T. Keller, Delaram Khamari, Elena Khomyakova, Anastasia Khvorova, Peter Kierulf, Kwang Pyo Kim, Thomas Kislinger, Mikael Klingeborn, David J. Klinke, Miroslaw Kornek, Maja M. Kosanović, Árpád Ferenc Kovács, Eva-Maria Krämer-Albers, Susanne Krasemann, Mirja Krause, Igor V. Kurochkin, Gina D. Kusuma, Sören Kuypers, Saara Laitinen, Scott M. Langevin, Lucia R. Languino, Joanne Lannigan, Cecilia Lässer, Louise C. Laurent, Gregory Lavieu, Elisa Lázaro-Ibáñez, Soazig Le Lay, Myung-Shin Lee, Yi Xin Fiona Lee, Debora S. Lemos, Metka Lenassi, Aleksandra Leszczynska, Isaac Ts Li, Ke Liao, Sten F. Libregts, Erzsebet Ligeti, Rebecca Lim, Sai Kiang Lim, Aija Linē, Karen Linnemannstöns, Alicia Llorente, Catherine A. Lombard, Magdalena J. Lorenowicz, Ákos M. Lörincz, Jan Lötvall, Jason Lovett, Michelle C. Lowry, Xavier Loyer, Quan Lu, Barbara Lukomska, Taral R. Lunavat, Sybren Ln Maas, Harmeet Malhi, Antonio Marcilla, Jacopo Mariani, Javier Mariscal, Elena S. Martens-Uzunova, Lorena Martin-Jaular, M. Carmen Martinez, Vilma Regina Martins, Mathilde Mathieu, Suresh Mathivanan, Marco Maugeri, Lynda K. McGinnis, Mark J. McVey, David G. Meckes, Katie L. Meehan, Inge Mertens, Valentina R. Minciacchi, Andreas Möller, Malene Møller Jørgensen, Aizea Morales-Kastresana, Jess Morhayim, François Mullier, Maurizio Muraca, Luca Musante, Veronika Mussack, Dillon C. Muth, Kathryn H. Myburgh, Tanbir Najrana, Muhammad Nawaz, Irina Nazarenko, Peter Nejsum, Christian Neri, Tommaso Neri, Rienk Nieuwland, Leonardo Nimrichter, John P. Nolan, Esther Nm Nolte-'t Hoen, Nicole Noren Hooten, Lorraine O'Driscoll, Tina O'Grady, Ana O'Loghlen, Takahiro Ochiya, Martin Olivier, Alberto Ortiz, Luis A. Ortiz, Xabier Osteikoetxea, Ole Østergaard, Matias Ostrowski, Jaesung Park, D. Michiel Pegtel, Hector Peinado, Francesca Perut, Michael W. Pfaffl, Donald G. Phinney, Bartijn Ch Pieters, Ryan C. Pink, David S. Pisetsky, Elke Pogge Von Strandmann, Iva Polakovicova, Ivan Kh Poon, Bonita H. Powell, Ilaria Prada, Lynn Pulliam, Peter Quesenberry, Annalisa Radeghieri, Robert L. Raffai, Stefania Raimondo, Janusz Rak, Marcel I. Ramirez, Graça Raposo, Morsi S. Rayyan, Neta Regev-Rudzki, Franz

L. Ricklefs, Paul D. Robbins, David D. Roberts, Silvia C. Rodrigues, Eva Rohde, Sophie Rome, Kasper Ma Rouschop, Aurelia Rughetti, Ashley E. Russell, Paula Saá, Susmita Sahoo, Edison Salas-Huenuleo, Catherine Sánchez, Julie A. Saugstad, Meike J. Saul, Raymond M. Schiffelers, Raphael Schneider, Tine Hiorth Schøyen, Aaron Scott, Eriomina Shahaj, Shivani Sharma, Olga Shatnyeva, Faezeh Shekari, Ganesh Vilas Shelke, Ashok K. Shetty, Kiyotaka Shiba, Pia R-M Siljander, Andreia M. Silva, Agata Skowronek, Orman L. Snyder, Rodrigo Pedro Soares, Barbara W. Sódar, Carolina Soekmadji, Javier Sotillo, Philip D. Stahl, Willem Stoorvogel, Shannon L. Stott, Erwin F. Strasser, Simon Swift, Hidetoshi Tahara, Muneesh Tewari, Kate Timms, Swasti Tiwari, Rochelle Tixeira, Mercedes Tkach, Wei Seong Toh, Richard Tomasini, Ana Claudia Torrecilhas, Juan Pablo Tosar, Vasilis Toxavidis, Lorena Urbanelli, Pieter Vader, Bas Wm Van Balkom, Susanne G. Van Der Grein, Jan Van Deun, Martijn Jc Van Herwijnen, Kendall Van Keuren-Jensen, Guillaume Van Niel, Martin E. Van Royen, Andre J. Van Wijnen, M. Helena Vasconcelos, Ivan J. Vechetti, Tiago D. Veit, Laura J. Vella, Émilie Velot, Frederik J. Verweij, Beate Vestad, Jose L. Viñas, Tamás Visnovitz, Krisztina V. Vukman, Jessica Wahlgren, Dionysios C. Watson, Marca Hm Wauben, Alissa Weaver, Jason P. Webber, Viktoria Weber, Ann M. Wehman, Daniel J. Weiss, Joshua A. Welsh, Sebastian Wendt, Asa M. Wheelock, Zoltán Wiener, Leonie Witte, Joy Wolfram, Angeliki Xagorari, Patricia Xander, Jing Xu, Xiaomei Yan, María Yáñez-Mó, Hang Yin, Yuana Yuana, Valentina Zappulli, Jana Zarubova, Vytautas Žėkas, Jian-ye Zhang, Zezhou Zhao, Lei Zheng, Alexander R. Zheutlin, Antje M. Zickler, Pascale Zimmermann, Angela M. Zivkovic, Davide Zocco, and Ewa K. Zuba-Surma. 2018. ‘Minimal Information for Studies of Extracellular Vesicles 2018 (MISEV2018): A Position Statement of the International Society for Extracellular Vesicles and Update of the MISEV2014 Guidelines’. Journal of Extracellular Vesicles 7(1):1535750. doi:10.1080/20013078.2018.1535750.

Tian, Youxi, Dong Tian, Xinsheng Peng, and Hong Qiu. 2024. ‘Critical Parameters to Standardize the Size and Concentration Determination of Nanomaterials by Nanoparticle Tracking Analysis’. International Journal of Pharmaceutics 656:124097. doi:10.1016/j.ijpharm.2024.124097.

Truong, Nhat Chau, Thao Nhi Huynh, Khuong Duy Pham, and Phuc Van Pham. 2020. 'The Role of Tumor-Derived Exosomes in Tumor Immune Escape: A Concise Review'. Biomedical Research and Therapy 7(11):4132–37. doi:10.15419/bmrat.v7i11.650.

Tsuchiya, Soken, Takeshi Fujiwara, Fumiaki Sato, Yutaka Shimada, Eiji Tanaka, Yoshiharu Sakai, Kazuharu Shimizu, and Gozoh Tsujimoto. 2011. 'MicroRNA-210 Regulates Cancer Cell Proliferation through Targeting Fibroblast Growth Factor Receptor-like 1 (FGFRL1)'. Journal of Biological Chemistry 286(1):420–28. doi:10.1074/jbc.M110.170852.

Tummala, Ramakumar, Wei Lou, Allen C. Gao, and Nagalakshmi Nadiminty. 2017. 'Quercetin Targets hnRNPA1 to Overcome Enzalutamide Resistance in Prostate Cancer Cells'. Molecular Cancer Therapeutics 16(12):2770–79. doi:10.1158/1535-7163.MCT-17-0030.

Urabe, Fumihiko, Yuta Yamada, Shutaro Yamamoto, Shunsuke Tsuzuki, Shoji Kimura, Takahiro Ochiya, and Takahiro Kimura. 2024. 'Extracellular Vesicles and Prostate Cancer Management: A Narrative Review'. Translational Andrology and Urology 13(3):442–53. doi:10.21037/tau-23-533.

US Preventive Services Task Force, David C. Grossman, Susan J. Curry, Douglas K. Owens, Kirsten Bibbins-Domingo, Aaron B. Caughey, Karina W. Davidson, Chyke A. Doubeni, Mark Ebell, John W. Epling, Alex R. Kemper, Alex H. Krist, Martha Kubik, C. Seth Landefeld, Carol M. Mangione, Michael Silverstein, Melissa A. Simon, Albert L. Siu, and Chien-Wen Tseng. 2018. 'Screening for Prostate Cancer: US Preventive Services Task Force Recommendation Statement'. JAMA 319(18):1901. doi:10.1001/jama.2018.3710.

Valadi, Hadi, Karin Ekström, Apostolos Bossios, Margareta Sjöstrand, James J. Lee, and Jan O. Lötvall. 2007. 'Exosome-Mediated Transfer of mRNAs and microRNAs Is a Novel Mechanism of Genetic Exchange between Cells'. Nature Cell Biology 9(6):654–59. doi:10.1038/ncb1596.

Vlaeminck-Guillem, Virginie. 2018. 'Extracellular Vesicles in Prostate Cancer Carcinogenesis, Diagnosis, and Management'. Frontiers in Oncology 8:222. doi:10.3389/fonc.2018.00222.

Wang, Qianyu, Gang Pan, Yu Zhang, Yiqin Ni, Yuzhu Mu, and Dingcun Luo. 2024. 'Emerging Insights into Thyroid Cancer from Immunotherapy Perspective: A Bibliometric Analysis'. Human Vaccines & Immunotherapeutics 20(1):2403170. doi:10.1080/21645515.2024.2403170.

Wang, Shuo, Peng Du, Yudong Cao, Jinchao Ma, Xiao Yang, Ziyi Yu, and Yong Yang. 2022. 'Cancer Associated Fibroblasts Secreted Exosomal miR-1290 Contributes to Prostate Cancer Cell Growth and Metastasis via Targeting GSK3β'. Cell Death Discovery 8(1):371. doi:10.1038/s41420-022-01163-6.

Wang, Y., M. Mikhailova, S. Bose, C. X. Pan, R. W. deVere White, and P. M. Ghosh. 2008. 'Regulation of Androgen Receptor Transcriptional Activity by Rapamycin in Prostate Cancer Cell Proliferation and Survival'. Oncogene 27(56):7106–17. doi:10.1038/onc.2008.318.

Webber, Jason P., Lisa K. Spary, Malcolm D. Mason, Zsuzsanna Tabi, Ian A. Brewis, and Aled Clayton. 2016. 'Prostate Stromal Cell Proteomics Analysis Discriminates Normal from Tumour Reactive Stromal Phenotypes'. Oncotarget 7(15):20124–39. doi:10.18632/oncotarget.7716.

Weber, K., and M. Osborn. 1969. 'The Reliability of Molecular Weight Determinations by Dodecyl Sulfate-Polyacrylamide Gel Electrophoresis'. The Journal of Biological Chemistry 244(16):4406–12.

Wei, Denghui, Weixiang Zhan, Ying Gao, Liyan Huang, Run Gong, Wen Wang, Ruhua Zhang, Yuanzhong Wu, Song Gao, and Tiebang Kang. 2021. 'RAB31 Marks and Controls an ESCRT-Independent Exosome Pathway'. Cell Research 31(2):157–77. doi:10.1038/s41422-020-00409-1.

Welsh, Joshua A., Deborah C. Goberdhan, Lorraine O'Driscoll, Clotilde Théry, and Kenneth W. Witwer. 2024. 'MISEV2023: An Updated Guide to EV Research and Applications'. Journal of Extracellular Vesicles 13(2):e12416. doi:10.1002/jev2.12416.

Weng, Hong, Kang-Ping Xiong, Wang Wang, Kai-Yu Qian, Shuai Yuan, Gang Wang, Fang Yu, Jun Luo, Meng-Xin Lu, Zhong-Hua Yang, Tao Liu, Xing Huang, Hang Zheng, and Xing-Huan Wang. 2023. 'Aspartoacylase Suppresses Prostate Cancer

Progression by Blocking LYN Activation'. Military Medical Research 10(1):25. doi:10.1186/s40779-023-00460-0.

Witwer, Kenneth W., and Clotilde Théry. 2019. 'Extracellular Vesicles or Exosomes? On Primacy, Precision, and Popularity Influencing a Choice of Nomenclature'. Journal of Extracellular Vesicles 8(1):1648167. doi:10.1080/20013078.2019.1648167.

Wong, Martin C. S., William B. Goggins, Harry H. X. Wang, Franklin D. H. Fung, Colette Leung, Samuel Y. S. Wong, Chi Fai Ng, and Joseph J. Y. Sung. 2016. 'Global Incidence and Mortality for Prostate Cancer: Analysis of Temporal Patterns and Trends in 36 Countries'. European Urology 70(5):862–74. doi:10.1016/j.eururo.2016.05.043.

Wu, Xiaoxuan, Peng Song, Shun Wang, Zhirong Qian, Jianming Ying, Shugeng Gao, and Wenbin Li. 2022. 'A Pan-Cancer Analysis of the Oncogenic Role of WD Repeat Domain 74 in Multiple Tumors'. Frontiers in Genetics 13:860940. doi:10.3389/fgene.2022.860940.

Wu, Yunjian, Kimberley C. Clark, Birunthi Niranjan, Anderly C. Chüeh, Lisa G. Horvath, Renea A. Taylor, and Roger J. Daly. 2023. 'Integrative Characterisation of Secreted Factors Involved in Intercellular Communication between Prostate Epithelial or Cancer Cells and Fibroblasts'. Molecular Oncology 17(3):469–86. doi:10.1002/1878-0261.13376.

Wu, Zilong, Zihao Xu, Boyao Yu, Jingtao Zhang, and Bentong Yu. 2020. 'The Potential Diagnostic Value of Exosomal Long Noncoding RNAs in Solid Tumors: A Meta-Analysis and Systematic Review' edited by K. Maemura. BioMed Research International 2020(1):6786875. doi:10.1155/2020/6786875.

Yan, Kai, Qing-Zhi Liu, Rong-Rong Huang, Yi-Hua Jiang, Zhen-Hua Bian, Si-Jin Li, Liang Li, Fei Shen, Koichi Tsuneyama, Qing-Ling Zhang, Zhe-Xiong Lian, Haixia Guan, and Bo Xu. 2024. 'Spatial Transcriptomics Reveals Prognosis-associated Cellular Heterogeneity in the Papillary Thyroid Carcinoma Microenvironment'. Clinical and Translational Medicine 14(3):e1594. doi:10.1002/ctm2.1594.

Yang, Xi, Zhiyong Guo, Feng Sun, Wei Li, Alan Alfano, Hermela Shimelis, Mingyuan Chen, Angela M. H. Brodie, Hegang Chen, Zhen Xiao, Timothy D. Veenstra, and

Yun Qiu. 2011. ‘Novel Membrane-Associated Androgen Receptor Splice Variant Potentiates Proliferative and Survival Responses in Prostate Cancer Cells’. Journal of Biological Chemistry 286(41):36152–60. doi:10.1074/jbc.M111.265124.

Yeh, Shuyuan, Yueh-Chiang Hu, Mujib Rahman, Hui-Kuan Lin, Cheng-Lung Hsu, Huei-Ju Ting, Hong-Yo Kang, and Chawnshang Chang. 2000. ‘Increase of Androgen-Induced Cell Death and Androgen Receptor Transactivation by BRCA1 in Prostate Cancer Cells’. Proceedings of the National Academy of Sciences 97(21):11256–61. doi:10.1073/pnas.190353897.

Yu, Jihang, Zhixiang Wang, and Yi Wang. 2022. ‘BrdU Incorporation Assay to Analyze the Entry into S Phase’. Pp. 209–26 in Cell-Cycle Synchronization. Vol. 2579, Methods in Molecular Biology, edited by Z. Wang. New York, NY: Springer US.

Zhang, Lin, and Dihua Yu. 2019. ‘Exosomes in Cancer Development, Metastasis, and Immunity’. Biochimica et Biophysica Acta (BBA) - Reviews on Cancer 1871(2):455–68. doi:10.1016/j.bbcan.2019.04.004.

Zhang, Rongxin, Te Bu, Ruidan Cao, Zhelong Li, Chen Wang, Bing Huang, Mengying Wei, Lijun Yuan, and Guodong Yang. 2022. ‘An Optimized Exosome Production Strategy for Enhanced Yield While without Sacrificing Cargo Loading Efficiency’. Journal of Nanobiotechnology 20(1):463. doi:10.1186/s12951-022-01668-3.

Zhang, Yuefei, Yiqing Li, Pan Liu, Dacheng Gong, Hui Zhou, Wenjuan Li, Huilun Zhang, Wenfang Zheng, Jiaqi Xu, Hongqiang Cheng, Xue Zhang, and Yuehai Ke. 2021. ‘Phosphatase Shp2 Regulates Biogenesis of Small Extracellular Vesicles by Dephosphorylating Syntenin’. Journal of Extracellular Vesicles 10(5):e12078. doi:10.1002/jev2.12078.

Zhao, Yan, Meili Shen, Liangqiang Wu, Haiqin Yang, Yixuan Yao, Qingbiao Yang, Jianshi Du, Linlin Liu, Yapeng Li, and Yuansong Bai. 2023. ‘Stromal Cells in the Tumor Microenvironment: Accomplices of Tumor Progression?’ Cell Death & Disease 14(9):587. doi:10.1038/s41419-023-06110-6.

Zhao, Yi, Benjamin S. Simpson, Naomi Morka, Alex Freeman, Alex Kirkham, Daniel Kelly, Hayley C. Whitaker, Mark Emberton, and Joseph M. Norris. 2022. ‘Comparison of Multiparametric Magnetic Resonance Imaging with Prostate-Specific Membrane

Antigen Positron-Emission Tomography Imaging in Primary Prostate Cancer Diagnosis: A Systematic Review and Meta-Analysis'. Cancers 14(14):3497. doi:10.3390/cancers14143497.

Zheng, Hongmei, Yuting Zhan, Sile Liu, Junmi Lu, Jiadi Luo, Juan Feng, and Songqing Fan. 2018. 'The Roles of Tumor-Derived Exosomes in Non-Small Cell Lung Cancer and Their Clinical Implications'. Journal of Experimental & Clinical Cancer Research 37(1):226. doi:10.1186/s13046-018-0901-5.

Zhou, Weiying, Miranda Y. Fong, Yongfen Min, George Somlo, Liang Liu, Melanie R. Palomares, Yang Yu, Amy Chow, Sean Timothy Francis O'Connor, Andrew R. Chin, Yun Yen, Yafan Wang, Eric G. Marcusson, Peiguo Chu, Jun Wu, Xiwei Wu, Arthur Xuejun Li, Zhuo Li, Hanlin Gao, Xiubao Ren, Mark P. Boldin, Pengnian Charles Lin, and Shizhen Emily Wang. 2014. 'Cancer-Secreted miR-105 Destroys Vascular Endothelial Barriers to Promote Metastasis'. Cancer Cell 25(4):501–15. doi:10.1016/j.ccr.2014.03.007.

19 SCIENTIFIC CONTRIBUTION AND AWARDS

19.1 Presentations at National and International Conferences (First Author only)

- "74. Kongress der Deutschen Gesellschaft für Urologie e.V.", (DGU) 2022, Hamburg, Germany
- "19. Jahrestagung der Deutsche Prostatakarzinom Konsortium", (DPKK) 2022, Homburg/Saar, Germany
- "29th Meeting of the EAU Section of Urological Research",(ESUR) 2023, Basel, Switzerland

19.2 Poster Presentations at National and International Conferences (First Author only)

- "12. AUF-Symposium", 2021, Virtual
- "27th Meeting of the EAU Section of Urological Research",(ESUR) 2021, Virtual
- "28th Meeting of the EAU Section of Urological Research", (ESUR) 2022, Innsbruck, Austria
- "AACR Special Conference on Advances in Prostate Cancer Research", 2023, Denver, USA
- "38th Meeting of the EAU", (EAU) 2023, Milan, Italy
- "10th Mildred Scheel Cancer Conference", 2023, Bonn Germany

19.3 Awards and Prizes

- Research Prize from the "Verein der Freunde des UKS e.V." at the Saarland University Hospital (2022, €5000)
- DAAD Travel Grant as part of the "GradUS Global Program" at Saarland University (2023, €2400)

20 CURRICULUM VITAE

The curriculum vitae was removed from the electronic version of the doctoral thesis for reasons of data protection.

Tag der Promotion: 04.05.2026
Dekan: Univ.-Prof. Dr. med. dent. Matthias Hannig
Berichterstatter: Prof. Dr. rer. nat. Steffi Urbschat
Prof. Dr. Dr. Philipp Staber